Department of Chemistry and Materials Science

Printed enzymatic glucose/air batteries: performance, stability and mass-manufacturing

Saara Tuurala

Aalto University

DOCTORAL DISSERTATIONS

Aalto University publication series
DOCTORAL DISSERTATIONS 83/2017
VTT SCIENCE 152

Printed enzymatic glucose/air batteries: performance, stability and mass-manufacturing

Saara Tuurala

A doctoral dissertation completed for the degree of Doctor of Science (Technology) to be defended, with the permission of the Aalto University School of Chemical Engineering, at a public examination held at the lecture hall Ke2 of the school on 19 May 2017 at 12.

Aalto University
School of Chemical Engineering
Department of Chemistry and Materials Science

Supervising professor
Associate Professor Lasse Murtomäki, Aalto University, Finland

Thesis advisors
Associate Professor Tanja Kallio, Aalto University, Finland
Research Team Leader Dr Maria Smolander, Technical Research Centre of Finland Ltd, Finland

Preliminary examiners
Associate Professor Scott Calabrese Barton, Michigan State University, The United States of America
Reader Daren Caruana, University College London, England

Opponent
Professor Edmond Magner, University of Limerick, Ireland

Aalto University publication series
DOCTORAL DISSERTATIONS 83/2017

VTT SCIENCE 152

ISBN 978-952-60-7412-2 (printed)
ISBN 978-952-60-7411-5 (pdf)
ISSN-L 1799-4934
ISSN 1799-4934 (printed)
ISSN 1799-4942 (pdf)
http://urn.fi/URN:ISBN:978-952-60-7411-5

ISBN 978-951-38-8537-3 (printed)
ISBN 978-951-38-8536-6 (pdf)
ISSN-L 2242-119X
ISSN 2242-119X (printed)
ISSN 2242-1203 (pdf)
http://urn.fi/URN:ISBN:978-951-38-8536-6

Unigrafia Oy
Helsinki 2017

Finland

441 697
Printed matter

Aalto University

Abstract

Aalto University, P.O. Box 11000, FI-00076 Aalto www.aalto.fi

Author
Saara Tuurala

Name of the doctoral dissertation
Printed enzymatic glucose/air batteries: performance, stability and mass-manufacturing

Publisher School of Chemical Engineering

Unit Department of Chemistry and Materials Science

Series Aalto University publication series DOCTORAL DISSERTATIONS 83/2017

Field of research Chemistry

Manuscript submitted 13 January 2017 **Date of the defence** 19 May 2017

Permission to publish granted (date) 20 March 2017 **Language** English

☐ **Monograph** ☒ **Article dissertation** ☐ **Essay dissertation**

Abstract

The enzymatic biofuel cell (EBFC) converts the chemical energy of biofuel into electricity via bioelectrochemical reactions. The use of enzymes confers many advantages over metal catalysts e.g. renewability and low toxicity. However, enzymes are fairly sensitive to changes in temperature, pH and moisture. For this reason, enzymes are typically immobilized on electrodes either by chemical or physical adsorption. The electrodes are usually immersed in a liquid cell containing an optimised electrolyte. Hence, the conventional EBFC configuration is not practical and for this reason, a new type of EBFC was developed.

In this thesis, screen printed enzymatic electrodes (4-12 cm^2) were fabricated on paper-based substrates using enzymatic inks creating thin (ca. 1 mm) and bendable EBFCs. The outcome of this thesis was a mass-manufacturable glucose/air biobattery that can be stored as dry and activated on demand by buffer. The power output of these biobatteries was on μW scale, however multiple suggestions for achieving higher performance are presented in this thesis. This biobattery could be integrated e.g. with low-power sensors, RFID tags or even cosmetic/medical skin patches.

At the anode, commercial glucose oxidase (GOx) and in-house purified aldose dehydrogenase (ALDH) were studied. At the cathode, two in-house purified laccases from *Trametes hirsuta* (ThL) and recombinant *Melanocarpus albomyces* were studied as well as one industrial laccase (EcoL). The fabrication methods included ink formulation using different carbon supports, biocompatible binders and enzyme-mediator pairs. First printing trials were performed in the laboratory using multiple enzyme-mediator pairs mixed with a commercial carbon-based ink. After that, the manufacturing was scaled up using GOx and EcoL mixed with in-house prepared graphite-based inks. The printed EBFCs were mainly characterised by means of electrochemistry.

In the laboratory, the best power output (P_{max} = 3.5 μW cm^{-2}) was achieved with an ALDH/ThL cell, which had an open circuit voltage (OCV) of 0.62 V and maximum energy output (***E***) of ca. 10 μWh cm^{-2}. The best GOx/ThL cell had an OCV of 0.38 V, P_{max} of 1.4 μW cm^{-2} and ***E*** of 5.5 μWh cm^{-2}. The pilot scale manufactured GOx/EcoL cells performed 50-90% less, which could be attributed to differences in the ink compositions as well as to the degradation of enzyme-mediator electrodes due to heating (23 °C vs. 70 °C) and storage (one day vs. one week). The stability of the printed enzymes (GOx and EcoL) was very good, they lost a maximum of 40% of their activity, regardless of the drying or storage temperature. However, when mediators were added into the inks, elevated drying temperatures accelerated the degradation, and 70-80% of the enzymatic activity was lost in 28 days. Moreover, the anode was found to be the limiting factor, and for this reason different approaches to increase the anode performance were tested.

Keywords enzymatic biofuel cell, enzymatic electrodes, biobattery, screen printing

ISBN (printed) 978-952-60-7412-2 **ISBN (pdf)** 978-952-60-7411-5

ISSN-L 1799-4934 **ISSN (printed)** 1799-4934 **ISSN (pdf)** 1799-4942

Location of publisher Helsinki **Location of printing** Helsinki **Year** 2017

Pages 170 **urn** http://urn.fi/URN:ISBN:978-952-60-7411-5

Tekijä
Saara Tuurala

Väitöskirjan nimi
Painetut entsymaattiset glukoosi/ilma paristot: suorituskyky, stabiilisuus ja massatuotanto

Julkaisija Kemian tekniikan korkeakoulu

Yksikkö Kemian ja materiaalitieteen laitos

Sarja Aalto University publication series DOCTORAL DISSERTATIONS 83/2017

Tutkimusala Kemia

Käsikirjoituksen pvm 13.01.2017 **Väitöspäivä** 19.05.2017

Julkaisuluvan myöntämispäivä 20.03.2017 **Kieli** Englanti

☐ **Monografia** ☒ **Artikkeliväitöskirja** ☐ **Esseeväitöskirja**

Tiivistelmä

Entsymaattinen biopolttokenno (EBPK) muuntaa biopolttoaineen kemiallisen energian sähköksi biosähkökemiallisten reaktioiden avulla. Entsyymien käyttö metallikatalyyttien sijaan tuo monia etuja mm. uusiutuvuuden ja myrkyttömyyden. Entsyymit ovat kuitenkin varsin herkkiä muutoksille lämpötilassa, pH:ssa ja kosteudessa. Tästä syystä entsyymit tyypillisesti immobilisoidaan elektrodeihin joko kemiallisen tai fysikaalisen adsorption avulla. Elektrodit useimmiten upotetaan nestekennoon, joka sisältää optimaalisen elektrolyytin. Näin ollen tavanomaisen EBPK:n kokoonpano ei ole käytännöllinen, mistä syystä kehitettiin uudenlainen EBPK-rakenne.

Tässä työssä painettiin silkkipainotekniikalla entsymaattisia elektrodeja (4-12 cm^2) paperipohjaisille alustoille luoden ohuita (n. 1 mm) ja taipuisia EBPK:ja. Työn tuloksena saatiin massatuotettava glukoosi/ilma bioparisto, joka voidaan säilyttää kuivana ja aktivoida tarpeen tullen puskuriliuoksella. Bioparistojen teho on µW-luokkaa, mutta useita parannusmahdollisuuksia tehon suurentamiseksi on esitelty tässä työssä. Bioparisto voisi soveltua esim. matalatehoisten sensorien, RFID-tunnisteiden tai jopa iholle asetettavien kosmeettisten/lääkinnällisten lappujen virtalähteiksi.

Anodientsyymeinä tutkittiin kaupallista glukoosioksidaasia (GOx) sekä VTT:llä tuotettua aldoosidehydrogenaasia (ALDH). Katodientsyymeinä tutkittiin kahta VTT:llä tuotettua lakkaasia, joista ensimmäisen alkuperä on *Trametes hirsuta* (ThL) ja toisen *Melanocarpus albomyces*. Näiden lisäksi tutkittiin teollista lakkaasia (EcoL). Menetelmät pitivät sisällään musteiden valmistusta erilaisten hiilien, bioyhteensopivien sidosaineiden ja entsyymi-mediaattori -parien avulla. Ensimmäiset painokokeet suoritettiin laboratoriossa käyttäen eri entsyymi-mediaattori -pareja sekoitettuna kaupalliseen hiilipohjaiseen musteeseen. Tämän jälkeen tuotanto laajennettiin käyttäen GOx ja EcoL entsyymejä yhdessä VTT:llä tuotettujen grafiittipohjaisten musteiden kanssa. Painetut EBPK:t karakterisoitiin pääsääntöisesti sähkökemiallisia tekniikoita käyttäen.

Paras laboratoriossa saavutettu tehotiheys (P_{max} = 3.5 µW cm^{-2}) saatiin ALDH/ThL-kennolla, jonka avoimenpiirinjännite (OCV) oli 0.62 V ja enimmäisenergia (***E***) n. 10 µWh cm^{-2}. Parhaan GOx/ThL-kennon OCV oli 0.38 V, P_{max} = 1.4 µW cm^{-2} ja ***E*** = 5.5 µWh cm^{-2}. Koe-erässä tuotettujen kennojen suorituskyky oli 50-90 % alhaisempi, koska käytetyt musteseokset olivat erilaiset sekä entsyymi-mediaattori -parien ikääntyminen kiihtyi kohotetun kuivatuslämpötilan (23 °C v. 70 °C) ja pidennetyn säilytyksen (yksi päivä v. yksi viikko) vuoksi. Painettujen entsyymien (GOx ja EcoL) stabiilius oli hyvä, sillä ne menettivät korkeintaan 40 % aktiivisuudestaan kuivatus- ja säilytyslämpötilasta riippumatta. Mediaattorien lisääminen musteisiin kiihdytti entsyymien ikääntymistä, ja 70-80 % aktiivisuudesta oli menetetty kuukauden säilytyksen aikana. Anodi todettiin olevan rajoittava tekijä, minkä vuoksi erilaisia tapoja testattiin anodin suorituskyvyn parantamiseksi.

Avainsanat entsymaattinen biopolttokenno, entsymaattiset elektrodit, bioparisto, silkkipainatus

ISBN (painettu) 978-952-60-7412-2 **ISBN (pdf)** 978-952-60-7411-5

ISSN-L 1799-4934 **ISSN (painettu)** 1799-4934 **ISSN (pdf)** 1799-4942

Julkaisupaikka Helsinki **Painopaikka** Helsinki **Vuosi** 2017

Sivumäärä 170 **urn** http://urn.fi/URN:ISBN:978-952-60-7411-5

Preface

The research presented in this thesis was carried out in the research team of Printed Sensors and Electronic Devices at the VTT Technical Research Centre of Finland (VTT) during the period 2009-2015. The work was part of two national projects, funded by the Finnish Funding Agency for Innovation (Tekes). I also received a personal grant from VTT for writing the thesis. The thesis was finalised during my study leave and I am grateful to the Finnish Education Fund for supporting me financially with an adult education allowance. This thesis was academically approved at the School of Chemical Engineering at Aalto University (formerly Helsinki University of Technology).

First of all, I want to thank my professor Lasse Murtomäki for the opportunity to be a part time doctoral student under his supervision. I am also grateful to my advisors Associate Professor Tanja Kallio and Research Team Leader Dr Maria Smolander for your guidance and advice throughout the work. This thesis work included a lot of practical work and I want to thank my colleagues Anu Vaari, Asta Pesonen and Kaisa Kiri for your help in that. Colleagues Harry Boer and Anu Koivula, thank you for your advice on the enzymes used in this thesis. Colleagues Otto-Ville Kaukoniemi and Tiina Maaninen, thank you for your contribution in the pilot scale manufacturing process. I also want to thank my former colleagues Matti Valkiainen, Johanna Uotila, Leo von Hertzen and Jari Keskinen for your contributions to this work. I am also grateful to Mikael Bergelin, Jan-Erik Eriksson and Pia Sjöberg from Åbo Akademi and to Peter Jenkins for your advice in the bioelectrochemical part of this work and for helping me with my publications. My office roommates Marja Vilkman and Reetta Grenman, thank you for your support and humour.

I want to thank Professor Shelley D. Minteer and Professor Plamen Atanassov for the opportunity to visit your laboratories and learn about enzyme immobilisation and paper-based biofuel cells. Stephanie Maltzman, Stephanie Bortz, Zana Brower, Nina Zulic Hausmann, Lindsey Pelster, Carolin Schneider-Lau, Kyle Sjöholm, Claudia Narváez Villarrubia, Omar Garcia, Jared Roy, Michael Moehlenbrock, Rob Arechederra, Lisa Palmer, Marja Murray, Gustavo Ciniciato - thank you for your friendship, I felt like home because of you.

I would also like to express my sincere gratitude to my pre-examiners Associate Professor Scott Calabrese Barton and Reader Daren Caruana for your constructive comments and analysis. I was able to improve my thesis through your contribution.

In addition to academic support, I am grateful for my dear friends. Thank you for your endless support and for helping me enjoy life outside work. Niina Hagman and Frank Russi, Maija and Tuukka Heikinheimo, Jenni Antikainen and Markku Laine, Miia and Toni Fohlin, Johanna Metsomaa and Kalle Anttila, Ulpu Remes, Katriina Valkeapää, Helinä Pohjanlehto, Sanna Keskioja, Tanja and Mikko Noranta, Ville Aarnikko, Teemu Lohenoja - I would not have made it without you.

Finally, to my whole family - thank you for your support throughout my whole life. Thank you Auli and Jyrki Pirttikoski for being great parents and my younger siblings Henri, Kasperi and Matleena for being there. To my pillar of strength Erik Goussev - you have been the one who secured my way all the way to the top.

Helsinki, April 24, 2017,

Saara Tuurala

List of publications

This thesis is based on the following original publications, which are referred to in the text as I–VI. The publications are reproduced with kind permission from the publishers.

I **Tuurala, S.**, Lau, C., Atanassov, P., Smolander, M., and Minteer, S.D. (2012) Characterization and Stability Study of Immobilized PQQ-Dependent Aldose Dehydrogenase Bioanodes. *Electroanalysis 24(2)*, 229-238.

II Jenkins, P., **Tuurala, S.**, Vaari, A., Valkiainen, M., Smolander, M., and Leech, D. (2012) A comparison of glucose oxidase and aldose dehydrogenase as mediated anodes in printed glucose/oxygen enzymatic fuel cells using ABTS/laccase cathodes. *Bioelectrochemistry 87*, 172-177.

III Jenkins, P., **Tuurala, S.**, Vaari, A., Valkiainen, M., Smolander, M., and Leech, D. (2012) A mediated glucose/oxygen enzymatic fuel cell based on printed carbon inks containing aldose dehydrogenase and laccase as anode and cathode. *Enzyme and microbial technology 50(3)*, 181-187.

IV **Tuurala, S.**, Kaukoniemi, O.V., von Hertzen, L., Uotila, J., Vaari, A., Bergelin, M., Sjöberg, P., Eriksson, J.E., and Smolander, M. (2014) Scale-up of manufacturing of printed enzyme electrodes for enzymatic power source applications. *Journal of Applied Electrochemistry 44(7)*, 881-892.

V **Tuurala, S.**, Kallio, T., Smolander, M., and Bergelin, M. (2015) Increasing performance and stability of mass-manufacturable biobatteries by ink modification. *Sensing and Bio-Sensing Research 4*, 61-69.

VI **Tuurala, S.**, Kallio, T., Smolander, M., and Bergelin, M. (2015) Increasing operational lifetime of printed enzymatic power sources using superabsorbent polymers as anode support. *Energy Technology 3*, 1080-1083.

Author's contributions

Publication I Saara Tuurala conducted the study plan, electrochemical measurements and data analysis, and was the main author of the publication. The SEM imaging was conducted by Dr Carolin Lau.

Publication II Saara Tuurala prepared the enzymatic inks, assembled the biofuel cells and conducted the electrochemical characterisation of the cells together with the first co-author. Saara Tuurala took an active part in the data analysis and writing of the publication. The synthesis of the mediators and the solution phase studies were conducted by Dr Peter Jenkins.

Publication III Saara Tuurala prepared the enzymatic inks, assembled the biofuel cells and conducted the electrochemical characterisation of the cells together with the first co-author. Saara Tuurala took an active part in the data analysis and writing of the publication. The synthesis of the mediators and the solution phase studies were conducted by Dr Peter Jenkins.

Publication IV Saara Tuurala planned the electrochemical measurements and enzyme stability study of printed enzyme electrodes. Saara Tuurala carried out all the electrochemical measurements and data analysis related to them, as well as data analysis of the enzyme stability and microscopy study of printed enzymatic electrodes. Saara Tuurala took an active part in the development of the enzymatic inks. Saara Tuurala was the main author of the publication. The solution phase studies of enzyme-mediator pairs were conducted by Dr Mikael Bergelin and Dr Jan-Erik Eriksson. The base ink drying experiments for the roll-to-roll manufacturing were conducted by Leo von Hertzen. Dr Tiina Maaninen and Otto-Ville Kaukoniemi were in charge of the roll-to-roll manufacturing and Saara Tuurala took part in the printing process. The microscopy imaging of the printed electrodes was conducted by Dr Tiina Maaninen.

Publication V Saara Tuurala conducted the study plan, electrochemical measurements and data analysis, and was the main author of the publication. Dr Tiina Maaninen was in charge of the roll-to-roll manufacturing. The microscopy imaging of the printed electrodes was conducted by Dr Tiina Maaninen.

Publication VI Saara Tuurala conducted the study plan, electrochemical measurements and data analysis, and was the main author of the publication.

Contents

Abbreviations and symbols

List of abbreviations

ABTS	2,2′-azino-bis(3-ethylbenzothiazoline-6-sulfonic acid) di-ammonium salt
$ABTS^{+}$	first oxidation state of ABTS
$ABTS^{2+}$	second oxidation state of ABTS
ALDH	aldose dehydrogenase
BFC	biofuel cell
BOD	bilirubin oxidase
CA	chronoamperometry
CB	carbon black
CMC	carboxymethyl cellulose
CP	chronopotentiometry
CV	cyclic voltammetry
DET	direct electron transfer
EBFC	enzymatic biofuel cell
EcoL	Ecostone laccase
FAD	flavin adenine dinucleotide
$FADH_2$	reduced form of FAD
FcMeOH	ferrocenemethanol
FDH	fructose dehydrogenase
GDH	glucose dehydrogenase
GOx	glucose oxidase
iV-curve	polarisation curve
L-cell	liquid cell

LOx	lactate oxidase
MaL	*Melanocarpus albomyces* laccase
MET	mediated electron transfer
mGDH	membrane-bound GDH
MWCNT	multi-walled carbon nanotube
NHE	normal hydrogen electrode
OCV	open circuit voltage
ORR	oxygen reduction reaction
pI	isoelectric point
Pd/H_2	palladium-hydrogen
PEO	polyethylene oxide
PQQ	pyrroloquinoline quinone
$PQQH_2$	reduced form of PQQ
R2R	roll-to-roll
RFID	radio-frequency identification
rMaL	recombinant MaL
SAP	superabsorbent polymer
SEM	scanning electron microscopy
sGDH	soluble GDH
TBAB	tetrabutylammonium bromide
ThL	*Trametes hirsuta* laccase
TMPD	*N,N,N′,N′*-tetramethyl-*p*-phenylenediamine

List of symbols

A	area
c	concentration
D	diffusion coefficient
E	electric potential
$\boldsymbol{E}$	energy density
$E^{0'}$	formal potential
E_a	anodic potential
E_c	cathodic potential
$E_{cut\text{-}off}$	cut-off potential
F	Faraday constant
I	current
K_m	Michaelis-Menten constant
K_S	dissociation constant
k	reaction rate constant
n	number of electrons
R	gas constant
T	temperature
$\boldsymbol{Q}$	charge density
v	scan rate
v_0	reaction rate
V_{max}	maximum reaction rate

1. Introduction

1.1 Motivation - Why an enzymatic biofuel cell?

As portable and wearable electronics become more and more common in our everyday lives, there is a clear need for flexible and sustainable power sources. Electronics are planned to be integrated into e.g. household devices, clothing and even the human body, and they need to be almost indistinguishable, meaning in practice as thin, flexible and disposable as possible.

Although current battery chemistries (e.g. Zn/MnO_2, Zn/air and Li-ion) are being converted from their solid form to printed flexible platforms (see e.g. [1]–[5]), they still face many challenges. First of all, the use of metals as active materials introduces issues of disposability, toxicity and availability. In addition, the need for a specific electrolyte between the anode and cathode layers affects the manufacturing process as well as the shelf-life. Applying and sealing of a moist electrolyte between the anode and cathode is a demanding manufacturing step. If the electrolyte leaks out from the cell during storage, the cells soon become dry and lose their functionality. Hence, there is a need for alternative, environmentally friendly battery configurations.

For the reasons outlined above, a new type of printed battery was developed in this thesis. This battery uses enzymes as catalysts and converts the chemical energy of biofuel into electrical energy. The fuel at the anode is sugar and that at the cathode is oxygen from air. The use of enzymes as catalysts confers many advantages over metal catalysts: 1) they are renewable, 2) they operate in mild conditions, 3) they have no toxicity issues, and 4) they can selectively oxidise different renewable fuels (e.g. sugars and alcohols).

Research on enzymes as biocatalysts in biofuel cells (BFC) began in the early 1960s, and the first enzymatic BFC (EBFC) was produced in 1964 [6]. EBFCs were first studied by NASA in order to find ways to recycle human waste into usable energy in space crafts. However, due to poor performance and stability the research was not active until 1980s, when researchers started to study methanol oxidation by enzymes. In 1998 Palmore et al. [7] demonstrated complete oxidation of methanol to CO_2 by enzymatic cascade. Since then, the group led by Shelley Minteer has developed immobilised enzyme cascade electrodes for full oxidisation of methanol, ethanol, glycerol, lactate and sugar to carbon dioxide in an EBFC [8]–[12]. Through electrical wiring of enzymes, Adam Heller's group demonstrated a miniaturised glucose/air EBFC operating in a grapefruit [13]–[15]. The group led by Evgeny Katz has demonstrated the operation of EBFCs e.g. in living clams and a snail as well as operation of a pacemaker powered by an implantable EBFC [16]–[18]. In addition, self-powered electrochemical devices utilising EBFCs have been developed, such as biosensors, memristors, and immunoassays [19]–[21]. Hence, the three main applications for EBFCs are implantable BFCs, self-powered sensors, and power supplies for small portable and wearable power devices [22]–[25]. The greatest challenges facing EBFC-based technology are their rather poor power generation and stability,

and bulky design [26]. These three aspects were studied in this thesis by developing enzymatic inks and assembling EBFCs using printed enzymatic electrodes. The printing process of these inks was first demonstrated in the laboratory and then scaled up to pilot scale manufacture.

1.2 Objective - From liquid phase biofuel cell to printed thin biobattery

The most common type of EBFC contains a liquid chamber into which both anode and cathode electrodes are inserted (Figure 1a). Optimally, the anode and cathode enzymes are fully immobilised into the electrode structures and no separator is needed due to the high selectivity of enzymes. However, typically an ion exchange membrane is needed to prevent anode and cathode chemicals from mixing together.

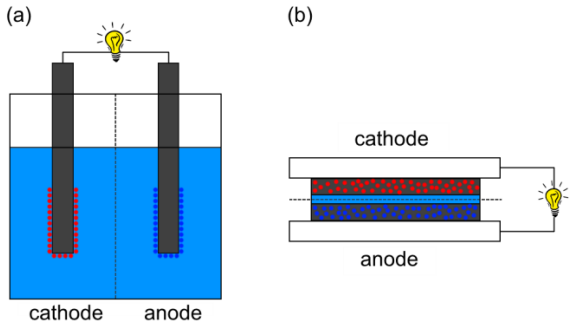

Figure 1. (a) Schematic of a conventional liquid-chamber EBFC. The electrodes consist of graphite rods on which the anode and cathode enzymes are immobilised. (b) Schematic of a planar EBFC. The electrodes are manufactured by printing enzymatic carbon-based inks on an electrically conductive substrate. The immobilised anode and cathode enzymes are represented as blue and red spheres, respectively.

In order to make EBFCs portable and easy to integrate for thin applications, the conventional structure needs to be changed. By mimicking a planar fuel cell structure and producing enzymatic electrodes by a printing process, a layered EBFC configuration was created (Figure 1b). Although this design miniaturises the cell structure, as well as simplifying the manufacturing process, it still faces many challenges, mainly related to enzyme stability and functionality. Hence, the objective of this thesis was to develop a printable, stable and scalable biobattery that can be stored dry and activated on demand. The main research questions were:

- How to develop enzyme-containing inks? (Publications I-V)
- What affects the performance and stability of printed electrodes? (Publications I-VI)
- Is it possible to demonstrate their production by printing in pilot scale? (Publications IV and V)

1.3 Progression - From laboratory to pilot scale manufacturing

As the main challenge when working with enzymes is their stability, they need to be protected against changes in temperature, pH and moisture. Immobilisation is a way to maintain the 3D structure of an enzyme

and thus its activity. Immobilisation can increase the molecular rigidity of an enzyme as well as create a protected microenvironment. There are many types of immobilisation techniques, such as covalent attachment or physical adsorption to a support, entrapment in a matrix or cross-linking of an enzyme [27]–[30], and the best immobilisation strategy is enzyme-specific. Consequently, the first task of this work was to study different polymer structures for immobilising and stabilising a very sensitive anode enzyme (Publication I).

Another challenge related to BFCs is their relatively poor electrochemical performance. This can be optimised by selecting the most suitable mediator molecules for shuttling electrons between the active site of the enzyme and the electrode surface. The use of osmium-based redox complexes as optional mediator molecules was investigated in printable enzyme electrodes, and fully printable BFCs were manufactured (Publications II and III).

As the printing process of enzyme electrodes was demonstrated to be successful in laboratory screen-printing, the next challenge was to scale up the printing process to a roll-to-roll (R2R) pilot scale. As there are many process steps in R2R manufacturing, including rotary screen-printing and drying of inks, they needed to be investigated (Publication IV). As a result, the printing process was scaled up from laboratory to pilot scale, and functional enzyme-containing electrodes were manufactured.

Although scale-up was successfully achieved, there were still challenges concerning the anode stability. For this reason, the anode-ink was reformulated in order to achieve better mechanical and functional stability (Publication V). As the last optimisation and stabilisation approach, a glue-like biocompatible polymer was introduced into the anode as a supporting element (Publication VI).

The outcome of this thesis work is a single-use, disposable and moisture-activated thin biobattery for µ-power applications, which can be manufactured on an industrial scale. The work flow of the whole thesis work is illustrated in Figure 2.

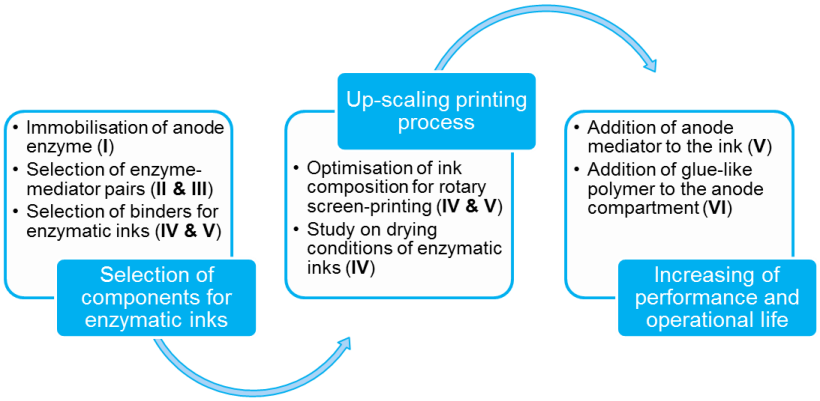

Figure 2. Progression of the thesis work.

2. The glucose/air biofuel cell

Any BFC is a fuel cell that contains biological catalysts [31]. Typically, the biocatalysts used are microorganisms or enzymes [32]. The operational principle of an EBFC [33], [34], using glucose and oxygen as fuel, is illustrated in Figure 3. On the anode, glucose is oxidised by an enzyme to gluconolactone, and on the cathode, oxygen is reduced by another enzyme to water, as shown in Equations (1) and (2).

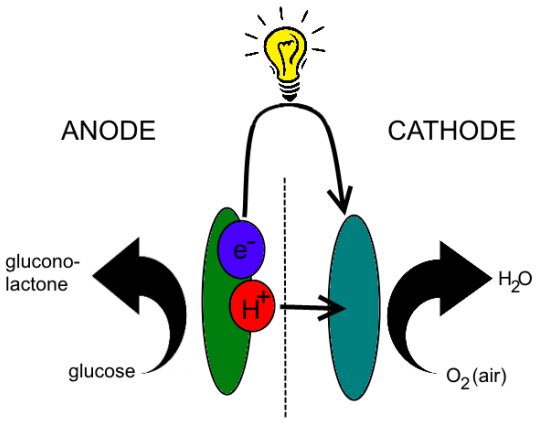

Figure 3. Illustration of the operational principle of a glucose/air EBFC.

$$\text{glucose} \xrightarrow{\text{anode enzyme}} \text{gluconolactone} + 2e^- + 2H^+ \quad (1)$$

$$\frac{1}{2}O_2(\text{air}) + 2e^- + 2H^+ \xrightarrow{\text{cathode enzyme}} H_2O \quad (2)$$

2.1 Enzymes as catalysts

Most metal catalysts catalyse a wide range of reactions, and hence they are usually not very selective. By contrast, enzymes are often highly selective, catalysing only very specific reactions. Enzymes lower the activation energy of certain biochemical reactions by providing an alternative reaction pathway. Enzymes take part in the reaction but they do not undergo permanent changes. In common with other catalysts, enzymes can only alter the rate of reaction, not the reaction equilibrium. [35]

Some enzymes consist of a protein and a cofactor, which is a chemical compound required for the protein's biological activity. Cofactors can be either organic or inorganic. Organic cofactors may be tightly or even covalently bound to the enzyme (e.g. flavin); they are called prosthetic groups. Organic molecules which are not permanently bound to the enzyme, but are involved directly in an enzyme-catalysed reaction (e.g. vitamin C) and combine temporarily with the enzyme-substrate complex, are called coenzymes. It must be mentioned, however, that this terminology can be slightly different in different sources [36]. Inorganic

cofactors are usually positively charged metal ions (e.g. Fe^{2+}, Mg^{2+} or Zn^{2+}) which bind temporarily to the active site of the enzyme, giving an intense local positive charge to the protein. Some enzymes or enzyme complexes require several cofactors, and in many cases the cofactor includes both an organic and an inorganic component (e.g. heme).

Enzyme proteins are often spherical, and in order to catalyse their reactions they must maintain their secondary and tertiary structures [37]. The intra- and intermolecular bonds that stabilise a protein structure are disrupted by changes in temperature, pH and hydration, which affects the overall conformation and thus the catalytic activity of the enzyme. Enzyme activity can also be affected by other molecules. Inhibitors and activators are molecules that decrease and increase enzyme activity, respectively, by binding to the active site of the enzyme.

In order to generate electricity, the selected enzymes need to be oxidoreductases due to their ability to catalyse electron transfer from one molecule to another. For comparison, transferases enact the transfer of specific functional groups from one molecule to another, and no electricity can be harvested. Many redox enzymes catalyse reactions at potentials that are close to the theoretical oxidation or reduction potentials of their substrates. This is most suitable for power sources because a high cell potential is needed for high power output. As an example, at pH 7 the theoretical oxidation potential of glucose is -0.42 V and the theoretical reduction potential of oxygen is 0.82 V, which would generate a cell potential of 1.24 V. Other characteristics needed from enzymes for power source applications are high turnover of the substrate (activity), stability and availability. These characteristics must be taken into account when large-scale manufacturing of biobatteries is planned.

2.1.1 Enzyme kinetics

During catalysis, an enzyme substrate (ES) complex is formed by binding the substrate (S) into the active site of the enzyme (E), finally resulting in a reaction product (P). The stability of the ES is related to the affinity of the substrate for the particular enzyme, and is characterized by its dissociation constant, K_s, for the ES complex:

$$\mathrm{E} + \mathrm{S} \underset{k_{-1}}{\overset{k_1}{\rightleftarrows}} \mathrm{ES} \xrightarrow{k_2} \mathrm{E} + \mathrm{P}, \tag{3}$$

$$K_\mathrm{s} = \frac{k_{-1} + k_2}{k_1}, \tag{4}$$

where *k's* are the reaction rate constants for each individual reaction. As $k_2 >> k_{-1}$, the term k_2 is referred to as the catalytic rate constant or turnover number, k_{cat} (typically in the order of 10^3 s^{-1}), and K_s is called the Michaelis-Menten constant, K_m. The overall rate of formation of P is given by the Michaelis-Menten equation:

$$[\mathrm{E}_0] = [\mathrm{E}] + [\mathrm{ES}], \tag{5}$$

$$v_0 = \frac{k_\mathrm{cat}[\mathrm{E}_0][\mathrm{S}]}{[\mathrm{S}] + K_\mathrm{m}} = \frac{V_\mathrm{max}[\mathrm{S}]}{K_\mathrm{m} + [\mathrm{S}]}, \tag{6}$$

where maximum reaction rate, V_{max}, is achieved when all of the available enzymes are bound with the substrate.

2.1.2 Anode enzymes for glucose oxidation

There are two main groups of enzymes that use glucose as their principal substrate: glucose oxidases (GOx) and glucose dehydrogenases (GDH). The category depends on the enzyme's ability to react with external electron acceptors. GOxs are defined as oxidoreductases that can utilize oxygen as the external electron acceptor, whereas GDHs are defined as oxidoreductases that are unable to utilize oxygen as the electron acceptor and instead transfer electrons to various natural and artificial electron acceptors [38].

GOxs are generally very stable and available enzymes, which have their cofactor tightly bound in the protein but show low activity. GDHs on the other hand have high turnover of their substrate, but they may require a soluble cofactor and are typically unstable [38], [39]. Hence, from the point of view of a power source, the two enzyme groups have both advantageous and disadvantageous characteristics. For this reason, both commercial GOx and in-house purified GDH-like enzymes were tested as anode enzymes in EBFC.

Glucose oxidase (EC 1.1.3.4) catalyses specifically the oxidation of *β*-D-glucose to D-glucono-δ-lactone and hydrogen peroxide (H_2O_2), as shown in Equations (7) and (8). The reaction mechanism is based on a concert transfer of a proton from glucose to a basic group on the enzyme and a direct hydride transfer from glucose to the cofactor [40], [41]. The cofactor of GOx is flavin adenine dinucleotide (FAD), which is tightly bound to the protein; hence it is a prosthetic group. FAD works as the initial electron acceptor and is reduced to $FADH_2$, after which it is oxidised back to FAD by the final electron acceptor, molecular oxygen, which is reduced to H_2O_2. The redox potential of free FAD is -0.22 V vs. normal hydrogen electrode (NHE) and the redox reaction of FAD-GOx occurs at around -0.2 V vs. NHE [42]–[45]. The reduction potential of O_2 to H_2O_2 is 0.29 V vs. NHE at pH 7.

$$\mathrm{GOx(FAD)} + \mathrm{glucose} \rightarrow \mathrm{GOx(FADH_2)} + \mathrm{gluconolactone} \tag{7}$$

$$\mathrm{GOx(FADH_2)} + \mathrm{O_2} \rightarrow \mathrm{GOx(FAD)} + \mathrm{H_2O_2} \tag{8}$$

GOx is found in several species of fungi and insects (e.g. honeybee) and functions as an antibacterial substance in nature by killing bacteria with H_2O_2. GOx is often extracted from *Aspergillus niger*, a fungus which causes black mould on certain fruits and vegetables and is commercially available at a reasonable price.

GOx is a homodimer with an average diameter of 8 nm and molecular mass between 150-180 kDa, typically 160 kDa. The isoelectric point (pI) of GOx is around pH 4 (see e.g. Wilson and Turner [39] and references therein). The substrate-binding domain of GOx is characterised by a deep pocket with FAD located on its base [46]; hence the substrate and oxygen must transfer deep into the enzyme in order to become oxidised and reduced, respectively. The crystal structure of GOx is shown in Figure 4.

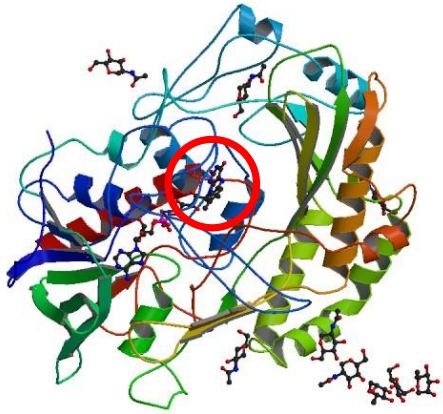

Figure 4. Crystal structure of monomeric GOx enzyme from *Aspergillus niger*. FAD is shown as a ball-and-stick representation inside the protein (circled in red). Protein chains are coloured from the N-terminus (green) to the C-terminus (blue) using a rainbow colour gradient. Image from the RCSB PDB (www.rcsb.org) of PDB ID 1GAL, original data from Hecht et al. [46].

Quinoprotein GDH (EC 1.1.5.2) refers to at least two distinct groups of GDHs harbouring pyrroloquinoline quinone (PQQ) as the redox cofactor: membrane-bound PQQ-GDH (mGDH) and water-soluble PQQ-GDH (sGDH). mGDHs have been reported from a variety of Gram-negative bacteria, and their substrate specificity, stability, and other features are strain-specific [38]. The physiological role of mGDH, coupled with the respiratory chain via ubiquinone, is the terminal oxidation of glucose.

Aldose dehydrogenase (ALDH) from Gram-negative *Gluconobacter oxydans* is a membrane-bound protein which can oxidise aldose sugars, e.g. glucose and xylose [47]. Like mGDH, ALDH has a prosthetic group PQQ which is the initial electron acceptor in the oxidising reaction of glucose, and ubiquinone is the natural electron acceptor as shown in Equations (9) and (10). The electrochemistry of both free PQQ and PQQ-GDHs is still poorly understood, but it is known that the reduction of PQQ takes place in two one-electron steps forming a semi-quinone between the fully oxidised and reduced forms. The reaction mechanism is assumed to proceed by base-catalysed hydride transfer, as in the case of GOx [48]–[50]. Because PQQ is very sensitive to pH and temperature, possessing at least five pK_as [51], the redox potentials for PQQ-GDHs are widely spread between ca. 0.005 and 0.105 V, being typically 0.09 V [52]–[55]. The redox potential of ubiquinone is 0.045 V vs. NHE at pH 7.

$$\mathrm{ALDH(PQQ)} + \mathrm{glucose} \rightarrow \mathrm{ALDH(PQQH_2)} + \mathrm{gluconolactone} \quad (9)$$

$$\mathrm{ALDH(PQQH_2)} + \mathrm{ubiquinone} \rightarrow \mathrm{ALDH(PQQ)} + \mathrm{ubiquinol} \quad (10)$$

The main advantage of using quinoproteins in power source applications is their typical insensitivity to oxygen and hence no H_2O_2 is formed in the reaction. However, O_2 has been reported to act as an electron

acceptor for mGDHs in basic medium, which is probably due to unique properties of the active site of mGDH. At neutral pH and in the presence of a suitable artificial electron acceptor, O_2 is not consumed [56].

mGDHs are partly homologous to other PQQ-dependent enzymes (except sGDH), notably to amino acid residues surrounding PQQ. Hence, the structure of ALDH can be expected to follow the common tertiary structure of PQQ-dependent enzymes [48], [49], [57]. Like other mGDHs, ALDH has a molecular mass of 87 kDa and is a monomeric enzyme [47]. The pI of mGDH from *Gluconobacter suboxydans* is 7.8 [58], and it is probably the same enzyme as ALDH [47]. Hence ALDH is a more basic enzyme than GOx.

2.1.3 Cathode enzymes for oxygen reduction

In a glucose/air EBFC, the reduction of dissolved or atmospheric O_2 to water at the cathode occurs via four proton – four electron transfer (oxygen reduction reaction, ORR). The achievement of a low-overpotential ORR at pH close to neutral is one of the most difficult electrocatalytic reactions in the field of small substrate activation. Whereas most metal catalysts require high overpotentials, multi-copper oxidases, such as laccases and bilirubin oxidases (BOD), have demonstrated low-overpotential ORR at close to neutral pH and for this reason the study of enzymatic cathodes has focused mainly on laccases and BODs (see e.g. [59]–[63]). In this thesis, laccases were selected as the cathode enzyme due to VTT's in-house expertise in their production and characterisation.

Laccases (EC 1.10.3.2) belong to a group of polyphenol oxidases containing four copper atoms in the catalytic centre (Figure 5a). Laccases catalyse ORR to water, accompanied by the oxidation of a substrate, typically p-diphenol or other phenolic compounds, as shown in Equations (11) and (12). As oxygen is usually present in their environment, laccases do not need the addition or synthesis of a low molecular weight cofactor.

$$4\text{p-diphenol} \xrightarrow{\text{Laccase, T1}} 4\text{p-benzoquinone} + 4e^- \tag{11}$$

$$O_2 + 4e^- + 4H^+ \xrightarrow{\text{Laccase, T2/T3}} 2H_2O \tag{12}$$

Laccases have two separate copper sites: a mononuclear site (T1 copper ion) and a trinuclear site that is a cluster of T2, T3, and T3´ copper ions (Figure 5). Reducing substrates are oxidized close to the mononuclear site due to its high redox potential of ca. 790 mV vs. NHE, although the potential of the T1 Cu sites varies between laccases. Electrons are then transferred through a Cys-His pathway into the trinuclear site where O_2 is reduced to water at around 400 mV vs. NHE. Although the copper-binding site arrangement into domains varies remarkably between different laccases, the geometries of the copper sites are very similar [64]. Typically, the molecular weight of fungal laccases is 60-70 kDa and their pI is ca. 4.0 [65].

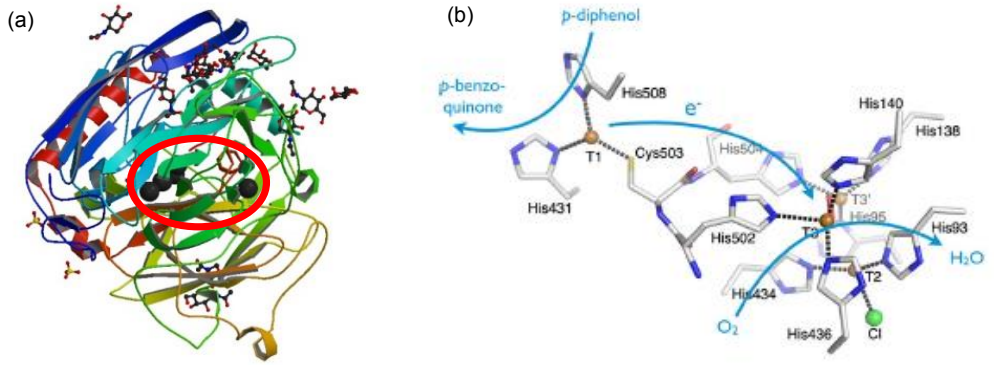

Figure 5. (a) Crystal structure of recombinant laccase from *Melanocarpus albomyces* (rMaL). Protein chains are coloured from the N-terminus (green) to the C-terminus (blue) using a rainbow colour gradient. The Cu-atoms are represented as black spheres, where T1 is closest to the outer layer of the protein and the T2/T3 trinuclear site is located inside the enzyme (circled in red). Image from the RCSB PDB (www.rcsb.org) of PDB ID 2IH8, original data from Hakulinen et al. [66]. (b) Copper sites as observed in MaL and the electron pathway. (Reprinted from [64] with permission.)

Laccases are typically found in plants and fungi (see e.g. [67], [68]). Their natural occurrence is related to e.g. degradation of biopolymers, detoxification and lignin polymerization (see e.g. [65], [69]). Most laccases are extracellular enzymes, which makes their purification procedures relatively easy. In addition, laccases generally exhibit a considerable level of stability in the extracellular environment, probably due to their high extent of glycosylation [70]. Nowadays laccases are widely used in different applications, e.g. in bio-bleaching, biological pulping, wine stabilisation, waste detoxification and decontamination (see e.g. [65], [67], [71] and references therein).

Three different laccases were used in this thesis. Two of them were produced in-house from *Trametes hirsuta* (ThL) and *Melanocarpus albomyces* (MaL, produced as a recombinant enzyme in the fungus *Trichoderma reesei*). ThL is considered to be a high potential laccase (E^0 = 700-800 mV), whereas MaL is a low potential laccase (E^0 ≤ 500 mV). The two enzymes also have different pH optima: pH 3-5 for ThL and pH 4-7 for MaL depending on the substrate [59], [72]. One industrial laccase, Ecostone LCL 45 from AB Enzymes (EcoL), was used in the pilot manufacturing trials (Publications IV-VI).

2.2 Electron transfer from enzyme to the electrode

2.2.1 Direct electron transfer

In direct electron transfer (DET) the enzyme and current collector are in direct contact, and electrons pass from the electrode to the reducing redox centre of the enzyme. DET allows the use of the full thermodynamic potential of the enzyme, without the overpotential of electron transfer from the enzyme to a mediator. In biosystems, electron transfer rates within and between species, as well as between electrodes and species in their proximity, decay exponentially with the distance between the involved centres. Kinetics measurements

have shown that electrons can tunnel about 25 Å through proteins in biologically relevant time scales [73], although the electron transfer rates drop by a factor of ~10^4 when the distance between an electron donor and an acceptor is increased from 8 to 17 Å [74].

PQQ-dependent, heme-containing and FAD-dependent enzymes can undergo DET. For example, DET of PQQ-dependent alcohol dehydrogenase and FAD-dependent GOx has been characterized and their anodic operation demonstrated in BFCs. However, reduced GOx does not directly transfer electrons to conventional electrodes (e.g. Au or glassy carbon), because the distance between its redox centres and the electrode surface exceeds the distance across which electrons are transferred at sufficient rates [75]. In addition, ALDH has been shown to perform DET but with very poor efficiency [76], probably due to the fact that it does not contain a heme group.

DET of laccase is possible if the enzyme is favourably oriented at the surface of the electrode. If laccase is successfully immobilized to the electrode, oxygen reduction bioelectrocatalysis can be achieved at the redox potential of the T1 copper active site, and hence oxygen can be reduced at low overpotentials, especially with high-potential laccases [63], [77], [78]. As an example, VTT's ThL has been shown to achieve DET on glassy carbon electrode by immobilizing laccase into a well-designed dual-layer architecture of PEDOT[1] [79]. The ORR was achieved at 0.75 V vs. NHE at pH 4.5, which is close to the redox potential of the T1 Cu of ThL (0.78 V vs. NHE [59]).

2.2.2 Mediated electron transfer

In mediated electron transfer (MET), a redox-active molecule with reversible electron transfer properties is used to act as an electron shuttle between the electrode surface and the enzyme active site. The redox potential of the mediator must be close to the redox potential of the active site, but also ensure sufficient driving force for optimizing bioelectrocatalytic activity. A study by Gallaway and Calabrese Barton showed that the bimolecular rate constants for the mediator-laccase reaction are highly dependent on mediator potential [80]. If the potential difference between the laccase T1 Cu site and mediator (ΔE_{et}) exceeded 300 mV, no dependence of ΔE_{et} on the bimolecular rate constant was observed. For laccase of *T. versicolor* (formal potential, $E^{0'}$ = 0.82 V), the optimum mediator potential was determined to be 0.66 V vs. NHE. Babanova et al. [52] studied quinone-modified surfaces with PQQ-GDH and indicated the optimal potential difference between the enzyme and mediator to be 148 ± 25 mV.

MET generally offers a higher current density than DET, if the mediator-enzyme system has been optimized. However, MET introduces an additional level of complexity, and electrode performance becomes a matter of mediator stability, as well its effect on the enzyme stability.

MET is compatible with almost all naturally occurring oxidoreductase enzymes and co-enzymes. In the case of glucose oxidation, mediator in its oxidised form is reduced by the anodic enzyme (GOx or ALDH). Next, the mediator transfers to the electrode surface and becomes oxidised again by releasing electrons (Equation (13)). In the case of ORR by laccase, mediator in its reduced form oxidizes by releasing electrons to the enzyme and transfers to the electrode surface to become reduced again (Equation (14)).

$$\mathrm{glucose} + \mathrm{med_{ox}} \xrightarrow{\mathrm{GOx/ALDH}} \mathrm{gluconolactone} + \mathrm{med_{red}} + 2\mathrm{H^+} \quad (13)$$

$$2\mathrm{O_2} + \mathrm{med_{red}} + 4\mathrm{H^+} \xrightarrow{\mathrm{Laccase}} 2\mathrm{H_2O} + \mathrm{med_{ox}} \quad (14)$$

[1] poly(3,4-ethylenedioxythiophene)

2.3 Potential losses in EBFC

Although the theoretical potential of a glucose/air BFC is 1.24 V, this is rarely achieved in practice. This is due to overpotentials present in the cell. The most significant losses are the activation and reaction overpotentials due to slow electron transfer at the solid electrode surface and slow chemical reactions. Typically, enzyme co-factors have relatively high activation overpotentials, and for this reason glucose is oxidised at approximately 200 mV higher potentials than its theoretical potential. In the case of GOx and ALDH, the oxidation potentials of glucose are approximately at -0.2 and 0.1 V vs. NHE, respectively. In the case of laccases, activation overpotentials are significantly lower, because laccases do not have co-factors. As mediators are used to shuttle electrons between electrode surface and enzyme, the activation overpotential is even higher, and thus the cell potential lower. The cell potential generation is illustrated in Figure 6.

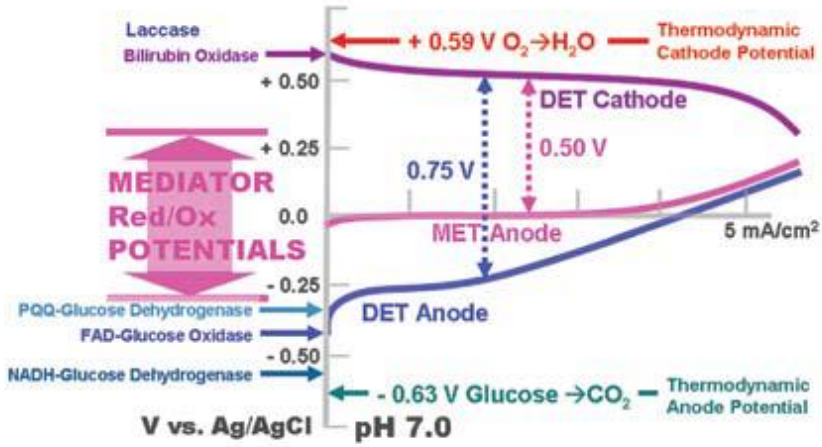

Figure 6. Principle of cell potential generation in an EBFC. The maximum oxidation potentials for glucose and the corresponding thermodynamic potential for ORR (pH 7) are indicated vs. Ag/AgCl reference electrode. Redox potentials of several enzymes and their corresponding co-factors are shown. (Reprinted from [22] with permission from The Electrochemical Society. Copyright 2007, The Electrochemical Society.)

Other losses in the electrode potential come from the ohmic resistance of the cell and the concentration overpotential. The former is attributed to cell design. It includes electrical conductivity of electrodes and current collectors, as well as proton conductivity between and through the electrolyte and the membrane. Concentration overpotential takes place at high current densities, when the transport of fuel and mediator into and out the enzymes, as well as the transport of a mediator from the enzyme to the electrode surface and back is too slow to maintain the reaction rate needed.

2.4 Mass transport in EBFC

Sufficient mass transport in an electrochemical cell is the key for high current densities. Efficient biocatalysis requires that both substrates and products freely diffuse inside and outside the immobilisation support. Enzyme immobilisation into polymers typically increases mass transfer limitations decreasing the reaction rate. Poor mass transfer can also aggravate product inhibition or induce undesirable pH gradients [30] leading to loss in enzymatic activity. High resistance for the mass transfer tends to build a concentration difference between the bulk phase and the sites of reaction, thus slowing down the reactions and leading to polarization of the electrodes. In the case of a mediated system, the mediator mass transport can have even higher impact on the reaction rate than enzyme kinetics [81].

In order to maximise power density, 3D electrodes have been developed. However, 3D electrodes are only valuable if they provide efficient mass transport. The presence of sufficient mass transport enables one to balance the overall effective surface area against porosity. This ensures that the maximum number of catalytic sites are available without suffering the blockage of fuel transport, which will be the case if the pore size is too small [33]. The electrodes should consist of multi-dimensional and multi-directional pores [34]. Multi-dimensionality provides both small pores to support enzyme stabilisation and high loading densities, and larger ones to support mass transport of liquid phase species. Multi-directionality provides higher surface area and permeability to liquid phase fuel transport, but it will eventually decrease structural strength if too extensive. It must be emphasised that the transport of the liquid phase species through a pore structure is only the first step; once the substrate has diffused to the enzyme surface, it must also cross an additional boundary layer that can also retard the mass transfer.

In the absence of assisted fluid flow, the mass transfer involves diffusion and migration [82]. Diffusion is the movement of ions and molecules due to concentration gradients whereas migration is the movement of charged species under the influence of a potential or electric field. Species subject to transport mechanisms in a mediated EBFC are fuels and reaction products; mediators both in oxidised and reduced forms; and buffer-electrolyte. Hence, multiple mass transfer processes both can be identified in a printed EBFC as illustrated in Figure 7.

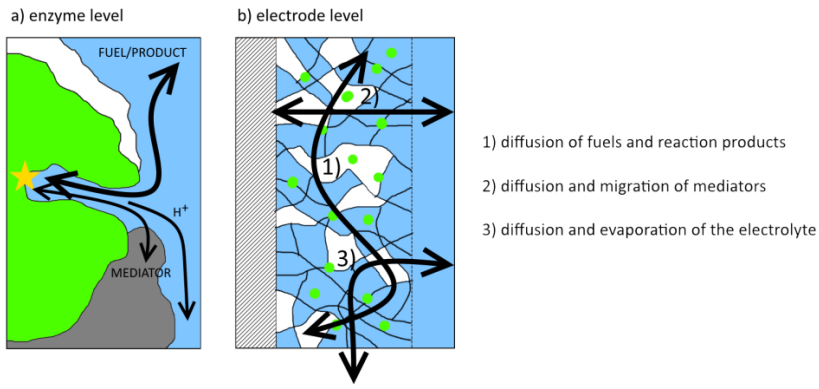

Figure 7. Schematic of different mass transport processes in a printed EBFC anode on a) enzyme level and b) electrode level. Enzymes (green), carbon support (grey, wires) and polymer (white) form the base of the electrode as they are immobilised.

3. Experimental methods

The first enzymatic anodes in this thesis were manufactured on carbon paper by drop-casting (Publication I). Printed enzymatic electrodes were manufactured by formulating inks and printing them on cellulose-based substrates (Publications II-V). Three different printing methods were used: rod-coating, laboratory scale screen printing and pilot scale rotary screen printing. The morphology of the printed electrodes was studied and their enzymatic activity was measured using various analytical techniques suitable for BFCs [83]. Most of the measurements conducted in this thesis were electrochemical measurements, including voltammetry, potentiometry, amperometry and coulometry.

Drop-casted bioanodes were characterized separately in a liquid phase cell (Publication I). Printed EBFCs were assembled using three different configurations. In the first configuration, printed electrodes were sandwiched between planar graphite current collectors (Publications II-V). In the second configuration, an inert reference electrode was inserted between the anode and cathode inside the separator in order to measure the anode and cathode potentials individually (Publications II-IV). In the third configuration, rotary screen printed electrodes were manufactured on PET-coated cardboard. Commercial carbon ink, used as a current collector, was printed first on the PET side of the cardboard and enzymatic inks were printed on top of that. The EBFCs were assembled by sandwiching the electrodes on top of each other, separated by membrane, and compressed between planar end-plates. (Publications IV-V).

3.1 Manufacturing methods

3.1.1 Immobilisation and stabilisation of enzymes

When enzymes are purified and removed from their natural environment, they may need to be immobilised and stabilised into structures that can mimic their optimal surroundings. Different immobilisation techniques utilizing polymers have been very successful for this purpose, including physical entrapment and covalent binding [30], [84]. In Publication I, two different modified polymers were used to encapsulate ALDH. Both polymers are micellar, but their chemical microenvironments are very different [85]. The first polymer was Nafion-based and the second chitosan-based. In Publications II and III, commercial carbon-based ink with a low concentration of volatile organic compounds was used to prepare enzymatic inks. This ink was enhanced with multi-walled carbon nanotubes (MWCNT) in order to increase its electron transfer properties (see Appendix A for more details). In Publications IV-V, in-house produced graphite-based inks were prepared and tested using different concentrations of polymers. Polymers tested were polyethylene oxide (PEO), carboxymethyl cellulose (CMC) and medium molecular weight chitosan.

3.1.2 Preparation of enzymatic inks

Catalytic inks are principally made of solvents, binders, conductive components and active components. In this thesis water, water-soluble polymers, carbon, and enzymes and mediators were used, respectively. Rheology and surface chemistry of the ink are fundamental material characteristics that describe ink flow and wetting of the substrate [86]. The rheological behaviour of screen-printable ink should preferably be thixotropic: the ink is thick when resting and becomes thinner when squeezed and pressed through the screen [87]. The adhesion and surface chemistry can be studied via the strength of attraction between the substrate material and the ink - the higher the substrate's surface free energy relative to the ink's surface

tension, the greater is the attraction. As an example, the typical surface free energy of polymers is ca. 30-40 mN cm^{-1} and the surface tension of water is 72 mN cm^{-1}, rendering water-based inks unsuitable for printing on untreated polymers [88].

Rheology and the surface tension of an ink can be tailored by using different polymers and solvents. Due to the use of enzymes, water was selected as the main solvent of the inks. For this reason, water-soluble polymers had to be used as binders.

In addition to ink characteristics, drying is also a crucial step in R2R manufacturing. Hence, drying of enzymatic inks was studied at different temperatures. Enzymatic activity of the dried electrodes was measured immediately after drying and after 14 and 28 days of storage at room temperature and in a fridge (Publication IV).

Typically, a base ink containing graphite powder and binder polymer (dissolved in water) was prepared. Enzymatic inks were mixed by adding enzyme and mediator into the base ink. Buffer solution was used to adjust the thickness of the ink. Different concentrations of enzyme and mediator were also studied (Publications IV and V).

3.1.3 Printing process of enzymatic electrodes

The aim of this thesis work was to investigate how production of printable enzymatic electrodes can be scaled up from laboratory scale to R2R pilot production. First trials were conducted in the laboratory using rod-coating and a laboratory scale screen printer. The rod-coating technique was used in Publications II and III. Both a laboratory scale screen printer and a pilot scale rotary screen printer were used in Publications IV and V.

Rod-coating was performed using a K Hand Coater (RK Print Coat Instruments Ltd.) with a rod-producing wet layer of 40 µm (Figure 8a). Filter paper (Whatman 1, 180 µm thick) was typically used as the printing substrate. Printed layers were left to dry at room temperature overnight. The electrodes were cut from the substrates for cell assembly (typically 4 cm^2 or 12.25 cm^2).

Laboratory scale screen printing was carried out with a semi-automatic Kent SP-400 screen printer (Figure 8b). The printing screen mesh was NMC EX 31-100 (producing a 70 µm thick wet ink layer), and typically the printing substrate was an insulator paper (Terkab Ilam Delfort Group, 33 µm thick). Enzymatic inks were screen-printed onto an A4-size substrate and dried at room temperature overnight. Each electrode was typically 12.25 cm^2 and the electrodes were cut from the A4-sheet before assembly.

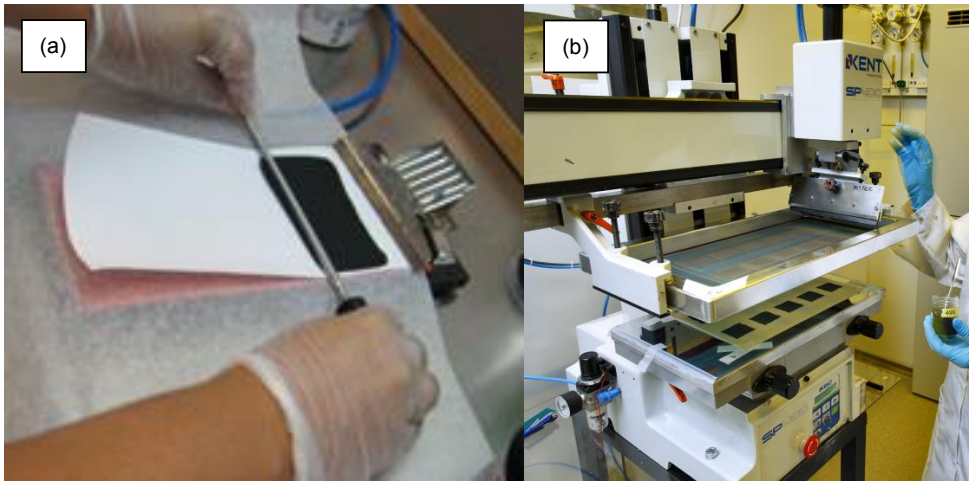

Figure 8. (a) Rod-coating system and (b) Kent SP-400 screen printer used in this thesis work.

Pilot scale rotary screen printing was performed with VTT's modular ROKO printing machine with a printing speed of 2 m min^{-1} (Figure 9a). Gallus BY Mesh 64 (thickness 200 µm, producing a 100 µm thick wet ink layer) printing screens were used for all the inks. A roll of PE-coated cardboard was used as the printing substrate (Figure 9b). Printed layers were dried on the printing line with three 0.9 m long hot air blasting dryers (81 s total drying time). Current collectors (12.25 cm^2) were printed first using a commercial carbon-based ink and dried at 145 °C. Enzymatic electrodes (9 cm^2) were printed on current collectors in a separate printing run. The anode ink was dried at 72 °C and the cathode ink at 65 °C. Layouts of the printing screens can be found in Supplementary Material 1 in Publication IV.

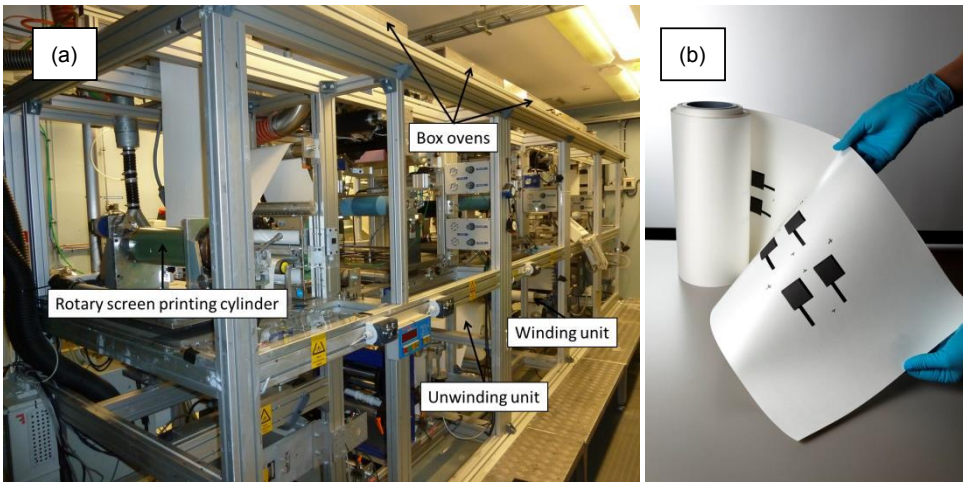

Figure 9. (a) Schematic of VTT's ROKO R2R pilot line and (b) a roll of printed enzymatic electrodes. (Publication IV)

3.2 Morphology of electrodes

Morphology of the electrodes was studied using scanning electron microscopy (SEM) for electrode structure (Publication I), a Dektak stylus profilometer for thickness and a Wyko white light interferometer for roughness (Publications IV and V). Visual determination by means of photography was also used to study adhesion of the printed layer (Publication VI).

3.3 Enzyme activity measurements of printed electrodes

Detection of enzymatic activity of printed electrodes was based on measuring the consumption of dissolved oxygen in the enzymatic reactions, Equations (8) and (14). Dissolved oxygen was measured using a fibre-optic oxygen meter (OXY-10 PreSens). The principle of the meter is based on the quenching of luminescence caused by collision between molecular oxygen and luminescent dye molecules in the excited state [89]. Values for oxygen consumption rate obtained for different electrodes were used for relative comparison, not to determine their absolute quantitative activity. (Publication IV)

3.4 Cell assemblies

3.4.1 Liquid cell

Liquid cell (L-cell) configuration is a modification of the traditional diffusion cell design illustrated in Figure 1a. L-cell (Figure 10) reduces the distance between the cathode and the anode. A platinum gas diffusion electrode is hot-pressed to a Nafion® 112 membrane and clamped between two glass tubes. Thus, the

cathode is in direct contact with air, which eliminates limitations of lack of oxygen. The upper glass tube contains the bioanode and the fuel solution forming a half enzymatic BFC. This cell assembly was used in Publication I, in which immobilised ALDH anodes were characterized.

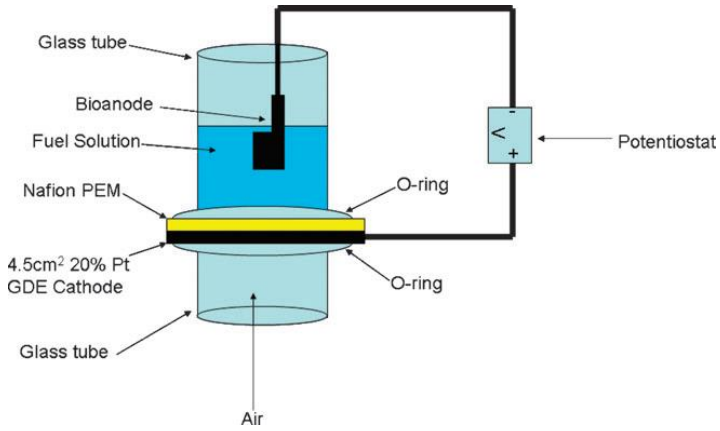

Figure 10. Schematic of the L-cell design used for half enzymatic BFCs with air-breathing platinum cathodes. (Reprinted from [26] with permission.)

3.4.2 Stand-alone cell

Stand-alone cell configuration (Figure 2 in Publication III) was used to characterize EBFCs that were assembled using printed electrodes, both at the anode and cathode. The electrodes (typically 12.25 cm^2) were printed on a cellulose-based substrate and sandwiched between graphite end-plates. The printed sides of the electrodes were facing graphite, and no additional membrane was needed between the electrodes. Glucose (50 mg) was spread on the anode before moisturising the cell. The anode end-plate contained holes through which cells were moisturized by pipetting 400 µl of electrolyte into the cells.

3.4.3 Pd/H_2 reference electrode cell

Individual electrode potentials of the anode and cathode half cells were measured using a thin reference electrode inside the separator-membrane. A palladium-hydrogen (Pd/H_2) electrode was chosen due to its inert characteristics especially in acidic electrolyte. Palladium is known to be an excellent hydrogen absorber, able to absorb 900 times its own volume of hydrogen at room temperature. As solid palladium foil is electrochemically charged by hydrogen, these two phases form a constant potential of approximately +50 mV vs. NHE. This potential is independent of the amount of hydrogen absorbed over a wide range. This makes Pd/H_2 an ideal material for a reference electrode, because in hydrogen saturated form it will not disturb the flow of ions in the fuel cell. This reference electrode was adapted from the study by Fleischmann and Hiddleston [90]. Cells were assembled by sandwiching the anode and cathode layers (typically 6.25 cm^2) between graphite current collectors and placing a hybrid separator-membrane layer between the anode and cathode. A Pd/H_2 reference electrode was placed inside the hybrid layer (Figure 1 in Publication II). The

anode and cathode layers were moisturised by 200 µl of buffer-electrolyte (25 mg glucose in 50 mM Na-succinate pH 5).

3.4.4 Cardboard cell

Pilot-manufactured printed enzymatic electrodes were cut from cardboard rolls as illustrated in Figure 11a. First, the anode was moisturised with the glucose-containing buffer electrolyte and the separator was placed on top of the anode. The cathode was then moisturised with the buffer-electrolyte and electrodes were sandwiched between flat plates to ensure even compression pressure (Publications IV and V). In Publication VI, superabsorbent polymers (SAP) were tested as an anode support. In this case the SAP-powder was spread on the anode before moisturizing it. SAP-powder absorbed the anode electrolyte and swelled before the cell assembly, preventing electrolyte from leaking out of the cell (Figure 11b).

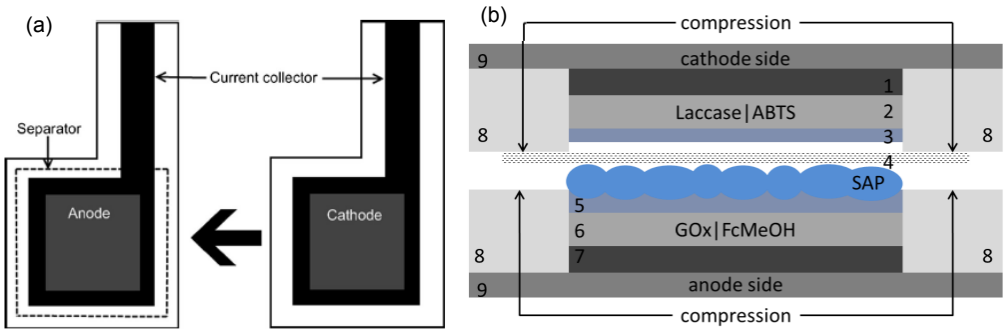

Figure 11. (a) Illustration of the electrode assembly of pilot scale fabricated enzymatic electrodes on cardboard substrate. (Publication IV); (b) Cross-sectional schematic of the cell assembly with SAP on the anode side. The numbers indicate different layers of the cell: 1) printed current collector, 2) printed cathode, 3) cathode electrolyte, 4) membrane, 5) anode electrolyte, 6) printed anode, 7) printed current collector, 8) rubber seal, and 9) printing substrate (cardboard). (Publication VI)

3.5 Electrochemical methods

In order to understand the intermolecular electron transfer between substrates and enzymes, and intramolecular electron transfer between different redox centres within one macromolecule, it is important to measure the redox potentials of enzymes, their co-factors and mediators. The thermodynamic equilibrium potential, *E*, of an electrode reaction is given by the Nernst equation [91]:

$$E = E^{0\prime} + \frac{RT}{nF} ln\left(\frac{c_O}{c_R}\right), \quad (15)$$

where c_O and c_R are the concentrations of the oxidized and reduced species, respectively, and

$E^{0\prime}$ = formal potential
R = gas constant
T = temperature
n = number of electrons
F = Faraday constant.

At equilibrium, the cell potential, E_{cell}, is:

$$E_{cell} = E_c - E_a, \quad (16)$$

where

E_c = potential at the cathode
E_a = potential at the anode.

3.5.1 Voltammetric measurements

Voltammetry is a very common method for characterizing enzyme-containing electrodes. In cyclic voltammetry (CV), the electrode potential is scanned linearly as a function of time and the resulting current is measured. With CV, the redox potential of the enzyme, cofactor or mediator can be determined. Voltammetry can also show the enzyme's ability to catalyse fuel oxidation or oxygen reduction by either DET or MET. In a reversible redox system, the formal potential can be determined from the voltammogram (Figure 12) and Equation (17):

$$E^{0\prime} = \frac{E_a^p + E_c^p}{2}, \quad (17)$$

where

E_a^p = potential of the oxidation peak (anodic)
E_c^p = potential of the reduction peak (cathodic).

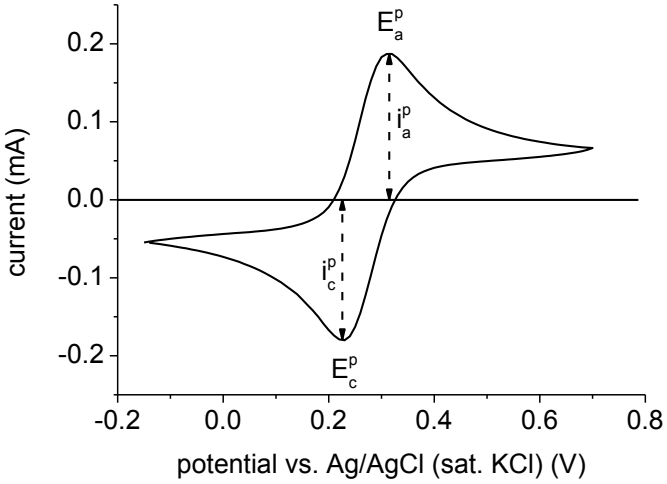

Figure 12. Cyclic voltammogram at 25 mV s^{-1} of an Au-electrode (r = 2.5 mm) in 1 M KCl with 7.5 mM $Fe(CN)_6^{3-}/Fe(CN)_6^{4-}$. The anodic and cathodic peak potentials are indicated as well as the peak currents. The counter electrode was Pt-wire and the reference electrode Ag/AgCl (sat. KCl). (Unpublished)

When scanning the potential at different scan rates, the Randles-Ševčik equation can be used, which at 25 °C reduces to [91]:

$$I^{\mathrm{p}} = 268{,}600\, n^{3/2} A D^{1/2} c v^{1/2}, \qquad (18)$$

where

I^{p} = peak current [A]
A = area of the electrode [cm^2]
D = diffusion coefficient [$cm^2\ s^{-1}$]
c = concentration of the analyte [mol cm^{-3}]
v = scan rate [V s^{-1}].

In practice this means that for a reversible process the peak currents of the redox reactions are linearly dependent on the square root of the scan rate. This theory can be used to study electron transport properties and the active area of different electrode materials (see Appendix A for more details).

3.5.2 Potentiometric measurements

Potentiometry measures the potential between a working electrode and a reference or counter electrode. In the case of enzymatic electrodes, it is an advantage that the enzymes are typically highly selective for a certain analyte, which makes this measurement technique very informative. The potential measured can be

related to the concentration of the analyte of interest. For this reason, potentiometry is one of the most common and simplest evaluation tools to measure the electrochemical potential of a cell at open circuit (OCV). However, this provides information about the thermodynamics but not the kinetics of the cell.

One variant of potentiometry is chronopotentiometry (CP), in which a constant current is applied to the working electrode and the potential of the cell is measured as a function of time. This technique was used to study the operating life of the biobattery (Publications IV-VI). A polarisation curve (iV-curve) can be measured as the current is increased from OCV to a cut-off potential ($E_{\text{cut-off}}$) in steady-state steps. The CP technique was used in Publications II-IV.

3.5.3 Amperometric measurements

Amperometry is a measurement of electric current as a function of time or electrode potential. In chronoamperometry (CA), a constant potential is applied to the cell and the current output of the cell is measured as a function of time. CA measures transient current response under a specific potential until the cell reaches a steady state. Bio-anodes are typically characterised by measuring their calibration curve by CA (Publication I). The potential of the bioanode is maintained constant, ensuring continuous oxidation reaction, and substrate is added to the electrolyte in suitable steps. The current is measured versus substrate concentration, c, and deriving Equation (19) from Equation (6) it is possible to determine maximum biocatalytic current, I_{max}, and Michaelis-Menten constant, K_{m}.

$$I = \frac{I_{\max} c}{K_{\text{m}} + c} \tag{19}$$

The iV-curve can be measured as the potential is reduced from OCV to a $E_{\text{cut-off}}$ in steady-state potential steps. This technique was used in Publications IV-VI.

3.5.4 Coulometric measurements

In coulometry, constant current or potential is applied to the cell in order to convert the analyte from one oxidation state to another. In this thesis, a constant resistor was used to discharge the biobatteries. Since the total charge is measured, this technique can determine the coulombic efficiency and the energy density of a battery. Electrical charge density ($\boldsymbol{Q}$) and electrical energy density ($\boldsymbol{E}$) were calculated from the measurement data according to Equations (20) and (21). This technique was used in Publications I-VI.

$$\boldsymbol{Q} = \int \frac{I}{A}\, dt = \int \frac{E}{AR}\, dt \tag{20}$$

$$\boldsymbol{E} = \int \frac{P}{A}\, dt = \int \frac{EI}{A}\, dt = \int \frac{E^2 R}{A}\, dt \tag{21}$$

4. Research contribution

This chapter presents the measurement results and their contribution to the research topics defined in Chapter 1.2. Main results both from published and unpublished research are presented as well as conclusions for the following research. A short discussion on each topic is also presented.

4.1 Immobilized ALDH Bioanodes (Publication I)

In Publication I, ALDH was immobilized on carbon paper using two different polymers. The first polymer tested was tetrabutylammonium bromide (TBAB)-modified Nafion and the second was butanal-modified chitosan. Both polymers are micellar and can be used to immobilise and stabilise different enzymes on carbon electrodes. ALDH anodes were characterized both in three-electrode and L-cell configuration using TMPD as mediator.

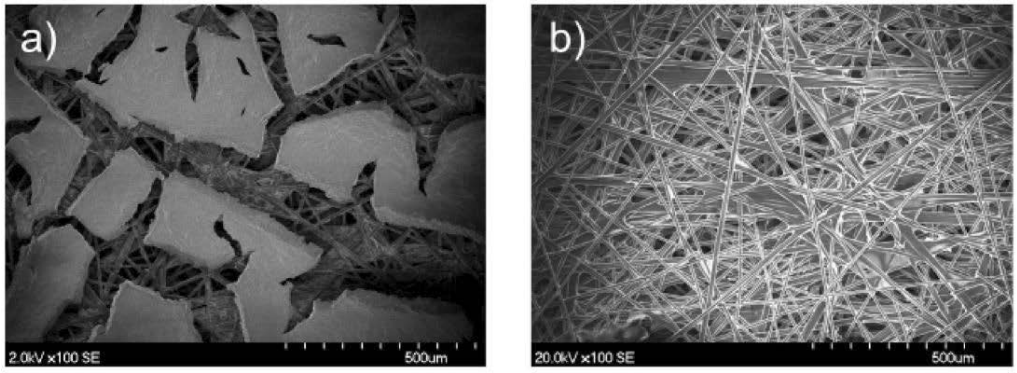

Figure 13. SEM images of (a) TBAB-modified Nafion/ALDH and (b) butanal-modified chitosan/ALDH on Toray paper, 100x magnification. (Publication I)

SEM images (Figure 13) of the electrodes showed that the polymer spread differently on the carbon support: chitosan forms an even layer, whereas Nafion dries forming polymer blocks. The micellar structure of hydrophobically modified chitosan is also larger and less ordered than that of Nafion. These physical properties of enzyme layers were also observed in electrochemical measurements, storage stability and leaching of enzyme. For example, the maximum current density of butanal-modified chitosan bioanodes was fourfold that of TBAB-modified Nafion (Figure 14a), but the storage stability was significantly better with the latter polymer (Figure 14b). The Michaelis-Menten constant (K_m) was the same with both polymers, as was operational stability. Characteristics of the ALDH anodes are presented in Table 1.

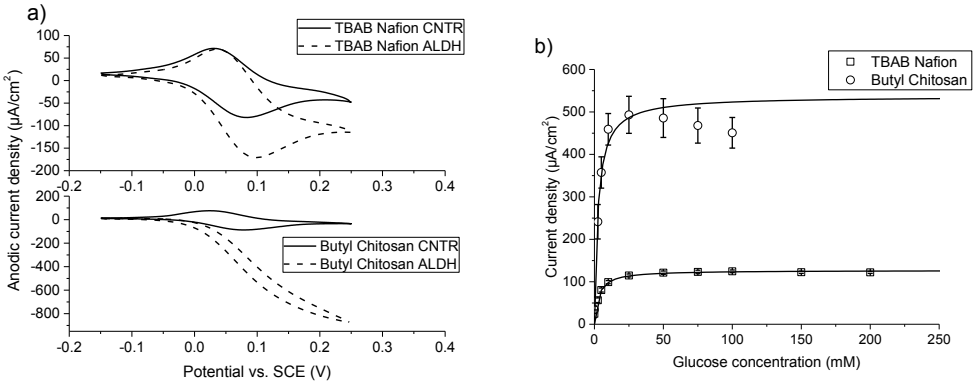

Figure 14. (a) Cyclic voltammogram and (b) calibration curve of immobilized ALDH enzyme on carbon paper. (Publication I)

Table 1. Characteristics of bioanodes and a half enzymatic BFC made of immobilised ALDH.

	Butanal chitosan	TBAB Nafion
K_m	2.6 ± 0.6 mM	2.9 ± 0.6 mM
I_{max}[a]	493 ± 44 µA cm^{-2}	121 ± 4 µA cm^{-2}
I_{max}[b]	220 ± 31 µA cm^{-2}	112 ± 35 µA cm^{-2}
P_{max}[b]	15 ± 1 µW cm^{-2}	10 ± 4 µW cm^{-2}
E_{24h}[b]	102 ± 8 µWh cm^{-2}	75 ± 14 µWh cm^{-2}
Leaching$_{max}$	28%	4%
Stability$_{RT,30d}$	0%	app. 60%
Stability$_{4C,30d}$	app. 25%	app. 70%

[a] From calibration curve, three electrode setup

[b] From L-cell setup, Pt cathode and Nafion 112 membrane

This study showed that ALDH enzyme could be used as an anode enzyme in a fuel cell setup. For this reason, the next study concentrated on testing ALDH in a fully enzymatic fuel cell setup. For mass-manufacturing of enzymatic electrodes, the choice of suitable immobilising polymer had to be considered in terms of performance, price and suitability for screen printing. Due to the biocompatibility and availability of chitosan, it appeared to be a better choice for large scale manufacturing. The only drawback of chitosan was its leaching, because ALDH was stored in buffer, but this was not seen as a problem in the future as the biobatteries were planned to be stored as dry.

4.2 Printed mediated ALDH/ThL EBFCs (Publications II and III)

In Publications II and III, fully printed EBFCs were developed using a rod-coating printing technique. The cells were characterized both in stand-alone and Pd/H_2 reference electrode cell configurations. The former

was used to measure energy density by coulometry and the latter to measure power-curves with CP. The enzyme on the anode was ALDH or GOx and on the cathode ThL or rMaL. Different osmium-based compounds were tested as redox mediators in addition to conventional mediators, i.e. TMPD for anode and ABTS for cathode (Table 2). Overall, the results showed that the best EBFC performance was achieved by using ALDH and ThL as the anode and cathode enzymes, respectively.

Table 2. Redox potential and OCV of individual electrodes using different enzyme-mediator couples. OCV values were measured in a Pd/H_2 cell. They were not published in Publications II and III.

Enzyme	Mediator	Redox potential (mV vs. Ag/AgCl)	$OCV_{electrode}$ (mV vs. NHE)
ThL	ABTS	500, pH 4.5	810 ± 50, pH 5
ThL	$[Os(dcbpy)_2(4\text{-}AMP)Cl]PF_6$	445, pH 4.5	670 ± 50, pH 5
rMaL	ABTS	500, pH 7	700, pH 6.5
ALDH	TMPD	70, pH 7	260 ± 60, pH 5
ALDH	$Os(bpy)_2Cl_2$	0, pH 7	180 ± 20, pH 5
GOx	TMPD	70, pH 7	400, pH 5
GOx	$Os(bpy)_2Cl_2$	0, pH 7	400, pH 5

Unpublished Pd/H_2 cell measurements (Figure 15 and Figure 16) showed that although solution phase studies indicated a redox potential of 700 mV vs. NHE for the ThL/ABTS couple, the OCV of ThL/ABTS cathode was 810 mV in the case of a full EBFC. This potential is higher than would have been expected. Additionally, GOx electrodes showed higher OCV than expected, which can be attributed to the fact that at pH 7 and pH 5 the reduction of O_2 to H_2O_2 occurs at 0.29 V and 0.4 V vs. NHE, respectively. Thus decreasing the anode pH increases the potential in the case of GOx. Other enzyme-mediator couples showed predictable OCV potentials (Table 2). The same behaviour was also seen in the OCV of EBFCs (Table 3): the highest OCV was 620 mV, although solution phase studies predicted only 500 mV.

The reason for higher ThL/ABTS potential in a fuel cell setup should be discussed. Laccase-mediator systems (LMS) have previously been shown to oxidise aromatic alcohols and hydrocarbons even though the oxidation potential was higher than the redox potential of the LMS [92]–[94]. ABTS undergoes two one-electron redox reactions at ca. 680 and 1090 mV vs. NHE at pH 4-5 [92], [93], [95], which correspond to the oxidation/reduction of ABTS/$ABTS^{\cdot+}$ and $ABTS^{\cdot+}$/$ABTS^{2+}$, respectively. The stabilities of these redox states are dependent on solution composition, pH and electrode material. Although high potential laccases have their T1 Cu site redox potential at ca. 790 mV vs. NHE, which is almost 300 mV lower than the oxidation reaction of $ABTS^{\cdot+}$/$ABTS^{2+}$, the oxidation reaction is possible at a very slow rate. By using the Nernst equation (15), and redox potentials of $ABTS^{\cdot+}$/$ABTS^{2+}$ and ThL T1 Cu, it is possible to calculate the equilibrium constant $K = {}^{c_O}/_{c_R} = 5.32 \cdot 10^{-6}$. This reaction is thermodynamically unfavourable but possible if the reac-

tion is driven forward by a follow-up process that irreversibly removes one of the products from the equilibrium of the first reaction [92], [93]. As an example, results reported by Bourbonnais et al. [92] showed that bulk electrolysis of ABTS and veratryl alcohol ($E_{p,a}$ = 1175 mV) at 585 mV (vs. Ag/AgCl) resulted in the formation of veratraldehyde, thus showing that ABTS can be oxidised to $ABTS^{2+}$ at significantly lower potential than expected. In addition, Dong et al. [96] reported that addition of graphene into a laccase-ABTS system increased the removal of labetalol, which was attributed to the formation and release of $ABTS^{2+}$.

Hence, this data suggests that in the case of ThL/ABTS couple incorporated into MWCNT-modified carbon ink, both redox reactions of ABTS can take place. This is possible because ThL is a high potential laccase with a redox potential of the T1 Cu site ca. 780 mV at pH 6.5 and ca. 840 mV at pH 5 (see Appendix B), which is sufficient to slowly oxidize $ABTS^{\cdot+}$ to $ABTS^{2+}$. This was also visually seen as the biofuel cells were opened after use: both blue-green ($ABTS^{\cdot+}$) and purple ($ABTS^{2+}$) colours were noticed. As both cations were present on the cathode side, and being separated with a semipermeable membrane from the anode, an unpredictable high cathode potential was created.

Table 3. OCV, maximum power density and energy density of different cathode-anode pairs. OCV values were not published in Publications II and III.

Cathode	Anode	OCV (mV)	P_{max} (μW cm^{-2})	***E*** as V > 200 mV (μWh cm^{-2})	Duration of the measurement (h)
ThL/ABTS	ALDH/ $Os(bpy)_2Cl_2$	620 ± 10	3.50	11.1 ± 5.5	47
ThL/ABTS	ALDH/TMPD	560 ± 10	1.67	10.7 ± 2.8	74
ThL/ $[Os(dcbpy)_2(4\text{-}AMP)Cl]PF_6$	ALDH/ $Os(bpy)_2Cl_2$	490 ± 10	0.39	16.3 ± 2.2	123
ThL/ $[Os(dcbpy)_2(4\text{-}AMP)Cl]PF_6$	ALDH/TMPD	430 ± 10	0.30	4.4 ± 0.1	58
rMaL/ABTS	ALDH/ $Os(bpy)_2Cl_2$	520	0.50	15	98
rMaL/ABTS	ALDH/TMPD	470	0.39	9	78
ThL/ABTS	GOx/TMPD	370	0.28	0.12	2.0
ThL/ABTS	GOx/ $Os(bpy)_2Cl_2$	360	0.17	0.02	0.8

The maximum power density was measured using CP with addition of 0.2 μA every minute (referred to as fast scan). In order to obtain high power from the cell, both the potential and current density need to be maximized. Therefore, the cells with highest OCV can be predicted to give the best performance provided that the rate of electron transfer between enzyme-mediator and mediator-electrode is sufficient. Fast scan iV-curves (Figure 15 and Figure 16) showed that ThL worked significantly better than rMaL. ThL also per-

formed better with ABTS than [Os(dcbpy)$_2$(4-AMP)Cl]PF$_6$. ALDH/TMPD was unstable at higher current densities than ALDH/Os(bpy)$_2$Cl$_2$ and GOx electrodes were very unstable and did not perform well. The highest power density was achieved with ALDH/Os(bpy)$_2$Cl$_2$ anode and ThL/ABTS cathode.

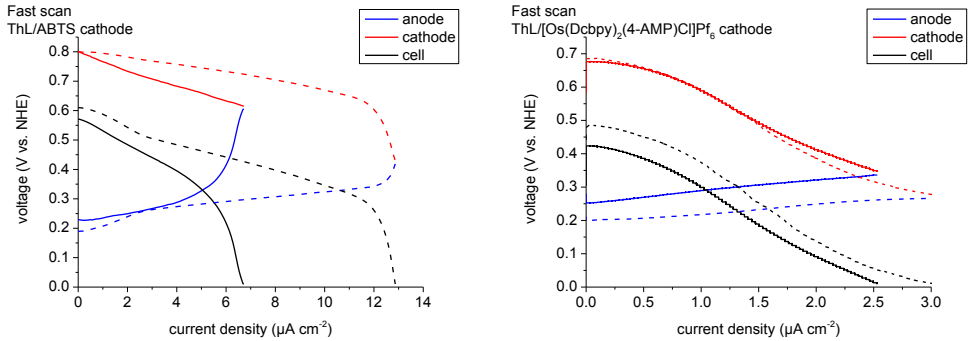

Figure 15. iV-curves of EBFCs with ALDH anode using TMPD (solid) or Os(bpy)$_2$Cl$_2$ (dashed) as mediator. The cathode was ThL/ABTS (left) or ThL/[Os(dcbpy)$_2$(4-AMP)Cl]PF$_6$ (right). Geometrical cell area 6.25 cm^2. Fast scan was measured using CP in 0.2 µA intervals every minute. (Unpublished)

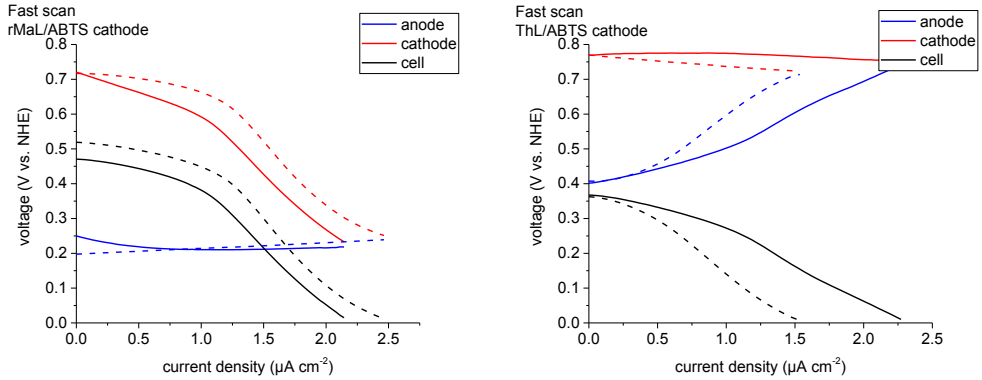

Figure 16. iV-curves (left) of ALDH/rMaL EBFCs with TMPD (solid) or Os(bpy)$_2$Cl$_2$ (dashed) as anode mediators. iV-curves (right) of GOx/ThL EBFCs with TMPD (solid) or Os(bpy)$_2$Cl$_2$ (dashed) as anode mediators. The cathode mediator was ABTS in all cases. (Unpublished)

Surprisingly, stand-alone cell measurements (referred to as slow scans) showed that the ALDH/ThL cell with osmium-mediators both on the anode and cathode was the most stable. The second best slow scan performance was achieved with ALDH-anode and rMaL-cathode. Overall, this data showed that fast scan measures the maximum catalytic performance of different enzyme-mediator pairs, whereas slow scan indicates the long-term stability of enzyme-mediator pairs. For this reason, it is important to pay attention to the

measurement techniques used in order to study the appropriate characteristics, in this case maximum power output vs. maximum energy output.

4.3 Scale-up of manufacturing (Publication IV)

In Publication IV, the manufacturing process of enzymatic electrodes was scaled up from laboratory to pilot scale. The idea was to select materials which were as commercially applicable as possible. For this reason, some materials were chosen based on their availability, price and safety over their performance.

The first task was to modify in-house made inks for screen printing. Due to the use of enzymes, a water-based buffer solution was chosen as the medium of the ink. The selection of the binder was made between CMC and PEO due to their water solubility and safety. Graphite was selected as the conductive component of the ink. Carbon nanotubes were rejected due to their difficult handling properties in large quantities and relatively high price. Due to its availability, price and stability, GOx was preferred as the anode enzyme rather than ALDH. Three different ferrocene-based redox molecules were tested as anode mediators for GOx with regard to their safety. TMPD was rejected due to its poor performance with GOx, as observed in Publications II and III. Ferrocenemethanol (FcMeOH) showed the highest catalytic current at the lowest potential (half wave potential around 250 mV vs. Ag/AgCl). Laccase/ABTS was chosen as the cathode enzyme-mediator pair due to its good functionality and stability, even though ABTS is relatively expensive.

Performance properties of the laboratory scale screen printed electrodes were characterized with CP measurements (Figure 17a). It was clear that PEO functioned better as the binder in GOx/ThL cells. Both enzyme activity (oxygen consumption) of laccase and Pd/H_2 cell measurements showed that the laccase cathode was inactivated when CMC was used as the binder. This was most probably due to the anionic nature of CMC, which acts as a resin, trapping positively charged ThL into the structure and thereby deactivating the enzyme.

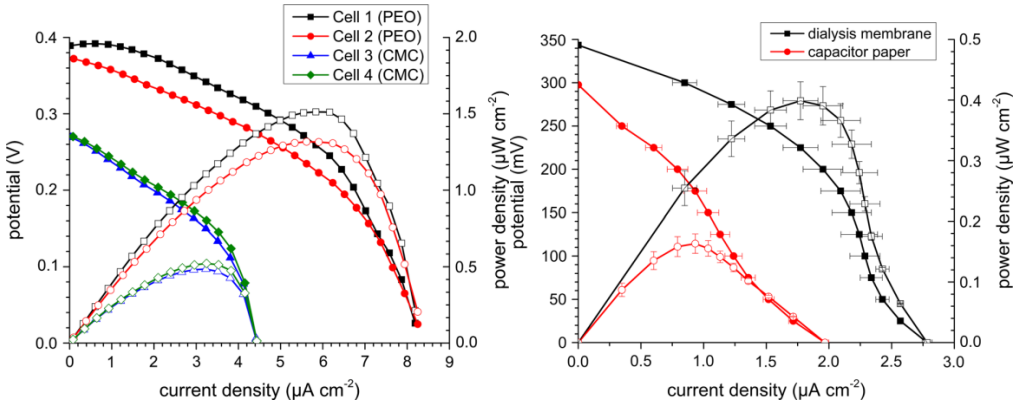

Figure 17. iV and power curves of EBFCs manufactured using a laboratory scale screen printer (left) and a pilot scale rotary screen printer (right). Two different binders and separators were tested for ink preparation and cell assembly. (Publication IV)

Drying experiments (1 min at elevated temperature) with enzymatic inks showed that enzymes alone can withstand relatively high temperatures; even a temperature of 90 °C reduced the enzymatic activity only by 20-30% (Figure 18). After 28 days of storage at room temperature, the residual activity was still 50-60% of the original. However, when the mediators were mixed into the enzymatic inks, the activity of the electrodes decreased dramatically during storage. After 28 days, the activity was only around 20-30% of the initial level. This indicates that mixing mediators with the enzymes in the ink may not be the best strategy in terms of stability.

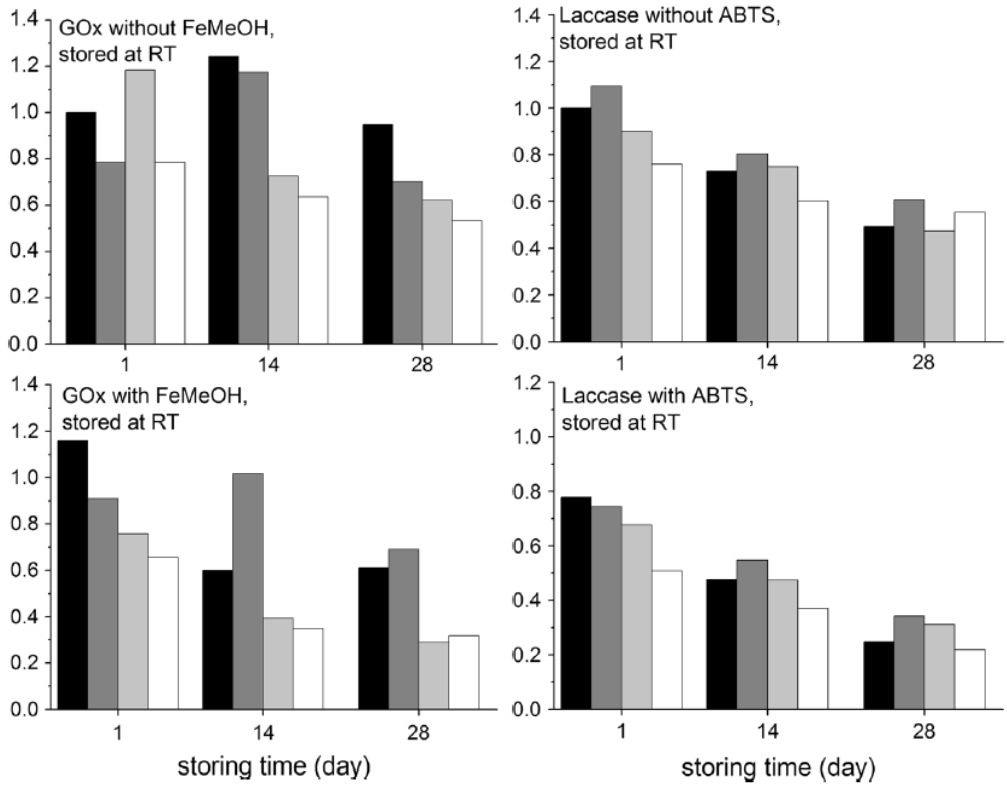

Figure 18. Relative enzyme activity (oxygen consumption) of GOx and EcoL electrodes dried at different temperatures and stored at room temperature. Drying temperatures were 23 °C (black), 50 °C (dark grey), 70 °C (light grey) and 90 °C (white). (Publication IV)

For pilot scale manufacturing, the ink needed to be modified in order to have good print quality in rotary screen printing. Therefore, the base ink contained a higher amount of graphite and a lower amount of binder solution. The base ink was diluted in situ with buffer during the printing trial. The amounts of mediators were also decreased due to their limited availability for large ink batches. First the mediator amount was 40% of

that used in laboratory inks, and in order to compensate for this reduction, a higher amount (2.5-fold) of enzyme was added to the inks. In the pilot printing trial, the inks had to be diluted further with buffer solution in order to adjust the viscosity of the ink. In the end, the composition of the pilot printing inks was drastically different from that of the inks prepared for the laboratory screen printer (Table 4). The amounts of enzyme and mediator per electrode were approximately 190% and 30%, respectively, of those in the laboratory inks. This difference was reflected in the electrochemical performance of the EBFCs assembled using pilot-manufactured electrodes (Figure 17b). The maximum performance (P_{max} and I_{max}) of pilot-manufactured cells was approximately 70% lower than those of the laboratory manufactured cells; the energy output was as much as 90% lower. This can be attributed to the lower amount of mediator as well as to the degradation of enzyme-mediator electrodes due to heating (ca. 70 °C) and storage (ca. one week).

Table 4. Composition of inks used in laboratory screen printing and pilot scale rotary screen printing, and electrochemical performance of EBFCs assembled using these enzymatic electrodes.

	Laboratory scale manufacturing (GOx/ThL)	Pilot scale manufacturing (GOx/EcoL)
Graphite amount in wet ink (wt.%)	37	46
Binder amount in the ink (wt.% $g^{-1}_{graphite}$)	7	3.6
Enzyme amount in the ink (nkat $g^{-1}_{graphite}$)	1000	1544
Mediator amount in the ink (µmol $nkat^{-1}$)	0.06	0.01
OCV (mV)	380 ± 8	345 ± 5
P_{max} (µW cm^{-2})	1.4 ± 0.1	0.4 ± 0.03
I_{max} (µA cm^{-2})	8.35 ± 0.04	2.78 ± 0.04
E as V > 200 mV (µWh cm^{-2})	5.5 ± 0.2	0.6 ± 0.1

4.4 Increasing the performance of the GOx/FcMeOH anode (Publication V)

In Publication V, the long-term stability of the pilot-manufactured electrodes was studied. Based on the laboratory experiments, the anode mediator appeared to be ageing during storage. As a consequence, a new batch of anode ink was developed and the amount of the anode mediator was increased. In addition, in order to increase the physical stability of the enzymatic anode layer, the ink composition was altered by adding more binder (both PEO and chitosan) into the ink. Finding the optimum amount of PEO, chitosan and FcMeOH in the ink was not straightforward, because they all appeared to affect the cell performance. How-

ever, after several laboratory ink experiments the final ink for manufacturing of the second pilot anode contained almost twice the amount of the binder and the mediator. On the other hand, the amount of graphite in the wet ink was 20% lower than in the first pilot ink, which meant a lower amount of enzyme per electrode (Table 5).

Table 5. Composition of the second pilot anode ink. The values in square brackets represent characteristics of the first pilot anode ink.

	2nd Pilot scale manufacturing (GOx/FcMeOH)
Graphite amount in wet ink (wt.%)	37 [46]
Binder amount in the ink (wt% $g^{-1}_{graphite}$)	7.1 [3.6]
Enzyme amount in the ink (nkat $g^{-1}_{graphite}$)	1622 [1544]
Mediator amount in the ink (µmol $nkat^{-1}$)	0.02 [0.01]
OCV (mV)	341 ± 1 [345 ± 5]
P_{max} (µW cm^{-2})	0.59 ± 0.02 [0.4 ± 0.03]
I_{max} (µA cm^{-2})	4.4 ± 0.1 [2.78 ± 0.04]
E as V > 200 mV (µWh cm^{-2})	0.88 ± 0.01 [0.6 ± 0.1]

The second pilot ink enhanced the electrochemical performance of the cells significantly, even though the amount of enzyme per electrode was lower. The improvement was due to the increase in the mediator amount (1.7-fold). However, neither this increase nor adding chitosan into the ink stabilized the anodes - they degraded at same rate as before. On the other hand, physical rigidness did increase, seen as an increased reducibility and an even ink layer.

4.5 SAPs as anode support (Publication VI)

In Publication VI, the operational lifetime of the pilot-manufactured enzymatic biobatteries was extended by adding a super-absorbent polymer (SAP) to the anode side. Addition of SAPs did not significantly increase the maximum power density or the current density. Improved operational stability was most probably due to better contact between anode-membrane-cathode interfaces, which was seen as lowering of IR drops by 14%, and better moisture management in the cell. Images (Figure 1 in Publication VI) also showed that the addition of SAPs prevented delamination of the enzymatic cathode layer from the current collector layer. Water transport through the membrane from the anode to the cathode and moisture retention of the cells were also increased. As an outcome, both electric charge density and energy density were doubled when SAPs were added to the anode (Table 6).

Table 6. Cell characteristics without and with addition of SAP on the anode. Charge and energy density values were calculated using $E_{cut\text{-}off}$ = 200 mV.

	no SAP	SAP 1	SAP 2
OCV (mV)	347 ± 4	367 ± 4	366 ± 3
I_{max} (µA cm^{-2})	4.4 ± 0.1	4.2 ± 0.1	4.0 ± 0.1
P_{max}	0.59 ± 0.01	0.58 ± 0.01	0.63 ± 0.01
Q (µAh cm^{-2})	4.52 ± 0.05	7.1 ± 0.2	9.9 ± 0.4
E (µWh cm^{-2})	1.14 ± 0.02	1.87 ± 0.01	2.63 ± 0.05

4.6 Further improvements of enzymatic inks

4.6.1 Increase of anode performance by increasing GOx/FcMeOH in the ink and changing the substrate to carbon fibre paper

The possibility to increase the performance of EBFC by increasing the amounts of biocatalyst-components in the anode ink and printing them on a porous carbon fibre felt (Kevra, 20 g m^{-2}) was studied. The base ink was DuPont modified with MWCNTs (as in Publications II and III). The original amount of GOx and FcMeOH in the ink used in samples 1-5 was 400 nkat ml$^{-1}_{ink}$ and 0.125 µmol nkat^{-1}, respectively (Table 7). A threefold amount of GOx and FcMeOH was used in samples 6-10. The cathode ink contained 400 nkat ml$^{-1}_{ink}$ and 0.125 µmol nkat^{-1} of ThL and ABTS in the ink, respectively, and it was used in all samples.

The inks were rod-coated on the carbon felt. Electrodes (4 cm^2) were cut from the substrate before assembly. In cells 1-2 and 6-8 one anode print was used. In cells 3-5 and 9-10 three anode prints were used on top of each other. The layers were assembled between graphite current collectors and separated by a dialysis membrane. The cells were activated by adding 200 µl of buffer electrolyte (25 mg glucose in 50 mM Na-succinate pH 4.5).

Electrochemical characterisation was performed with CP. OCV was measured for two hours (Figure 19a), after which constant current was applied to the cell, increasing the current by 0.1 µA every 20 min (Figure 19b). Each measurement was terminated when the cell potential reached 200 mV.

Table 7. Different cells. E1 represents carbon fibre electrodes containing a 1-fold amount of enzyme and mediator, whereas E3 represents electrodes containing a 3-fold amount of enzyme and mediator. Values are means ± standard deviation. (Unpublished)

Cells	Anode	OCV (mV)	***Q*** (µAh cm^{-2})	***E*** (µWh cm^{-2})
1-2	1 x E1	350 ± 30	5 ± 4	1 ± 1
3-5	3 x E1	410 ± 40	29 ± 3	7 ± 1
6-8	1 x E3	380 ± 60	21 ± 5	6 ± 1
9-10	3 x E3	470 ± 10	60 ± 20	19 ± 9

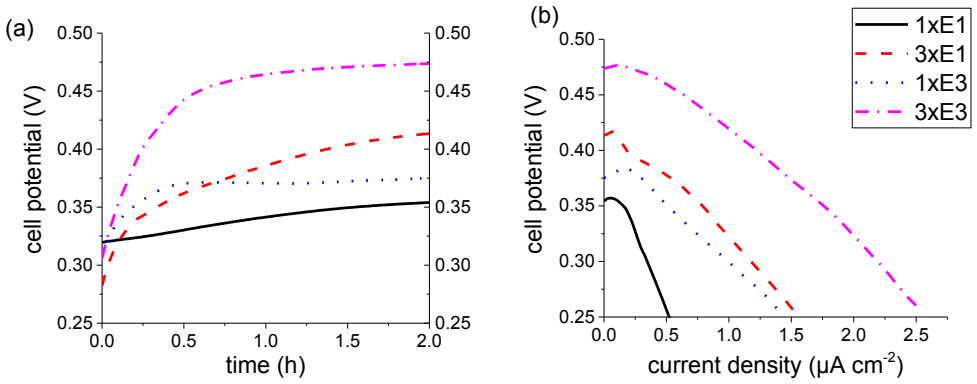

Figure 19. (a) OCV of EBFCs using different amounts of FcMeOH/GOx in the ink and either one or three printed layers on top of each other. (b) CP measurement of the cells. The curves represent average values. (Unpublished)

These preliminary results showed that the GOx-anode could be tailored by adding more catalytic components into the inks and printing them on carbon felt, as well as by stacking electrode materials. The more catalytic components in the ink, the higher were the OCV (most probably due to an increased amount of reduced form of FcMeOH on the electrode surface), charge and energy output. This data suggested that multilayer printing could also be a means to increase the cell performance.

4.6.2 Changing graphite to carbon black in enzymatic inks

The possibility to substitute carbon black (CB, Printex XE2) for graphite in enzymatic inks was studied. Figure 20 shows SEM images of both carbons used; CB is a very fine powder, whereas graphite is coarser.

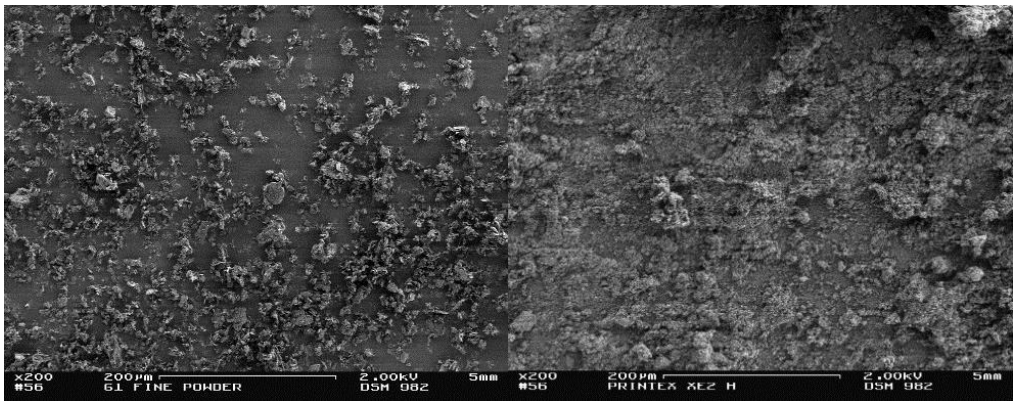

Figure 20. SEM of dry graphite (left) and carbon black (right) powders. Magnification x200. (Unpublished)

Inks without active components were characterised with the ferro/ferricyanide redox couple as described in Appendix A. Both inks contained carbon, PEO (7 wt.% g^{-1}_{carbon}) and buffer (Table 8). The amounts of graphite and CB in the inks were 39 wt.% and 8.7 wt.%, respectively. Cyclic voltammograms showed that the redox peaks of the graphite ink were lower compared with those of the CB ink (Figure 21). In addition, CB ink showed capacitive behaviour as its CV curves were rectangular shaped. This can be attributed to the different surface areas of the carbons: ca. 10-100 m^2 g^{-1} for synthetic graphites and 1000 m^2 g^{-1} for Printex XE2. This indicates that these two carbon powders may exhibit different properties in enzymatic inks.

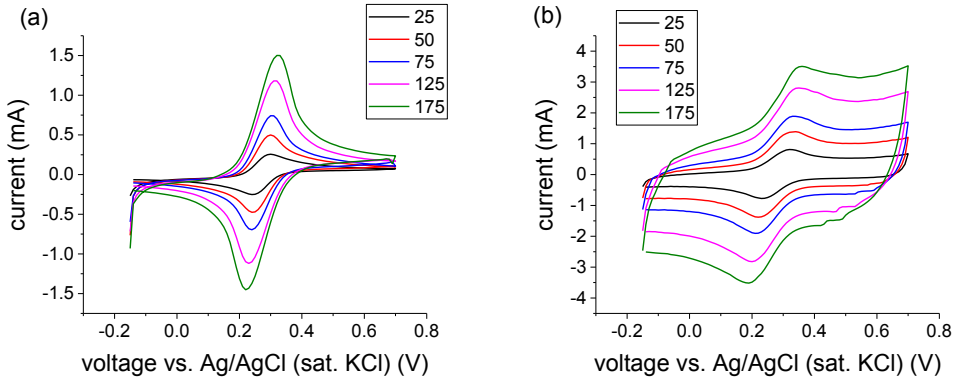

Figure 21. Voltammograms of $F_3Fe(CN)_6/F_4Fe(CN)_6$ on glassy carbon electrodes coated with (a) graphite ink and (b) CB ink. (Unpublished)

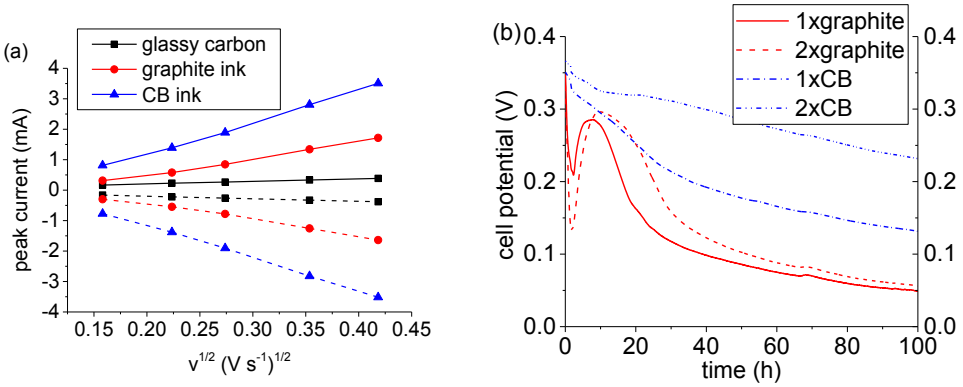

Figure 22. (a) Randles-Ševčik plot of different carbon-based inks on a GC electrode. The electrolyte was 1 M KCl with 7.5 mM of $F_3Fe(CN)_6/F_4Fe(CN)_6$. Pt-wire was used as counter electrode and Ag/AgCl (sat. KCl) as reference electrode. (b) Discharge-curve (constant load of 75 kΩ) of GOx||ThL cells using two different carbon-based inks. The cell area was 12.25 cm^2 and 50 mg of glucose in 400 µl of 50 mM Na-succinate buffer (pH 4.5) was used to moisturise the cells. 1x indicates one layer and 2x two layers of anode ink. (Unpublished)

The Randles-Ševčik plot also showed significantly different slopes (Figure 22a). The increase in the slopes of the Randles-Ševčik plot is attributed to an increased electrode area, *A*, in Equation (18). Slopes for the graphite ink and CB ink were 4.9×10^{-3} and 1.1×10^{-2}, respectively. According to these experiments, the active area of the CB ink is 2.2 times greater than that of the graphite ink. As each electrode contained 4 µl of ink, there was ca. 1.56 mg of graphite and 0.348 mg of CB per electrode. Considering the surface areas of these carbons, a 2.2x increase is reasonable.

When enzymatic inks were prepared from these two carbon materials, different ink compositions were necessary to make them printable (Table 8). The amount of GOx and FcMeOH was the same in both inks, but the dry amount of carbon was significantly different. This had to be taken into account when the cells were compared. In practice, each wet anode (12.25 cm^2) print was weighed and the amount of enzyme per print was calculated according to the weight and ink composition. The printing was done directly on graphite current collectors using a printing screen (mesh NMC EX 31-100). Tests were made of both one-layer and two-layer printing.

Table 8. Compositions of the anode graphite ink and the CB ink. (Unpublished)

	graphite ink	CB ink
carbon	2.5 g (39 wt.%)	0.375 g (8.7 wt.%)
PEO (5 wt.% in H_2O)	3.5 ml	0.525 ml
buffer (50 mM Na-succinate pH 4.5)	0.4 ml	3.4 ml
GOx (1400 nkat)	560 nkat g^{-1}_{carbon}	3730 nkat g^{-1}_{carbon}
FcMeOH (19 mg)	0.06 µmol $nkat^{-1}$	0.06 µmol $nkat^{-1}$

The difference in the active area of the inks can be seen in the discharge curves (Figure 22b), as the CB ink performs significantly better than the graphite ink. In fact, the energy outputs of the cells with similar amounts of GOx/FcMeOH were twofold (Table 9). The OCV was also stable and high when the CB ink was used. This indicates that the type of carbon support, especially its active area, in enzymatic inks plays a very important role. Electrochemical properties of home-made carbon inks provide useful preliminary data for planning of the actual enzyme-containing inks. By using a high surface area carbon support it is possible to create a printed BFC/supercapacitor hybrid that is self-charged.

Table 9. Characteristics of test cells. The rows emphasised in light grey denote comparable cells in terms of active component amount. Values are means ± standard deviation (n = 3). (Unpublished)

Anode layer	OCV at 1.5 h (mV)	Weight of wet anode (g)	Calculated enzyme activity per anode (nkat)	***E*** (µWh cm^{-2})
1xgraphite	220 ± 40 *	0.15 ± 0.01	33	1.10 ± 0.04
2xgraphite	140 ± 70 *	0.31 ± 0.06	77	1.8 ± 0.4
1xCB	340 ± 10	0.24 ± 0.09	78	3.9 ± 0.7
2xCB	362 ± 1	0.35 ± 0.09	114	12 ± 5

* unstable

5. Discussion

5.1 Performance

Several factors contribute to the performance of printed biobatteries. First of all, the selection of enzyme-mediator pairs is crucial. In the case of the cathode, high potential laccase (ThL) is preferred due to its capability to reduce oxygen to water close to the theoretical potential. In order to guarantee sufficient electron transfer into laccase, several mediators were tested, of which ABTS appeared to be the most suitable. ThL was able to oxidise both redox states of ABTS; the highest cathode potential was ca. 800 mV vs. NHE (Publications II and III).

Selection of the anode enzyme-mediator pair was made between GOx and ALDH (Publications II and III). The highest performance was achieved using ALDH with an osmium-mediator. The lowest anode potential was ca. 200 mV vs. NHE. The second-best performance was achieved with TMPD, showing an OCV of ca. 300 mV vs. NHE. However, due to the limited availability of ALDH, GOx was preferred as the enzyme. Neither osmium complexes nor TMPD performed well in printed GOx electrodes. The mediator for GOx was selected from the group of ferrocene derivatives, from which FcMeOH showed the best catalytic current at the lowest potential of ca. 450 mV vs. NHE (Publication IV).

After the enzyme-mediator selection, the next step was to understand how the composition of enzymatic inks affects the cell performance. Components in the simplest inks are carbon powder, a binder, an enzyme, a mediator and solvent (aqueous buffer). The type of carbon powder plays an important role because the redox chemistry of mediators takes place on the powder surface. Therefore, the carbon support should have as high an active area as possible. In order to increase its active area, commercial carbon-based ink was modified with MWCNTs. Changing graphite powder to carbon black in the experimental inks improved the cell performance by doubling the 2D active area of the printed layers.

The type of binder must also be taken into account, because some water-soluble polymers may have ionic characteristics that affect the catalytic performance of enzymes. Comparing PEO and CMC showed that the cathode enzyme was not active when CMC was used, most probably due to the anionic property of CMC (Publication IV), and PEO was consequently selected as the preferred binder. The amount of binder is also an important factor for the cell performance. Too low an amount of binder makes the printed layer very fragile, and good conductivity is lost as well as good adhesion to the printing substrate (Publication IV and VI). On the other hand, too high an amount of binder increases concentration overpotentials, and free movement of mediators to the enzymes can be lost (Publication I).

Determining the optimum amounts of active components in the inks was rather complex, as it appears that the type and amount of carbon and the binder affect the optimum amount of enzyme and mediator. However, there were two findings that had good correlation. First, the amount of the mediator is one of the key factors in maximum performance. This is of course obvious, because the mediator carries the charge between the electrode and the enzyme. However, its amount cannot be arbitrarily increased. Second, the amount of available active enzymes as well as the active electrode area are related to the appropriate mediator amount. For example, with graphite, the maximum amount of FcMeOH in the ink is approximately 14 mg $g^{-1}_{graphite}$ (65 µmol $g^{-1}_{graphite}$). In order to function properly, the anode must have enough active enzyme available. In graphite ink with 7 wt.% of binder, an appropriate amount of GOx was ca. 1000 nkat $g^{-1}_{graphite}$. If the binder amount was only half of that, a twofold amount of GOx was needed. When a carbon support with a large active area was used, the amounts of active components could be increased, which led to an increase in the energy output. The maximum amounts of active components in the CB ink was not studied

in detail; this would be an interesting topic for further studies. The cell performance could also be increased by stacking anodes on top of each other or by multilayer printing.

Integration of biobatteries with electronics can also improve their performance. For example, with a combination of a stack of printed biobatteries and printed super-capacitors, 5 mA pulses (lasting 3 s) every 20 min could be generated (see Appendix C). This could extend the range of applications from μW scale to mW scale.

5.2 Stability

The stability of printed electrodes can be discussed from three points of view: stability during manufacturing, during storage, and during use. The first enzymatic electrodes were manufactured using the very sensitive ALDH enzyme, immobilised with Nafion or chitosan-based polymers. It was found that the Nafion-based polymer resulted in more stable electrodes in terms of storage stability, but most of the enzymatic activity (in this case available enzyme) was lost due to poor spreading onto the carbon paper. The chitosan-based polymer resulted in a more evenly coated surface on the carbon paper and hence in better electrochemical performance. As a consequence, alternatives to Nafion were searched for.

Since the enzyme electrodes are manufactured using water-based inks at room temperature, there is no dramatic decay in their activity. Especially if there is a long delay (> 1 h) between ink preparation and printing, selection of the solvent becomes important. In order to keep the inks stable, suitable binders and buffers should be used. As the electrodes are dried at elevated temperatures, their enzymatic activity typically decreases. The addition of mediators into the inks decreases the enzymatic activity further in the drying step, most probably due to accelerated thermal degradation as predicted by the Arrhenius equation (not shown).

During one month of storage, printed GOx electrodes lost a maximum of 20-30% of their enzymatic activity, whereas laccase lost 40%, regardless of the drying or storage temperature. However, when mediators were added into the inks, elevated drying temperatures accelerated the degradation, and 70-80% of the enzymatic activity was lost in 28 days. Drying at 50 °C was an exception, perhaps due to PEO's characteristics of having a crystalline melting temperature of 65 °C and being possible to crystallise at 50 °C [97]. It seems that especially GOx/FcMeOH anodes dried at 50 °C benefitted from this property, losing only 20-30% of their enzymatic activity in 28 days, regardless of whether they were stored at room temperature or in a fridge. For laccase/ABTS electrodes, storing in a fridge is most beneficial, as the electrodes lost only 40% of their enzymatic activity. Laccase/ABTS electrodes stored at room temperature degraded faster, ca. 60-70% of the activity being lost in 28 days. This may be due to the fact that storage conditions were neither air- nor moisture-free, and the reaction between laccase and ABTS could continue during storage, thus ageing the laccase electrodes.

Pilot-manufactured electrodes were also characterised electrochemically. Degradation of electrodes was also observed in these measurements. The anodes were found to be the limiting factor for cell performance. Especially the anode mediator degraded, but adding fresh mediator into the activation electrolyte restored the anode performance. Thus, not only the stabilisation of enzymes but also that of mediators is important. There are at least three degradation mechanisms of FcMeOH that can be considered: 1) As the anode ink is prepared, FcMeOH can be protonated by succinic acid (dicarboxylic acid) used for stabilisation of enzymes. This reaction leads to elimination the hydroxyl group from FcMeOH forming an α-ferrocenyl carbocation [98], which can further form new species or even denature GOx. 2) Ferrocene can be oxidised to ferrocenium cation which is unstable in the presence of dioxygen and water [99], [100]. This leads to formation of insoluble species. 3) Thermal decomposition of ferrocene due to heating [101].

Operational stability could be increased with suitable cell design, ensuring good electrical and ionic contacts between adjacent surfaces. This was achieved by adding SAP on the anode side, preventing the leakage of electrolyte and delamination of the cathode. In order to have good conductivity in both in-plane and cross-plane directions, the adhesion of printed layers is also very important. This was achieved by tailoring inks with chitosan, a more hydrophobic polymer than PEO.

It is important to study operational stability between enzyme-mediator pairs. The ALDH/TMPD pair appeared to be rather unstable, although the stability of the ThL/ABTS pair was very good on ALDH anodes. This was most probably due to the fact that no H_2O_2 is formed at the anode when ALDH is used. Since GOx is used in aerobic conditions, H_2O_2 is formed which degrades the laccase cathode [102]. FcMeOH can also react with H_2O_2, forming hydroxyl radicals and hydroxide ions via Fenton's chemistry, which again degrades the cells. Removing H_2O_2 from the anode by e.g. adding catalase could most probably stabilise the cells as reported in [103]. However, if dioxygen could be removed from the anode side, it would most probably stabilise both the enzyme and mediator.

5.3 Mass-manufacturing

Printing of enzymatic inks can be accomplished in mass-manufacturing. In order to move from laboratory scale rod- or screen-printing to rotary screen-printing, the enzymatic inks must be tailored to obtain certain characteristics. First of all, the inks must be homogenous and preferably thixotropic in order to maintain good ink flow on the screen. The rheological parameters of the ink can be tailored with solvents and binders. For example, the viscosity of water is ca. 1 cP, whereas for PEO (5 wt.% in H_2O) it is 8800-17600 cP and for medium molecular weight chitosan (1 wt.% in 1% acetic acid) 200-800 cP.

Adhesion between the ink and the printing substrate can be tailored either by selecting a substrate with surface free energy higher than the ink's surface tension (for water 72 mN m^{-1}) or by lowering the ink's surface tension. In this work, either cellulose- or carbon-based substrates were used. Surface tension of the ink was tailored with binders; the surface free energy of e.g. PEO is ca. 43 mN m^{-1}.

Drying of printed layers is a crucial step in R2R manufacturing. If the ink is still moist as the roll is wound after printing, the ink layer is destroyed. However, because delicate active components are used in the inks, over-drying them is also undesirable. Therefore, enzymatic inks need to be studied in terms of their heat tolerance. GOx and laccase appeared to tolerate heating very well.

If large-scale manufacturing of full biobatteries is the aim, at least six important steps must be considered: 1) mixing of the inks on demand; 2) printing and drying of the current collector layers on the substrate; 3) printing and drying of both the anode and cathode layers on the current collectors; 4) printing of an adhesive electrolyte-membrane hybrid on the top of the anodes and laminating the cathode side on it; 5) hot-pressing individual cells; and 6) cutting of individual cells.

The material costs of large-scale manufacturing are strongly dependent on the price of carbon, enzymes, and mediators, whereas paper-based substrates and polymers are available at a reasonable price. For example, the pilot-manufactured cells had an electrode area of 9 cm^2 and the dry matter content of each print was about 8 mg cm^{-2}. If the amount of the anode mediator is increased as suggested in the previous section, each electrode will contain approximately 1 mg of mediator. The enzyme amount should then be ca. 100 nkat. Commercial FcMeOH and ABTS cost around 50-60 € g^{-1} and enzymes 1-3 € kU^{-1}, meaning a total of 0.1-0.2 € per cell. Commercial CB-based inks can cost 1 € g^{-1}_{ink} and typical coverage is 100 cm^2 g^{-1}_{ink}, which adds 0.18 € per cell. Therefore, developing in-house made inks is important because it can lower the overall

costs. These costs apply naturally to small batches only; with larger amounts the costs are expected to be significantly lower.

Considering environmental aspects, each individual chemical should be studied as well as their possible side reactions. In this thesis, some chemicals were rejected due to their toxicity, although they performed well. An example is MWCNTs, because handling them requires very careful safety procedures. The use of osmium-complexes as mediators was successful especially with ALDH, but they were rejected due to their possible high toxicity and poor availability.

5.4 Comparison to other flexible EBFCs

Over the past few years, many research groups have started developing bendable and wearable EBFCs (Table 10). As an example, the highest P_{max} (0.12 mW cm^{-2} at 0.4 V) of single paper-based EBFC was reported with electrodes manufactured using GOx and BOD enzymes [104]. The highest power pulse (1.07 mW cm^{-2} with 4 mA cm^{-2} discharge current) was achieved with an EBFC/supercapacitor hybrid using GDH and BOD enzymes [105]. EBFCs constructed using fabrics have also been reported. The highest P_{max} (0.95 mW cm^{-2} at 0.36 V) was achieved with a fructose dehydrogenase (FDH)/BOD cell [106]. A stack of three cells generated almost threefold higher power density (2.55 mW cm^{-2} at 1.21 V) than a single cell. Jia et al. [107] demonstrated the use of lactate oxidase(LOx)/Pt-black cells on fabrics for powering electronics with human sweat (P_{max} = 0.1 mW cm^{-2} at 0.34 V). Multiple cells were printed on different garments for generating power for e.g. a LED or a digital watch during physical exercise.

Stretchable EBFCs have been developed and characterised on skin as epidermal patches for energy harvesting from sweat and even for wound healing and transdermal drug delivery. As examples, Ogawa et al. [108] demonstrated successful iontophoretic delivery of ascorbyl glucoside (used in anti-ageing treatments) through abdominal human skin using a commercial flow-through diffusion cell containing an enzyme cathode and anode. In another experiment, EBFC patches containing the fluorescent molecule rhodamine B (RB, 479 Da) were used on pigskin. When an iontophoretic current was applied (ca. 50 µA cm^{-2}) using the patch for 1 h, the penetration of RB under the anode was obviously enhanced as compared to the penetration under the cathode. The amount of RB penetration was increased by longer treatment for 6 h, or by applying a higher current (ca. 80 µA cm^{-2}) for 1 h. Tsubota et al. [109] demonstrated the use of an EBFC plaster for wound healing (on mouse skin), showing faster wound healing with the EBFC plaster than with a control plaster.

All the EBFCs mentioned here contain high surface area carbon materials, typically MWCNTs. The highest OCV and P_{max} were reported with mediator-less FDH/BOD EBFC fabricated on MWCNT-modified carbon fabric. The highest power pulse was generated with an EBFC/supercapacitor hybrid fabricated using carbon paper and buckypaper. The reason why the printed EBFCs presented in this thesis do not show such high power densities can be attributed to the lack of high surface area carbon materials and the low amounts of enzymes and mediators on the electrodes. For example, the EBFCs reported in this section contained tens or even hundreds of enzyme units per each electrode. The electrodes manufactured at VTT contain ca. 1-5 U of enzyme per electrode. In addition, the use of mediators brings mass transport limitations as well as challenges with stability compared to mediator-less EBFCs. Using 1000-fold amounts of enzymes, striving for mediator-less systems and utilising high surface area carbon support could lead to a printed glucose/air biobattery/supercapacitor system that can perform steadily on the mW scale.

Table 10. Different bendable and wearable EBFCs.

	Fuel	Anode/Mediator	Cathode	Carbon	OCV	P_{max}
Paper-based EBFCs						
Publications II and III (laboratory manufacturing)	glucose	ALDH/$Os(bpy)_2Cl_2$ (ca. 0.06 U cm^{-2})	ThL/ABTS (ca. 0.06 U cm^{-2})	DuPont ink MWCNT	0.62 V	3.5 µW cm^{-2} (at 0.32 V)
Publication IV (laboratory manufacturing)	glucose	GOx/FcMeOH (ca. 0.3 U cm^{-2})	ThL/ABTS (ca. 0.3 U cm^{-2})	graphite	0.38 V	1.4 µW cm^{-2} (at ca. 0.22 V)
Publications V and VI (pilot manufacturing)	glucose	GOx/FcMeOH (0.7-0.9 U cm^{-2})	EcoL/ABTS (ca. 0.8 U cm^{-2})	graphite	0.37 V	0.63 µW cm^{-2} (at ca. 0.2 V)
Zhang et al. [110]	glucose NAD^+	GDH	BOD	MWCNT[a]	0.56 V	13.5 µW cm^{-2} (at 0.33 V)
Shitanda et al. [104]	glucose	GOx/TTF[b] (400 U cm^{-2})	BOD (20 U cm^{-2})	Ketjenblack	0.55 V	0.12 mW cm^{-2} (at 0.4 V)
Wu et al. [111]	fructose	FDH (0.1 mg)	BOD (0.1 mg)	MWCNT	0.61 V	4.31 µW (at ca. 0.4 V)
Lau et al. [112]	ethanol NAD^+	ADH[c]+AlDH[d]/PMG[e] (100 U cm^{-2} of each enzyme)	BOD (10 U cm^{-2})	MWCNT[f]	0.53 V	35.5 µW cm^{-2} (at ca. 0.4 V)
Lau et al. [112]	methanol formaldehyde formic acid NAD^+	ADH+AlDH+FoDH[g]/PMG (10 U cm^{-2} of each enzyme)	BOD (10 U cm^{-2})	MWCNT[f]	0.55 V	26.9 µW cm^{-2} (at ca. 0.38 V)
Narvaez Villarrubia et al. [105]	glucose	GDH/MG[h] (9.93 mg)	BOD (80 mg)	Buckypaper	0.56 V	1.07 mW cm^{-2} (a pulse of 4 mA cm^{-2})

	Fuel	Anode/Mediator	Cathode	Carbon	OCV	P_{max}
Fabric-based EBFCs						
Haneda et al. [113]	fructose (in agarose film)	FDH (3400 U cm^{-2})	BOD (5 U cm^{-2})	MWCNT Ketjenblack	0.70 V	0.55 mW cm^{-2} (at 0.4 V)
Miyake et al. [106]	fructose	FDH	BOD	MWCNT	0.74 V	0.95 mW cm^{-2} (at 0.36 V)
Miyake et al. [106] (triple cell)	fructose	FDH	BOD	MWCNT	2.09 V	2.55 mW cm^{-2} (at 1.21 V)
Jia et al. [107]	lactate	LOx+BSA[i]/TTF·TCNQ[j]	Pt-black	CNT	0.67 V	100 µW cm^{-2} (at 0.34 V)
Stretchable EBFCs for skin						
Bandodkar et al. [114]	glucose	GOx+BSA/NQ[k]	Pt	MWCNT	ca. 0.4 V	ca. 125 µW cm^{-2} (at ca. 0.28 V)
Jia et al. [115]	lactate	LOx+BSA/TTF (ca. 16 U á electrode)	Pt black	MWCNT	ca. 0.5 V	44 µW cm^{-2} (at ca. 0.29 V)
Ogawa et al. [116]	fructose (in hydrogel film)	FDH	BOD	MWCNT SWCNT	0.74 V	0.25 mW cm-2 (at ca. 0.4 V)
Ogawa et al. [108] (transdermal drug delivery)	fructose (in hydrogel film)	FDH	BOD	MWCNT	0.75 V (on pig-skin)	60 µW cm^{-2} (at ca. 0.3 V on pigskin)
Tsubota et al. [109] (wound healing)	fructose (in gel film)	FDH	BOD	CNT	ca. 0.75 V	(0.4 mA cm^{-2} constant current for 12 h around a wound on a mouse skin)

[a] functionalised with ionic liquid, [b] TTF = tetrathiafulvalene, [c] ADH = alcohol dehydrogenase, [d] AlDH = aldehyde dehydrogenase, [e] PMG = polymethylene green, [f] coated with PMG, [g] FoDH = formate dehydrogenase, [h] MG = methylene green, [i] BSA = bovine serum albumin, [j] TCNQ = 7,7,8,8-tetracyanoquinodimethane, [k] NQ = 1,4-naphthoquinone

5.5 Suggestions for future research and development

Roughly 20 years ago, Palmore and Whitesides [31] suggested that the future work on BFCs should concentrate on the following question: “Is the activity available in biological catalysts sufficient, and in the right form, to provide the basis for a practical fuel cell?” This thesis work has proven that yes, EBFCs can provide sufficient amount of power for practical applications. However, there is still work to be done in the future in order to develop these biobatteries further:

- There is a need to study more the possible degradation processes of the cell. As this thesis work showed, both the enzymes and mediators degrade during the manufacturing, storing and use. The printed layers were also delaminating from the current collectors, which may be due to the degradation of the polymers in the inks. In order to optimise these cells, better understanding on degradation processes between the used chemical species is needed.
- More loss analysis of the system is needed to discover the restricting processes in the cell. Especially in the case of a mediated system, it is important to establish the rate limiting steps in the transfer of electrons from the mediator to the electrode surface and to determine the relevant mass transport and enzyme kinetic rates. Without these values, optimal design of 3D electrode structures cannot be achieved.
- Mass transfer characteristics of the 3D electrodes could be enhanced by patterned printing. Both hydrophobic and hydrophilic channels could be created forming a functional matrix. For an example, air cathodes need channels both for liquid and gas phase species.
- Optimisation of the cell structure should take into account that the anode should be free from oxygen, but at the same time, that is the fuel for the cathode. Drying of these cells is also problematic. For this reason, ways to prevent the electrolyte leakage or evaporation are needed.
- Exploring the possibility to use a multivariable management technique particularly for the mass production of these flexible biobatteries is essential. As some of the depositing techniques used in this thesis may need to be revised and changed, it can bring complexity to the manufacturing process.

6. Summary and conclusions

This thesis studied the possibility of manufacturing printed enzymatic biobatteries in large scale. The performance of laboratory-manufactured cells was compared to pilot-manufactured biobatteries. The selection of suitable enzyme-mediator pairs as well as binders and the carbon support of the enzymatic inks has significant effect on the biobattery performance and stability.

The anode and cathode were chosen to contain GOx/FcMeOH and high potential laccase/ABTS pairs, respectively. Although the ALDH enzyme performed very well on the anode, it was rejected due to its poor availability and stability. The stability in manufacturing, storage and during use should all be considered when an application of biobatteries for consumer products is planned. Immobilisation and stabilisation of both enzymes and mediators must be taken into account in order to maintain good performance.

The activity of enzymes could be maintained at 60-80% even though the enzymatic layers were dried at high temperatures and stored for one month at room temperature. However, when mediators were added into the inks, the degradation of enzymes was faster, and only 20-30% on the enzymatic activity was maintained after storing for one month. Therefore, the stabilisation of mediators should be studied in more detail in the future. The possibility of mediator-less electrodes, especially for the cathode side, seems plausible. This approach would increase the stability of the cell. Another suggestion is to add catalase to the anode side to remove H_2O_2. This could improve the operational stability of the biobatteries.

Applications that could benefit from this kind of batteries are disposable sensors or memory devices that are used for a few days at room temperature. At the moment, these printed biobatteries have demonstrated maximum power densities in the range of 1-3 μW cm^{-2} and maximum energy outputs ($E_{cut\text{-}off}$ = 200 mV) in the range of 10-20 μWh cm^{-2}. A battery the size of a credit card (ca. 50 cm^2) could generate 50-150 μW or 0.5-1 mWh. This level of power suffices for e.g. smart RFID tags or low energy Bluetooth in idle mode (some μAs). However, in active mode they need 10-15 mA current at ca. 2 V for waking up and transmitting data to a master receiver. This would require at least three biobatteries connected in series or a converter to boost the output voltage. In order to improve peak power generation, the integration of biobatteries with supercapacitors is recommended. Other suitable applications of biobatteries could be water leakage detection, cold chain detection (especially for frozen goods), and autonomous biosensors. Furthermore, other applications could also include microcurrent patches for skin and wounds if the power generation of printed biobatteries could be increased from μW scale to mW scale.

Bibliography

[1] M. Hilder, B. Winther-Jensen, and N. B. Clark, “Paper-based, printed zinc–air battery,” *J. Power Sources*, vol. 194, no. 2, pp. 1135–1141, Dec. 2009.

[2] K. T. Braam, S. K. Volkman, and V. Subramanian, “Characterization and optimization of a printed, primary silver-zinc battery,” *J. Power Sources*, vol. 199, pp. 367–372, 2012.

[3] A. M. Gaikwad, D. a. Steingart, T. Nga Ng, D. E. Schwartz, and G. L. Whiting, “A flexible high potential printed battery for powering printed electronics,” *Appl. Phys. Lett.*, vol. 102, no. 23, p. 233302, 2013.

[4] K. Fu, Y. Wang, C. Yan, Y. Yao, Y. Chen, J. Dai, S. Lacey, Y. Wang, J. Wan, T. Li, Z. Wang, Y. Xu, and L. Hu, “Graphene Oxide-Based Electrode Inks for 3D-Printed Lithium-Ion Batteries,” *Adv. Mater.*, vol. 28, no. 13, pp. 2587–2594, 2016.

[5] S. Suren and S. Kheawhom, “Development of a High Energy Density Flexible Zinc-Air Battery,” *J. Electrochem. Soc.*, vol. 163, no. 6, pp. A846–A850, 2016.

[6] A. T. Yahiro, S. M. Lee, and D. O. Kimble, “Enzyme utilizing bio-fuel cell studies,” *Biochim. Biophys. Acta*, vol. 88, pp. 375–383, 1964.

[7] G. T. R. Palmore, H. Bertschy, S. H. Bergens, and G. M. Whitesides, “A methanol/dioxygen biofuel cell that uses NAD+-dependent dehydrogenases as catalysts: application of an electro-enzymatic method to regenerate nicotinamide adenine dinucleotide at low overpotentials,” *J. Electroanal. Chem.*, vol. 443, pp. 155–161, 1998.

[8] P. K. Addo, R. L. Arechederra, and S. D. Minteer, “Evaluating enzyme cascades for methanol/air biofuel cells based on NAD+-dependent enzymes,” *Electroanalysis*, vol. 22, no. 7–8, pp. 807–812, 2010.

[9] R. L. Arechederra and S. D. Minteer, “Complete Oxidation of Glycerol in an Enzymatic Biofuel Cell,” *Fuel Cells*, vol. 9, no. 1, pp. 63–69, 2009.

[10] D. Sokic-Lazic and S. D. Minteer, “Citric acid cycle biomimic on a carbon electrode,” *Biosens. Bioelectron.*, vol. 24, no. 4, pp. 939–944, 2008.

[11] S. Xu and S. D. Minteer, “Enzymatic Biofuel Cell for Oxidation of Glucose to CO2,” *ACS Catal.*, vol. 2, no. 1, pp. 91–94, 2012.

[12] D. P. Hickey, F. Giroud, D. W. Schmidtke, D. T. Glatzhofer, and S. D. Minteer, “Enzyme cascade for catalyzing sucrose oxidation in a biofuel cell,” *ACS Catal.*, vol. 3, no. 12, pp. 2729–2737, 2013.

[13] A. Heller, “Electrical wiring of redox enzymes,” *Acc. Chem. Res.*, vol. 23, no. 5, pp. 128–134, 1990.

[14] T. Chen, S. C. Barton, G. Binyamin, Z. Gao, Y. Zhang, H.-H. Kim, and A. Heller, “A miniature biofuel cell,” *J. Am. Chem. Soc.*, vol. 123, no. 35, pp. 8630–8631, 2001.

[15] N. Mano, F. Mao, and A. Heller, “Characteristics of a Miniature Compartment-less Glucose-O2 Biofuel Cell and Its Operation in a Living Plant,” *J. Am. Chem. Soc.*, vol. 125, no. 21, pp. 6588–6594, 2003.

[16] L. Halámková, J. Halámek, V. Bocharova, A. Szczupak, L. Alfonta, and E. Katz, “Implanted biofuel cell operating in a living snail,” *J. Am. Chem. Soc.*, vol. 134, no. 11, pp. 5040–5043, 2012.

[17] A. Szczupak, J. Halámek, L. Halámková, V. Bocharova, L. Alfonta, and E. Katz, “Living battery – biofuel cells operating in vivo in clams,” *Energy Environ. Sci.*, vol. 5, no. 10, p. 8891, 2012.

[18] M. Southcott, K. MacVittie, J. Halámek, L. Halámková, W. D. Jemison, R. Lobel, and E. Katz, “A pacemaker powered by an implantable biofuel cell operating under conditions mimicking the human

blood circulatory system--battery not included.," *Phys. Chem. Chem. Phys.*, vol. 15, no. 17, pp. 6278–83, 2013.

[19] E. Katz, A. Bückmann, and I. Willner, "Self-powered enzyme-based biosensors," *J. Am. Chem. Soc.*, vol. 123, pp. 10752–10753, 2001.

[20] K. MacVittie and E. Katz, "Self-powered electrochemical memristor based on a biofuel cell--towards memristors integrated with biocomputing systems.," *Chem. Commun. (Camb).*, vol. 50, no. 37, pp. 4816–9, 2014.

[21] Y. Wang, L. Ge, P. Wang, M. Yan, J. Yu, and S. Ge, "A three-dimensional origami-based immuno-biofuel cell for self-powered, low-cost, and sensitive point-of-care testing," *Chem. Commun.*, vol. 50, no. 16, p. 1947, 2014.

[22] P. Atanassov, C. Apblett, S. Banta, S. Brozik, S. Calabrese Barton, M. Cooney, B. Y. Liaw, S. Mukerjee, and S. D. Minteer, "Enzymatic biofuel cells," *Electrochem. Soc. Interface*, vol. 16, pp. 28–31, 2007.

[23] A. Heller, "Miniature biofuel cells," *Phys. Chem. Chem. Phys.*, vol. 6, no. 2, p. 209, 2004.

[24] M. Rasmussen, S. Abdellaoui, and S. D. Minteer, "Enzymatic biofuel cells: 30 years of critical advancements," *Biosens. Bioelectron.*, vol. 76, pp. 91–102, 2016.

[25] A. J. Bandodkar and J. Wang, "Wearable Biofuel Cells: A Review," *Electroanalysis*, vol. 28, no. 6, pp. 1188–1200, 2016.

[26] M. J. Moehlenbrock and S. D. Minteer, "Extended lifetime biofuel cells," *Chem. Soc. Rev.*, vol. 37, no. 6, pp. 1188–1196, 2008.

[27] A. Illanes, "Stability of biocatalysts," *Electron. J. Biotechnol.*, vol. 2, no. 1, pp. 7–15, 1999.

[28] U. T. Bornscheuer, "Immobilizing enzymes: How to create more suitable biocatalysts," *Angew. Chemie - Int. Ed.*, vol. 42, no. 29, pp. 3336–3337, 2003.

[29] K. M. Polizzi, A. S. Bommarius, J. M. Broering, and J. F. Chaparro-Riggers, "Stability of biocatalysts.," *Curr. Opin. Chem. Biol.*, vol. 11, no. 2, pp. 220–5, Apr. 2007.

[30] U. Hanefeld, L. Gardossi, and E. Magner, "Understanding enzyme immobilisation," *Chem Soc Rev*, vol. 38, no. 2, pp. 453–468, 2009.

[31] G. T. R. Palmore and G. M. Whitesides, "Microbial and Enzymatic Biofuel Cells," in *Enzymatic Conversion of Biomass for Fuels Production*, M. E. Himmel, J. O. Baker, and R. P. Overend, Eds. American Chemical Society, 1994, pp. 271–290.

[32] S. Calabrese Barton, J. Gallaway, and P. Atanassov, "Enzymatic Biofuel Cells for Implantable and Microscale Devices," *Chem. Rev.*, vol. 104, no. 10, pp. 4867–4886, Oct. 2004.

[33] M. J. Cooney, V. Svoboda, C. Lau, G. Martin, and S. D. Minteer, "Enzyme catalysed biofuel cells," *Energy Environ. Sci.*, vol. 1, no. 3, pp. 320–337, 2008.

[34] S. D. Minteer, B. Y. Liaw, and M. J. Cooney, "Enzyme-based biofuel cells.," *Curr. Opin. Biotechnol.*, vol. 18, no. 3, pp. 228–34, Jun. 2007.

[35] G. M. Cooper, *The Cell: A Molecular Approach*, 2nd ed. Sunderland (MA): Sinauer Associates Inc., 2000.

[36] O. H. Hashim and N. A. Adnan, "Coenzyme, cofactor and prosthetic group — Ambiguous biochemical jargon," *Biochem. Educ.*, vol. 22, no. 2, pp. 93–94, 1994.

[37] C. O. Fagain, "Understanding and increasing protein stability," *Biochim. Biophys. Acta - Protein Struct. Mol. Enzymol.*, vol. 1252, no. 1, pp. 1–14, 1995.

[38] S. Ferri, K. Kojima, and K. Sode, “Review of glucose oxidases and glucose dehydrogenases: a bird’s eye view of glucose sensing enzymes.,” *J. Diabetes Sci. Technol.*, vol. 5, no. 5, pp. 1068–76, 2011.

[39] R. Wilson and A. Turner, “Glucose oxidase: an ideal enzyme,” *Biosens. Bioelectron.*, vol. 7, pp. 165–185, 1992.

[40] V. Leskovac, S. Trivić, G. Wohlfahrt, J. Kandrač, and D. Peričin, “Glucose oxidase from Aspergillus niger: The mechanism of action with molecular oxygen, quinones, and one-electron acceptors,” *Int. J. Biochem. Cell Biol.*, vol. 37, no. 4, pp. 731–750, 2005.

[41] M. Meyer, G. Wohlfahrt, J. Knäblein, and D. Schomburg, “Aspects of the mechanism of catalysis of glucose oxidase: a docking, molecular mechanics and quantum chemical study.,” *J. Comput. Aided. Mol. Des.*, vol. 12, no. 5, pp. 425–40, Sep. 1998.

[42] X. Zhang, D. Liu, L. Li, and T. You, “Direct Electrochemistry of Glucose Oxidase on Novel Free-Standing Nitrogen-Doped Carbon Nanospheres@Carbon Nanofibers Composite Film,” *Sci. Rep.*, vol. 5, p. 9885, 2015.

[43] X. Wu, F. Zhao, J. R. Varcoe, A. E. Thumser, C. Avignone-Rossa, and R. C. T. Slade, “Direct electron transfer of glucose oxidase immobilized in an ionic liquid reconstituted cellulose-carbon nanotube matrix.,” *Bioelectrochemistry*, vol. 77, no. 1, pp. 64–8, Nov. 2009.

[44] M. Zhao, Y. Gao, J. Sun, and F. Gao, “Mediatorless Glucose Biosensor and Direct Electron Transfer Type Glucose/Air Biofuel Cell Enabled with Carbon Nanodots,” *Anal. Chem.*, vol. 87, pp. 2615–2622, 2015.

[45] D. Ivnitski, K. Artyushkova, R. a. Rincón, P. Atanassov, H. R. Luckarift, and G. R. Johnson, “Entrapment of enzymes and carbon nanotubes in biologically synthesized silica: Glucose oxidase-catalyzed direct electron transfer,” *Small*, vol. 4, no. 3, pp. 357–364, 2008.

[46] H. J. Hecht, H. M. Kalisz, J. Hendle, R. D. Schmid, and D. Schomburg, “Crystal structure of glucose oxidase from Aspergillus niger refined at 2.3 Å resolution.,” *J. Mol. Biol.*, vol. 229, no. 1, pp. 153–172, 1993.

[47] J. Buchert, “A xylose-oxidizing membrane-bound aldose dehydrogenase of Gluconobacter oxydans ATCC 621,” *J. Biotechnol.*, vol. 18, pp. 103–113, 1991.

[48] A. Oubrie, H. J. Rozeboom, K. H. Kalk, A. J. Olsthoorn, J. A. Duine, and B. W. Dijkstra, “Structure and mechanism of soluble quinoprotein glucose dehydrogenase.,” *EMBO J.*, vol. 18, no. 19, pp. 5187–94, Oct. 1999.

[49] M. Yamada, K. Matsushita, C. T. Migita, and O. Adachi, “Escherichia coli PQQ-containing quinoprotein glucose dehydrogenase: its structure comparison with other quinoproteins,” *Biochim. Biophys. Acta*, vol. 1647, pp. 185–192, 2003.

[50] C. Anthony, “Pyrroloquinoline quinone (PQQ) and quinoprotein enzymes.,” *Antioxid. Redox Signal.*, vol. 3, no. 5, pp. 757–74, Oct. 2001.

[51] Y. Ohshiro and S. Itoh, “The Chemistry of PQQ and Related Compounds,” in *Principles and Applications of Quinoproteins*, V. L. Davidson, Ed. New York: Marcel Dekker, Inc., 1993, pp. 309–329.

[52] S. Babanova, I. Matanovic, and P. Atanassov, “Quinone-Modified Surfaces for Enhanced Enzyme-Electrode Interactions in Pyrroloquinoline-Quinone-Dependent Glucose Dehydrogenase Anodes,” *ChemElectroChem*, vol. 1, no. 11, pp. 2017–2028, 2014.

[53] D. Ivnitski, P. Atanassov, and C. Apblett, “Direct bioelectrocatalysis of PQQ-dependent glucose dehydrogenase,” *Electroanalysis*, vol. 19, no. 15, pp. 1562–1568, 2007.

[54] V. Flexer and N. Mano, “Wired pyrroloquinoline quinone soluble glucose dehydrogenase enzyme

electrodes operating at unprecedented low redox potential.," *Anal. Chem.*, vol. 86, no. 5, pp. 2465–73, 2014.

[55] V. Flexer, F. Durand, S. Tsujimura, and N. Mano, "Efficient direct electron transfer of PQQ-glucose dehydrogenase on carbon cryogel electrodes at neutral pH.," *Anal. Chem.*, vol. 83, no. 14, pp. 5721–7, Jul. 2011.

[56] A. R. Dewanti and J. A. Duine, "Reconstitution of Membrane-Integrated Quinoprotein Glucose Dehydrogenase Apoenzyme with PQQ and the Holoenzyme's Mechanism of Action," *Biochemistry*, vol. 37, no. 19, pp. 6810–6818, 1998.

[57] A. Oubrie, H. J. Rozeboom, K. H. Kalk, J. A. Duine, and B. W. Dijkstra, "The 1.7 A crystal structure of the apo form of the soluble quinoprotein glucose dehydrogenase from Acinetobacter calcoaceticus reveals a novel internal conserved sequence repeat.," *J. Mol. Biol.*, vol. 289, no. 2, pp. 319–333, 1999.

[58] M. Ameyama and E. Shinagawa, "D-Glucose dehydrogenase of Gluconobacter suboxydans: solubilization, purification and characterization," *Agric. Biol. Chem. Biol. Chem.*, vol. 45, no. 4, pp. 851–861, 1981.

[59] M. Frasconi, H. Boer, A. Koivula, and F. Mazzei, "Electrochemical evaluation of electron transfer kinetics of high and low redox potential laccases on gold electrode surface," *Electrochim. Acta*, vol. 56, no. 2, pp. 817–827, Dec. 2010.

[60] A. Christenson, S. Shleev, N. Mano, A. Heller, and L. Gorton, "Redox potentials of the blue copper sites of bilirubin oxidases," *Biochim. Biophys. Acta - Bioenerg.*, vol. 1757, no. 12, pp. 1634–1641, 2006.

[61] E. I. Solomon, U. M. Sundaram, and T. E. Machonkin, "Multicopper oxidases and oxygenases," *Chem. Rev.*, vol. 96, no. 7, pp. 2563–2605, 1996.

[62] E. I. Solomon, P. Chen, M. Metz, S.-K. Lee, and A. E. Palmer, "Oxygen Binding, Activation, and Reduction to Water by Copper Proteins.," *Angew. Chem. Int. Ed. Engl.*, vol. 40, no. 24, pp. 4570–4590, Dec. 2001.

[63] S. Shleev, A. Jarosz-Wilkolazka, A. Khalunina, O. Morozova, A. Yaropolov, T. Ruzgas, and L. Gorton, "Direct electron transfer reactions of laccases from different origins on carbon electrodes.," *Bioelectrochemistry*, vol. 67, no. 1, pp. 115–24, Sep. 2005.

[64] N. Hakulinen and J. Rouvinen, "Three-dimensional structures of laccases," *Cell. Mol. Life Sci.*, vol. 72, no. 5, pp. 857–868, 2015.

[65] P. Baldrian, "Fungal laccases - occurrence and properties.," *FEMS Microbiol. Rev.*, vol. 30, no. 2, pp. 215–42, Mar. 2006.

[66] N. Hakulinen, K. Kruus, A. Koivula, and J. Rouvinen, "A crystallographic and spectroscopic study on the effect of X-ray radiation on the crystal structure of Melanocarpus albomyces laccase," *Biochem. Biophys. Res. Commun.*, vol. 350, pp. 929–934, 2006.

[67] V. Madhavi and S. S. Lele, "Laccase: properties and applications," *BioResources*, vol. 4, no. 4, pp. 1694–1717, 2009.

[68] A. M. Mayer and R. C. Staples, "Laccase: New functions for an old enzyme," *Phytochemistry*, vol. 60, no. 6, pp. 551–565, 2002.

[69] S. Riva, "Laccases: blue enzymes for green chemistry," *Trends Biotechnol.*, vol. 24, no. 5, pp. 219–226, 2006.

[70] H. Claus, "Laccases: Structure, reactions, distribution," *Micron*, vol. 35, no. 1–2, pp. 93–96, 2004.

[71] U. N. Dwivedi, P. Singh, V. P. Pandey, and A. Kumar, "Structure-function relationship among

bacterial, fungal and plant laccases," *J. Mol. Catal. B Enzym.*, vol. 68, no. 2, pp. 117–128, 2011.

[72] M. Frasconi, G. Favero, H. Boer, A. Koivula, and F. Mazzei, "Kinetic and biochemical properties of high and low redox potential laccases from fungal and plant origin.," *Biochim. Biophys. Acta*, vol. 1804, no. 4, pp. 899–908, Apr. 2010.

[73] J. R. Winkler and H. B. Gray, "Long-Range Electron Tunneling," *J. Am. Chem. Soc.*, vol. 136, no. 8, pp. 2930–2939, 2014.

[74] S. Mayo, W. Ellis, R. Crutchley, and H. Gray, "Long-range electron transfer in heme proteins," *Science (80-.).*, vol. 233, no. 4767, pp. 948–952, 1986.

[75] Y. Degani and a Heller, "Direct Electrical Communication between Chemically Modified Enzymes and Metal Electrodes," *J. Phys. Chem.*, vol. 91, no. 6, pp. 1287–9, 1987.

[76] M. Smolander, G. Marko-Varga, and L. Gorton, "Aldose dehydrogenase-modified carbon paste electrodes as amperometric aldose sensors," *Anal. Chim. Acta*, vol. 302, pp. 233–240, 1995.

[77] A. Le Goff, M. Holzinger, and S. Cosnier, "Recent progress in oxygen-reducing laccase biocathodes for enzymatic biofuel cells," *Cell. Mol. Life Sci.*, vol. 72, no. 5, pp. 941–952, 2015.

[78] S. Shleev, J. Tkac, A. Christenson, T. Ruzgas, A. I. Yaropolov, J. W. Whittaker, and L. Gorton, "Direct electron transfer between copper-containing proteins and electrodes," *Biosens. Bioelectron.*, vol. 20, no. 12, pp. 2517–2554, 2005.

[79] X. Wang, R. Latonen, P. Sjöberg-Eerola, J.-E. Eriksson, J. Bobacka, H. Boer, and M. Bergelin, "Direct electron transfer of Trametes hirsuta laccase in a dual-layer architecture of poly (3, 4-ethylenedioxythiophene) films," *J. Phys. Chem. C*, vol. 115, pp. 5919–5929, 2011.

[80] J. W. Gallaway and S. A. C. Barton, "Kinetics of redox polymer-mediated enzyme electrodes," *J. Am. Chem. Soc.*, vol. 130, no. 26, pp. 8527–8536, 2008.

[81] C. Bourdillon, C. Demaille, J. Moiroux, and J. Savéant, "Catalysis and mass transport in spatially ordered enzyme assemblies on electrodes," *J. Am. Chem. Soc.*, vol. 117, pp. 11499–11506, 1995.

[82] N. Perez, "Mass Transport by Diffusion and Migration," in *Electrochemistry and Corrosion Science*, Springer International Publishing Switzerland, 2016, pp. 151–197.

[83] M. J. Moehlenbrock, R. L. Arechederra, K. H. Sjöholm, and S. D. Minteer, "Analytical techniques for characterizing enzymatic biofuel cells," *Anal. Chem.*, vol. 81, no. 23, pp. 9538–9545, 2009.

[84] A. Dwevedi, "Basics of Enzyme Immobilization," in *Enzyme Immobilization*, Springer International Publishing Switzerland, 2016, pp. 21–45.

[85] T. Klotzbach, M. Watt, Y. Ansari, and S. D. Minteer, "Effects of hydrophobic modification of chitosan and Nafion on transport properties , ion-exchange capacities , and enzyme immobilization," *J. Memb. Sci.*, vol. 282, pp. 276–283, 2006.

[86] J. B. Rosenholm, "Wetting of Surfaces and Interfaces: a Conceptual Equilibrium Thermodynamic Approach," in *Colloid Stability: The Role of Surface Forces, Part II*, vol. 2, T. F. Tadros, Ed. Weinheim: WILEY-VCH Verlag GmbH & Co. KGaA, 2007, pp. 1–83.

[87] K. Gilleo, "Rheology and Surface Chemistry for Screen Printing," *Screenprinting*, no. February, pp. 128–132, 1989.

[88] A. Falsafi, S. Mangibudi, and M. J. Owen, "Surface and Interfacial Properties," in *Physical Properties of Polymers Handbook*, 2nd ed., J. E. Mark, Ed. Springer Science & Business Media, 2007.

[89] H. Kautsky, "Quenching of luminescence by oxygen," *Trans. Faraday Soc.*, vol. 35, pp. 216–219, 1939.

[90] M. Fleischmann and J. N. Hiddleston, "A palladium-hydrogen probe electrode for use as a

microreference electrode," *J. Phys. E.*, vol. 1, no. 2, pp. 667–668, 1968.

[91] A. J. Bard and L. R. Faulkner, *Electrochemical Methods: Fundamentals and Applications*, 2nd ed. John Wiley & Sons, Inc, 2001.

[92] R. Bourbonnais, D. Leech, and M. G. Paice, "Electrochemical analysis of the interactions of laccase mediators with lignin model compounds.," *Biochim. Biophys. Acta*, vol. 1379, no. 3, pp. 381–390, 1998.

[93] A. Majcherczyk, C. Johannes, and A. Huttermann, "Oxidation of aromatic alcohols by laccase from Trametes versicolor mediated by the 2,2'-azino-bis-(3-ethylbenzothiazoline-6-sulphonic acid) cation radical and dication," *Appl. Microbiol. Biotechnol.*, vol. 51, no. 2, pp. 267–276, 1999.

[94] C. Johannes, A. Majcherczyk, and C. Johannes, "Natural Mediators in the Oxidation of Polycyclic Aromatic Hydrocarbons by Laccase Mediator Systems Natural Mediators in the Oxidation of Polycyclic Aromatic Hydrocarbons by Laccase Mediator Systems," *Appl. Environ. Microbiol.*, vol. 66, no. 2, pp. 524–528, 2000.

[95] M. Solís-Oba, V. M. Ugalde-Saldívar, I. González, and G. Viniegra-González, "An electrochemical-spectrophotometrical study of the oxidized forms of the mediator 2,2´-azino-bis-(3-ethylbenzothiazoline-6-sulfonic acid) produced by immobilized laccase," *J. Electroanal. Chem.*, vol. 579, no. 1, pp. 59–66, 2005.

[96] S. Dong, H. Xiao, Q. Huang, J. Zhang, L. Mao, and S. Gao, "Graphene Facilitated Removal of Labetalol in Laccase-ABTS System: Reaction Efficiency, Pathways and Mechanism," *Sci. Rep.*, vol. 6, no. February, p. 21396, 2016.

[97] Y. Tong, Y. Lin, S. Wang, and M. Song, "A study of crystallisation of poly(ethylene oxide) and polypropylene on graphene surface," *Polymer (Guildf).*, vol. 73, pp. 52–61, 2015.

[98] P. Peljo, L. Qiao, L. Murtomäki, C. Johans, H. H. Girault, and K. Kontturi, "Electrochemically controlled proton-transfer-catalyzed reactions at liquid-liquid interfaces: nucleophilic substitution on ferrocene methanol.," *Chemphyschem a Eur. J. Chem. Phys. Phys. Chem.*, vol. 14, no. 2, pp. 311–4, Feb. 2013.

[99] J. P. Hurvois and C. Moinet, "Reactivity of ferrocenium cations with molecular oxygen in polar organic solvents: Decomposition, redox reactions and stabilization," *J. Organomet. Chem.*, vol. 690, pp. 1829–1839, 2005.

[100] A. Singh, D. R. Chowdhury, and A. Paul, "A kinetic study of ferrocenium cation decomposition utilizing an integrated electrochemical methodology composed of cyclic voltammetry and amperometry," *Analyst*, vol. 139, pp. 5747–5754, 2014.

[101] A. Bhattacharjee, A. Rooj, D. Roy, and M. Roy, "Thermal Decomposition Study of Ferrocene [(C5H5)2Fe]," *J. Exp. Phys.*, vol. 2014, p. 8, 2014.

[102] R. D. Milton, F. Giroud, A. E. Thumser, S. D. Minteer, and R. C. T. Slade, "Hydrogen peroxide produced by glucose oxidase affects the performance of laccase cathodes in glucose/oxygen fuel cells: FAD-dependent glucose dehydrogenase as a replacement.," *Phys. Chem. Chem. Phys.*, vol. 15, no. 44, pp. 19371–9, 2013.

[103] A. Zebda, C. Gondran, A. Le Goff, M. Holzinger, P. Cinquin, and S. Cosnier, "Mediatorless high-power glucose biofuel cells based on compressed carbon nanotube-enzyme electrodes.," *Nat. Commun.*, vol. 2, no. May, p. 370, Jan. 2011.

[104] I. Shitanda, S. Kato, Y. Hoshi, M. Itagaki, and S. Tsujimura, "Flexible and high-performance paper-based biofuel cells using printed porous carbon electrodes.," *Chem. Commun.*, vol. 49, no. 94, pp. 11110–2, Dec. 2013.

[105] C. W. Narvaez Villarrubia, F. Soavi, C. Santoro, C. Arbizzani, A. Serov, S. Rojas-Carbonell, G.

Gupta, and P. Atanassov, “Self-feeding paper based biofuel cell/self-powered hybrid μ-supercapacitor integrated system,” *Biosens. Bioelectron.*, vol. 86, pp. 459–465, 2016.

[106] T. Miyake, K. Haneda, S. Yoshino, and M. Nishizawa, “Flexible, layered biofuel cells,” *Biosens. Bioelectron.*, vol. 40, no. 1, pp. 45–49, 2013.

[107] W. Jia, X. Wang, S. Imani, A. J. Bandodkar, J. Ramírez, P. P. Mercier, and J. Wang, “Wearable textile biofuel cells for powering electronics,” *J. Mater. Chem. A*, vol. 2, no. 43, pp. 18184–18189, 2014.

[108] Y. Ogawa, K. Kato, T. Miyake, K. Nagamine, T. Ofuji, S. Yoshino, and M. Nishizawa, “Organic Transdermal Iontophoresis Patch with Built-in Biofuel Cell,” *Adv. Healthc. Mater.*, vol. 4, no. 4, pp. 506–510, 2015.

[109] A. Tsubota, Y. Ogawa, T. Yamauchi, H. Kai, K. Yamasaki, and M. Nishizawa, “Development of a Therapeutic Device for Wound Healing with Enzymatic Biofuel Cells,” *Electrochem. Soc.*, vol. Meeting Ab, no. 53, p. 3903, Sep. 2016.

[110] L. Zhang, M. Zhou, D. Wen, L. Bai, B. Lou, and S. Dong, “Small-size biofuel cell on paper,” *Biosens. Bioelectron.*, vol. 35, no. 1, pp. 155–159, May 2012.

[111] X. E. Wu, Y. Z. Guo, M. Y. Chen, and X. D. Chen, “Fabrication of flexible and disposable enzymatic biofuel cells,” *Electrochim. Acta*, vol. 98, pp. 20–24, 2013.

[112] C. Lau, M. J. Moehlenbrock, R. L. Arechederra, A. Falase, K. Garcia, R. Rincon, S. D. Minteer, S. Banta, G. Gupta, S. Babanova, and P. Atanassov, “Paper based biofuel cells: Incorporating enzymatic cascades for ethanol and methanol oxidation,” *Int. J. Hydrogen Energy*, vol. 40, no. 42, pp. 14661–14666, 2015.

[113] K. Haneda, S. Yoshino, T. Ofuji, T. Miyake, and M. Nishizawa, “Sheet-shaped biofuel cell constructed from enzyme-modified nanoengineered carbon fabric,” *Electrochim. Acta*, vol. 82, pp. 175–178, 2012.

[114] A. J. Bandodkar, I. Jeerapan, J. M. You, R. Nuñez-Flores, and J. Wang, “Highly Stretchable Fully-Printed CNT-Based Electrochemical Sensors and Biofuel Cells: Combining Intrinsic and Design-Induced Stretchability,” *Nano Lett.*, vol. 16, no. 1, pp. 721–727, 2016.

[115] W. Jia, G. Valdés-Ramírez, A. J. Bandodkar, J. R. Windmiller, and J. Wang, “Epidermal Biofuel Cells: Energy Harvesting from Human Perspiration.,” *Angew. Chem. Int. Ed. Engl.*, vol. 52, no. 28, pp. 7233–7236, Jul. 2013.

[116] Y. Ogawa, Y. Takai, Y. Kato, H. Kai, T. Miyake, and M. Nishizawa, “Stretchable biofuel cell with enzyme-modified conductive textiles,” *Biosens. Bioelectron.*, vol. 74, pp. 947–952, 2015.

[117] S. J. Konopka and B. McDuffie, “Diffusion coefficients of ferri- and ferrocyanide ions in aqueous media, using twin-electrode thin-layer electrochemistry,” *Anal. Chem.*, vol. 42, no. 14, pp. 1741–1746, 1970.

[118] M. Smolander, H. Boer, M. Valkiainen, R. Roozeman, M. Bergelin, J.-E. Eriksson, X.-C. Zhang, A. Koivula, and L. Viikari, “Development of a printable laccase-based biocathode for fuel cell applications,” *Enzyme Microb. Technol.*, vol. 43, no. 2, pp. 93–102, Aug. 2008.

[119] C. Lau, E. R. Adkins, R. P. Ramasamy, H. R. Luckarift, G. R. Johnson, and P. Atanassov, “Design of Carbon Nanotube-Based Gas-Diffusion Cathode for O2 Reduction by Multicopper Oxidases,” *Adv. Energy Mater.*, vol. 2, no. 1, pp. 162–168, Jan. 2012.

[120] G. P. M. K. Ciniciato, C. Lau, A. Cochrane, S. S. Sibbett, E. R. Gonzalez, and P. Atanassov, “Development of paper based electrodes: From air-breathing to paintable enzymatic cathodes,” *Electrochim. Acta*, vol. 82, pp. 208–213, Nov. 2012.

[121] S. Tuurala, M. Smolander, J. Uotila, O.-V. Kaukoniemi, H. Boer, M. Valkiainen, A. Vaari, A. Koivula, and P. Jenkins, “Performance of a Printable Enzymatic Fuel Cell: Study on Mediated ThL Laccase Cathode,” *ECS Trans.*, vol. 25, no. 33, pp. 1–10, 2010.

[122] J. Keskinen, E. Sivonen, M. Bergelin, J. E. Eriksson, P. Sjöberg-Eerola, M. Valkiainen, M. Smolander, A. Vaari, J. Uotila, H. Boer, and S. Tuurala, “Printed Supercapacitor as Hybrid Device with an Enzymatic Power Source,” *Adv. Sci. Technol.*, vol. 72, pp. 331–336, Oct. 2010.

Appendix A: Electron transfer properties of ferro/ferricyanide on DuPont ink

Electron transfer properties of DuPont ink were studied on a glassy carbon (GC, r = 2.5 mm) electrode. Figure A1 shows the CV measurements (a-c) at different scan rates, and Randles-Ševčik plots (d) of three different electrodes: 1) GC, 2) GC coated with 4 µl of DuPont ink, and 3) GC coated with 4 µl of DuPont ink modified with MWCNTs (as in Publications II and III).

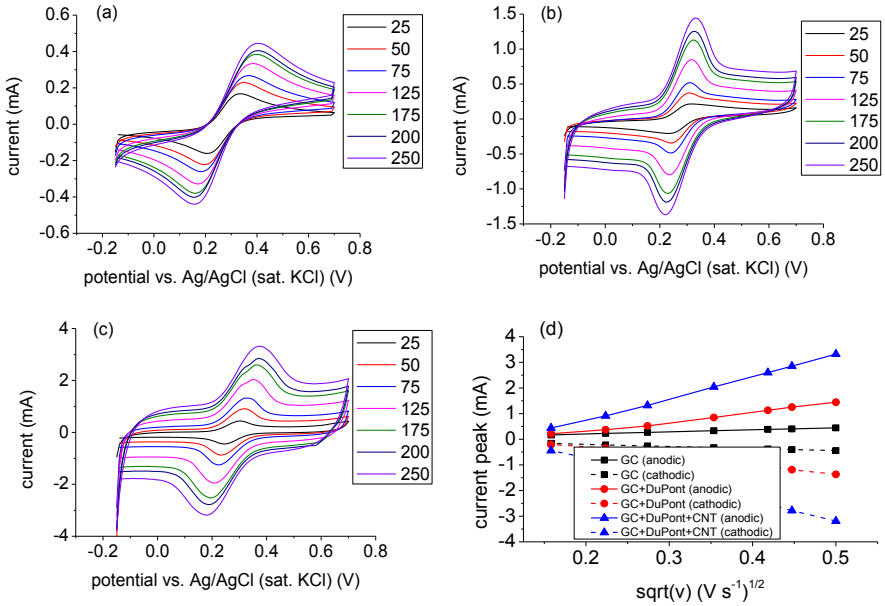

Figure A1. Cyclic voltammograms of (a) GC, (b) GC coated with DuPont ink, (c) GC coated with MWCNT-modified DuPont ink using different scan rates (mV s^{-1}), and (d) Randles-Ševčik plots of the electrodes studied. The electrolyte contained 7.5 mM $F_3Fe(CN)_6/F_4Fe(CN)_6$ in 1 M KCl. The counter electrode was Pt-wire and the reference electrode Ag/AgCl (sat. KCl). (Unpublished)

The slopes in the Panel (d) vary with the modification of the electrodes, which implies varying electrode surface area. The diffusion coefficient of the reactant can be calculated from the slopes. The slope of the GC electrode is 7.8×10^{-4} and Equation (18) leads to D = 4×10^{-6} cm^2 s^{-1}, which is rather close to the literature values (ca. 7×10^{-6} cm^2 s^{-1} [117]). For coated electrodes, the diffusion coefficient is assumed to be the same and the change in the slopes is attributed to an increased active area. The slope for GC/DuPont is 4.1×10^{-3} and for GC/MWCNT-modified DuPont 8.4×10^{-3}; hence doping with MWCNTs increased the active area of the electrode twofold. This was also observed by Smolander et al. [118], their measurements showed twofold higher current densities for MWCNT-modified DuPont ink containing ThL and ABTS.

Appendix B: Studying DET of ThL and rMaL in a fuel cell setup

One approach to increase the cell voltage is to utilise DET at the cathode, and hence DET of both ThL and rMaL was studied. Both laccases were immobilised on Toray paper (TGP-H-060, Fuel Cells Etc) and teflonised CB (prepared as in [119]). The electrolyte used in the measurements was 100 mM potassium phosphate buffer (KPB) with varying pH.

Toray paper electrodes

ThL solution was prepared by pipetting 100 µl of ThL (activity 156 U ml^{-1}) into 1.85 ml of KPB (pH 5), resulting in an enzyme activity of 8 U ml^{-1}. rMaL solution was prepared by pipetting 100 µl of rMaL (rMaL 138 U ml^{-1}) into 1.625 ml of KPB (pH 5), resulting in an enzyme activity of 8 U ml^{-1}. A piece of Toray paper was washed with ethanol and distilled water and dried at room temperature. Eight pieces were cut using a punching tool (r = 2.5 mm) and soaked into laccase solutions (four each) overnight at 4 °C.

The samples were measured the next day, attaching the Toray paper electrode on a glassy carbon electrode with a cup-formed holder made of Teflon. The measurement was made by measuring OCV for 1 h and then performing a CV from 800 mV to 0 mV vs. Ag/AgCl at a scan rate of 10 mV s^{-1}. The CV scan was repeated three times with 3 different samples.

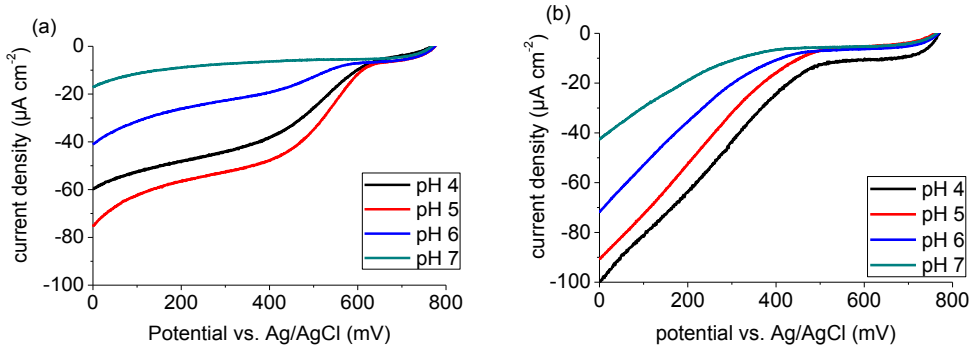

Figure B1. Cyclic voltammograms at varying pH of (a) ThL and (b) rMaL immobilised into Toray paper. Scan rate 10 mV s^{-1}. The electrolyte was bubbled with O_2. The curves represent average values of the third scan (n = 3). (Unpublished)

Cyclic voltammograms of the Toray paper electrodes in different pH values are shown in Figure B1. Both laccases indicated ORR without any use of a mediator, meaning that they were successfully immobilised into the Toray paper. The ORR starts at rather high potential with ThL, at ca. 600 mV vs. Ag/AgCl, which makes it a good cathode enzyme for BFC or battery applications. However, ThL is very sensitive to pH, showing its highest catalytic current at pH 5 but almost deactivating at pH 7. ThL also shows an interesting CV curve. The catalytic current of ORR increases dramatically between 600 and 500 mV vs. Ag/AgCl, but plateaus after that. rMaL on the other hand starts to catalyse ORR at ca. 500 mV vs. Ag/AgCl, with increasing catalytic current throughout the potential window. In addition, rMaL is not as sensitive to pH as ThL, still

catalysing ORR at pH 7. For this reason, rMaL could be a better cathode enzyme than ThL to couple with pH-sensitive anode enzymes.

Teflonised CB electrodes

ThL solution was prepared by pipetting 10 µl of ThL (780 U ml^{-1}) into 4.99 ml of KPB (pH 5), resulting in an enzyme activity of 1.56 U ml^{-1}. rMaL solution was prepared by pipetting 50 µl of rMaL (138 U ml^{-1}) into 4.95 ml of KPB (pH 5), resulting in an enzyme activity of 1.38 U ml^{-1}.

Toray paper was cut into a piece as illustrated in Figure B2. Small holes were punched in order to increase air diffusion through the material. 100 mg of teflonised CB was pressed onto Toray paper forming a round (r = 1.5 cm) area (see [120] for more details). 10 µl of ethanol was dropped on the teflonised CB and soaked into laccase buffer solution overnight at 4 °C. Three similar samples were prepared using both laccases.

The samples were measured the next day. The measurement setup is illustrated in Figure B2. A rectangular piece of filter paper (Whatman®) was placed between the laccase electrode and a Pt mesh. The cell was clamped together with a paperclip. The other end of the filter paper was soaked into KPB (pH 5), which caused the electrolyte to rise up into the cell. Ag/AgCl reference electrode was inserted into the electrolyte. OCV was measured for 1 h and CA was performed after that in 50 mV steps every 10 min from OCV to 0 V.

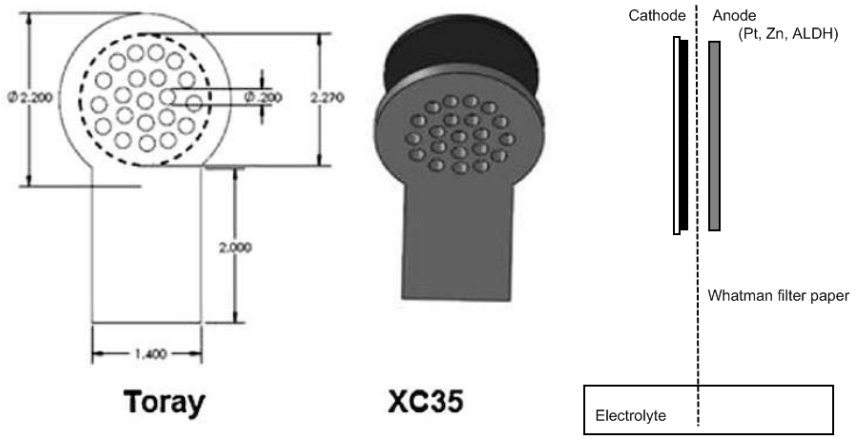

Figure B2. Left: schematic of the teflonised CB electrode (reprinted from [120] with permission). Right: Schematic of the test electrode setup. (Unpublished)

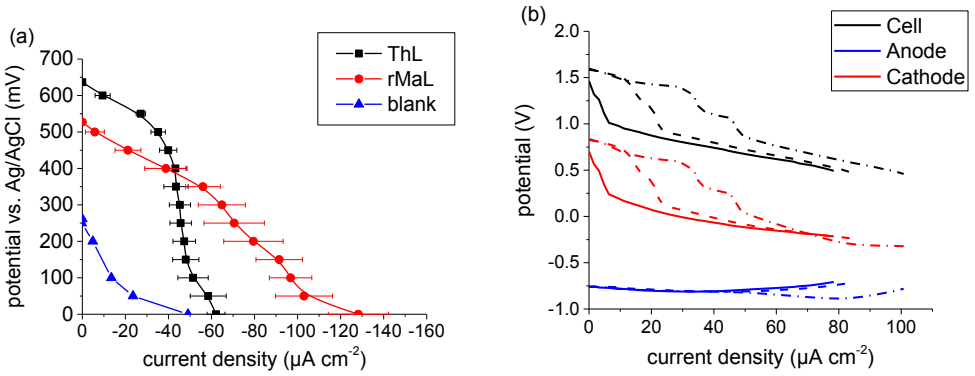

Figure B3. (a) Curves of CA measurement of teflonised CB laccase electrodes. Geometrical electrode area 7 cm^2. (b) Individual electrode potentials of CP measurement of $Zn_{sol.}$||ThL/ABTS cells. The printed cathodes contained different amounts of active components: 1x (solid), 10x (dash), and 100x (dash-dot). Geometrical cell area 6.25 cm^2. The original data was presented by Tuurala et al. in Figure 5 in [121]. Here the curves represent the average data (n = 2). (Unpublished)

CA measurements in Figure B3a showed that both laccases immobilised in teflonised CB catalyse ORR via DET. ThL electrodes have ca. 100 mV higher potential than rMaL electrodes between current densities 0-50 µA cm^{-2}, but after that the potential of ThL electrodes drops dramatically. rMaL electrodes on the other hand maintain their potential, which decreases almost linearly between current densities 50-100 µA cm^{-2}.

This behaviour of ThL at higher current densities was also observed in the author's earlier transaction publication [121]. Curves of individual electrode potentials from CP measurement of printed ThL/ABTS electrodes paired with solid Zn anode are shown in Figure B3b. Different amounts of ThL/ABTS were used in the inks. It was shown that increased amounts of catalytic components maintain the cathode, and thus cell potential, higher as current density increases. The highest OCV was 1.6 V, which corresponds to a cathode potential of 0.84 V.

This data indicated that ThL can catalyse ORR at high potential (ca. 700-800 mV), as long as the pH is between 4 and 5 and there is sufficient enzyme to keep the catalytic current high. rMaL on the other hand catalyses ORR at lower potential than ThL but tolerates neutral pH better. For this reason, it is important to know the application requirements for the cathode before the enzyme is selected.

Appendix C: A stack of biobatteries combined with printed supercapacitors

The use of biobatteries in mW-scale applications is still a question due to their modest power output. Therefore, the combination of printed biobatteries and printed supercapacitors was tested. In order to obtain higher voltage, three 12.25 cm^2 ALDH/ThL biobatteries with TMPD and ABTS mediators, prepared as in Publications II and III, were connected in series, creating an OCV of ca. 1.7 V. This stack was connected with two series-connected printed carbon-based supercapacitors (prepared as in [122]). The capacitance of the supercapacitors stack was approximately 0.2 F and the leakage current was3 µA at 1.2 V.

Both the stack of biobatteries and the stack of supercapacitors (pre-charged to 1 V) were subjected to a pulse test in which 5 mA pulses were drawn for 3 s while the potential was measured. The time between each pulse was 20 min. It was seen that three cells alone could not maintain the voltage (inset in Figure C1), and that the supercapacitors worked well, although the potential decreased during the pulses (Figure C1). In order to maintain the potential, a power source is needed to charge the supercapacitors between the pulses. Hence, the stack of supercapacitors was charged again to 1 V and connected with the stack of biobatteries. The same type of pulsing test was repeated, except that the first four pulses were taken every 10 min, after which they were taken every 20 min. The potential of the system remained at ca. 1 V for 10 hours, after which it started to decrease dramatically.

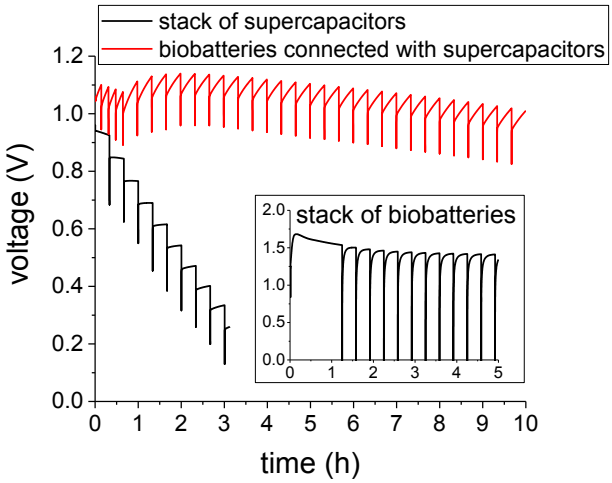

Figure C1. Voltage vs. time plot as a stack of biobatteries (inset), supercapacitors and a hybrid combination of both are discharged with pulses of 5 mA for 3 s. (Unpublished)

This measurement showed that printed biobatteries can be connected successfully with printed supercapacitors. The charging time of the capacitor between current pulses must be taken into account due to its high impact on the system performance. When these two stacks were connected, their combination was able to provide energy peaks of 12-17 mWs every 20 min for 15 h.

I

Tuurala, S., Lau, C., Atanassov, P., Smolander, M., and Minteer, S.D. (2012) Characterization and Stability Study of Immobilized PQQ-Dependent Aldose Dehydrogenase Bioanodes. *Electroanalysis* ***24(2)***, 229-238.

DOI: 10.1002/elan.201100546

Characterization and Stability Study of Immobilized PQQ-Dependent Aldose Dehydrogenase Bioanodes

Saara Tuurala,[a, b, c] *Carolin Lau*,[c] *Plamen Atanassov*,[c] *Maria Smolander*,*[a] *Shelley D. Minteer**[b, d]

[a] VTT Technical Research Centre of Finland, 02150 Espoo, Finland
tel: +358207225836; fax: +358207227071
[b] Saint Louis University, Department of Chemistry, St. Louis, MO, USA
tel: +1801-587-8325; fax: +1801-581-8181
[c] The University of New Mexico, Department of Chemical and Nuclear Engineering, Albuquerque, NM, USA
[d] University of Utah, Departments of Chemistry and Materials Science and Engineering, Salt Lake City, UT, USA
*e-mail: maria.smolander@vtt.fi; minteer@chem.utah.edu

Received: September 29, 2011
Accepted: November 16, 2011

Abstract
In this paper, glucose oxidizing bioanodes employing immobilized PQQ-dependent aldose dehydrogenase were prepared and characterized. The enzyme was immobilized on carbon paper in two different polymeric systems: tetrabutylammonium bromide (TBAB) modified Nafion and butanal modified chitosan. Characterization of the bioanodes included electron microscopy, electrochemical evaluation, as well as stability and leaching studies. Results indicate that the operational degradation was the same but the long term storage stability is better in the case of modified Nafion. The performance of the modified Nafion immobilized bioanodes stayed at 70% of the initial value after 60 days of storing at 4°C and 25°C. Compared to TBAB modified Nafion immobilized bioanodes, butanal modified chitosan immobilized bioanodes showed 50% activity after eight weeks storage at 4°C and one week storage at 25°C. However, the electrochemical properties of modified chitosan were better.

Keywords: PQQ-dependent aldose dehydrogenase, Biofuel cells, Bioanodes, Stability, Enzyme immobilization

DOI: 10.1002/elan.201100546

Supporting Information for this article is available on the WWW under http://dx.doi.org/10.1002/elan.201100546.

1 Introduction

Enzymatic biobatteries are a potential alternative to conventional batteries for low power applications. Due to the use of enzymes as catalysts and harmless organic materials employed as fuels, biobatteries are non-toxic, disposable and renewable. They could be used in many different applications e.g. active RFID tags, functional packages, small displays and cosmetic products. These functional disposable applications would require a battery that is biodegradable, cheap and thin. Hence, one of the most interesting ways of producing biobatteries is utilizing printing techniques, due to their potentially inexpensive mass production method [1]. This has been demonstrated in biocathode concept using laccase from *Trametes hirsuta* as the oxygen reducing enzyme [2]. These printed biocathodes maintained their enzymatic activity even for several months as stored dry, and the concept was proven to be potentially mass manufacture-able with reel-to-reel adjustable methods. The next step is to find a suitable, well performing bioanode for these biocathodes, and eventually demonstrate a printed fully enzymatic biobattery. In the simplest configuration, both the anode and cathode are prepared mixing all active components into a conductive ink, printed on conductive layers, separated by e.g. cellophane membrane and sandwiched between e.g. cardboard material (see Figure S1).

The enzyme of interest in this bioanode is PQQ-dependent aldose dehydrogenase. Aldose dehydrogenase (ALDH) from *Gluconobacter oxydans* is a bacterial membrane-bound quinoprotein, the cofactor of which is pyrroloquinoline quinone (PQQ), which is tightly bound to the apoenzyme. PQQ-dependent dehydrogenases present relatively new class of enzymes and have been showing great properties in biosensors [3–8]. In addition engineered PQQ-dependent glucose dehydrogenase (GDH) has been shown to work as an anode enzyme in a fully enzymatic biofuel cell with bilirubin oxidase (BOD) as cathode [9]. There are many advantages of using ALDH in analytical and amperometric applications due to its ability to oxidise different aldoses including glucose, xylose, galactose, mannose and arabinose [10]. In addition the presence of oxygen does not affect the catalytic activity of the enzyme, which is a problem in the case of glucose oxidase. ALDH enzyme was previously shown to work in amperometric sensors for xylose and glucose [3,4,11]. Due to the two electron oxidation reaction of glucose:

$$\beta\text{-D-glucose} + \text{ALDH-PQQ} \rightarrow \delta\text{-gluconolactone} + \text{ALDH-PQQH}_2$$

and other advantages mentioned earlier, ALDH is an ideal enzyme for bioanodes in enzymatic biofuel cells.

One of the many issues of concern for enzymatic biobatteries and biofuel cells is the immobilization and stabilization of enzymes at electrode surfaces. There are a variety of methods of immobilization including: physical adsorption, covalent binding/crosslinking, polymeric sandwich techniques, and encapsulation. Physical adsorption is a mild technique that frequently doesn't affect enzyme structure and function, but results in leaching of protein from the electrode over short time periods [12]. Covalent binding or crosslinking of enzyme to electrode surfaces is very useful for improving stability and eliminating leaching, but typically results in decreasing the enzyme activity due to structural changes of the protein upon functionalization and binding [13]. Polymeric sandwich techniques are also useful at decreasing leaching of protein, but the polymer coating employed to reduce enzyme leaching retards mass transport of substrate/fuel to the electrode and product away from the electrode and polymer coatings have not been shown to stabilize proteins [13]. Encapsulation techniques can be tailored to stabilize the enzyme at electrode structures [14–17]. However, different encapsulation polymers have different properties. This paper is focussed on evaluating and comparing two different polymeric strategies for encapsulation. Both strategies are micellar polymers, but the chemical microenvironments are very different between the two polymer systems.

The first strategy is employing tetrabutylammonium bromide modified Nafion for encapsulating aldose dehydrogenase. Research has shown that tetrabutylammonium bromide modified Nafion can successfully immobilize and stabilize different dehydrogenase enzymes at carbon electrodes [16]. This perfluorinated polymer system has micellar structures for encapsulating enzymes. The second strategy is the use of butanal modified chitosan, which is also a micellar polymer that has been used for immobilizing dehydrogenase enzymes [17]. However, the micellar structure of hydrophobically modified chitosan is larger and less ordered than Nafion, but the polymer is renewable and biodegradable [18]. This paper immobilizes aldose dehydrogenase in both polymeric systems at carbon bioanodes to understand the advantages and disadvantages of each system. This characterization is done by electron microscopy and electrochemical evaluation of bioanodes and complete biofuel cells, as well as studying stability and leaching via standard biochemistry techniques.

2 Experimental

2.1 Materials

Aldose dehydrogenase (ALDH) from *Gluconobacter oxydans* was produced as described in Smolander et al. [5], the protein content and activity was 6.2 mg/mL and 800 nkat/mL, respectively. Tetramethyl-*p*-phenylenediamine (TMPD, Sigma-Aldrich, T7394), tetra-*n*-butylammonium bromide (TBAB, Fluka, 86860), Nafion suspension (Sigma-Aldrich, product no. 274704), butyraldehyde (Sigma-Aldrich, 538191), sodium cyanoborohydride (Sigma-Aldrich, 156159), medium molecular weight chitosan (Sigma-Aldrich, product no. 448877), potassium phosphate monobasic (Sigma-Aldrich, P9791), potassium nitrate (Sigma-Aldrich, P8394), D-glucose (Sigma-Aldrich, product no. G5400), acetic acid (Fisher Scientific, A38–212), ethanol (Sigma-Aldrich, 459828) and methanol (Mallinckrodt Chemicals, 3016–22) were used without further purification. Distilled water was used as water in all preparations and experiments. Toray paper (Fuel Cell Earth, TGP-H-060) was used as the electrode substrate for prepared bioanodes and Nafion membrane (Nafion 212 Fuel Cell Store, 593263) as separator in full fuel cell setup.

2.2 Preparation of ALDH Bioanode

TBAB modified Nafion was prepared as per the procedure in [16]. Butanal modified chitosan was prepared as per the procedure in [17]. Toray paper was cut into pieces (geometrical electrode area 1 cm^2) and sonicated two times in ethanol for five minutes, rinsed three times with water and dried under desiccation. After drying, the connecting end of the electrode was dipped into hot paraffin wax to prevent wicking of electrolyte during experiments. 100 μL of ALDH enzyme was mixed with 150 μL of 100 mM potassium phosphate buffer (pH 6) and vortexed for 30 s. 250 μL of TBAB modified Nafion or butanal modified chitosan suspension was added into the enzyme solution and vortexed for 30 s. 100 μL of enzyme polymer mixture was pipetted on Toray paper electrode and let dry under fan at room temperature. After drying the electrodes were stored in 100 mM potassium phosphate buffer (pH 6) in the fridge overnight if not mentioned otherwise. Control electrodes were prepared with the same procedure, except the volume of enzyme solution was replaced with the same volume amount of 100 mM potassium phosphate buffer (pH 6).

2.3 Microscopic Characterization of Modified Nafion and Chitosan

Coated Toray paper electrodes were used as such to image the electrode surface and distribution of polymer on the carbon paper. In addition, gold grids were coated using 1 μL of the same enzyme polymer suspension as when in preparation of ALDH bioanodes to image the polymer itself. Scanning electron microscopy (SEM) was performed on a Hitachi S-5200.

2.4 Electrochemical Characterization of Immobilized ALDH Bioanode

CH Instruments' potentiostats were used for the electrochemical measurements. All measurements were performed using both TBAB modified Nafion and butanal modified chitosan immobilized ALDH bioanodes and repeated three times with separate samples. In half cell measurements, the counter electrode (CE) was a platinum mesh and reference electrode was a saturated calomel electrode (SCE). In full fuel cell measurements, the cathode electrode was a platinum mesh and the separator was a Nafion 212 membrane. The anodes were soaked in the electrolyte for 30 min before experiment. Potassium phosphate buffer (KPB) pH 6 containing 100 mM of potassium phosphate and 250 mM of potassium nitrate was used as the electrolyte.

2.4.1 Cyclic Voltammetry

Cyclic voltammetry (CV) was performed from −0.15 V to 0.25 V with a scan rate of 5 mV/s in half cell setup using ALDH bioanode as the working electrode (WE). The electrolyte was KPB with 0.5 mM of TMPD and 200 mM of glucose.

2.4.2 Amperometric Evaluation of Glucose Bioelectrocatalysis

Amperometric analysis of glucose bioelectrocatalysis was performed in a half cell with constant stirring of solution during the measurement. The electrolyte used was KPB with 0.5 mM of TMPD. First a CV (−0.15 V to 0.25 V, scan rate 5 mV/s) was performed to locate the potential of the anodic current peak, and then the potential of the WE was applied at above that potential (100 mV vs. SCE). After the current of the cell was stable, glucose was added into the electrolyte (2.5, 5, 10, 25, 50, 75, 100, 150 and 200 mM) every 10 min and the steady state current was measured. Control electrodes were measured.

2.4.3 Polarization Curve

A full biofuel cell setup was used with ALDH bioanode and a commercial Pt cathode separated by Nafion 212 in a standard H-cell configuration. The electrolyte used was KPB with 0.5 mM of TMPD and 50 mM of glucose on the anode side and KPB on the cathode side. First an open circuit potential (OCV) was measured until it was stable, after which a resistor was connected into the circuit (1010, 505, 100, 51, 15, 5, 1, 0.5, 0.1 kΩ) and changed every 20 min. The steady state potential was measured.

2.5 Operational and Storage Stability of Immobilized ALDH Bioanode

CH Instruments' potentiostats were used for the electrochemical measurements. All measurements were performed using both TBAB modified Nafion and butanal modified chitosan immobilized ALDH bioanodes and repeated three times with separate samples. In half cell measurements, the CE was a platinum mesh and reference electrode a SCE. In full fuel cell measurements, the cathode electrode was a platinum mesh and the separator was a Nafion 212 membrane. The anodes were soaked in the electrolyte for 30 min before experiment. KPB pH 6 containing 100 mM of potassium phosphate and 250 mM of potassium nitrate was used as the electrolyte.

2.5.1 Potentiostatic Study

A half cell setup with ALDH bioanode was used in this measurement. The electrolyte employed was KPB with 0.5 mM of TMPD and 50 mM of glucose. First a CV (−0.15 V to 0.25 V, scan rate 5 mV/s) was performed to locate the potential of the anodic current peak, and then the potential of the WE was set slightly over that potential (100 mV vs. SCE). The current was measured for 24 h.

2.5.2 Galvanostatic Study

A full fuel cell setup was used with ALDH bioanode and evaluated with a Pine Instruments WaveNow potentiostat/galvanostat. The electrolyte was KPB with 0.5 mM of TMPD and 50 mM of glucose on the anode side and KPB on the cathode side. First an OCV was measured until it was stable, after which 25 μA current was held. The potential of the cell was measured for 24 h.

2.5.3 Storage Time Stability

Prepared ALDH enzyme electrodes were stored in 100 mM potassium phosphate buffer pH 6, half of them in fridge at 4 °C and half at room temperature, for several weeks. Half cell setup was used to perform the measurements. The electrolyte was KPB with 0.5 mM of TMPD and 200 mM of glucose. Three CVs (−0.15 V to 0.25 V, scan rate 5 mV/s) were performed to measure the anodic current peak and the third CV was used as the result. In order to eliminate the current from the mediator, the anodic current of the controls was subtracted from the anodic current of the enzyme electrodes (at the potential of TMPD's current peak) which was divided by the anodic current of the controls. This ratio described portion of the current directly from the enzyme oxidizing glucose to gluconolactone.

2.5.4 Enzyme Leaching from the Polymer

Prepared enzyme electrodes were stored in 200 μL of potassium phosphate buffer (pH 6) in fridge at 4 °C. The buffer was collected after 1, 2, 3 and 15 days and replaced with fresh buffer. A bicinchoninic acid protein assay (BCA) was used to measure the protein content in the

buffer and the protein content on the prepared electrode was calculated.

3 Results and Discussion

All measurements were performed using both TBAB modified Nafion and butanal modified chitosan immobilized ALDH bioanodes and repeated three times with separate samples. The error bars were calculated as standard error of the mean.

3.1 Microscopic Characterization of Modified Nafion and Chitosan

SEM micrographs of coated Toray paper electrodes can be seen in Figure 1a–d. The first images were taken using 100× magnification and the second using 2000× magnification. In Figure 1e) and f) are the SEM images using Au grid as the holder and the used magnification is 50 000× and 35 000× for TBAB modified Nafion and butanal modified chitosan, respectively.

Figure 1a–d shows that the distribution of the polymer on Toray carbon paper is significantly different. TBAB modified Nafion forms a layer of polymer on top of the Toray paper after pipette coating of 100 μL of a 5% by wt alcoholic suspension, which cracks when it dries and may further crack during microscopic analysis at low vacuum. This results in areas of the electrode surface without immobilized biocatalyst, which will increase transport distances of the mediator and decrease electrochemical performance. In contrast, butanal modified chitosan forms a more uniform polymer layer on top of individual carbon fibers and no cracking was observed. It also appeared as though the modified chitosan penetrates throughout the carbon paper (i.e. the modified chitosan suspension wets the Toray paper better than the modified Nafion suspension). It is important to mention that the coating technique for Nafion could be optimized e.g. casting the Toray paper multiple times using smaller amount of polymer and hence avoiding cracking or using other thin film coating technologies. In addition, concentrations could be optimized to avoid cracking. On Au grid (Figure 1e and f), TBAB modified Nafion appears to form a porous layer of polymer. Butanal modified chitosan on the other hand forms a thin polymer layer without any noticeable pore structure at this magnification. This further suggests that chitosan coats the individual fibers of the Toray paper.

When these polymers are used for enzyme immobilization, it looks like that butanal modified chitosan offers a higher immobilized surface area due to its ability to penetrate into the carbon paper and coat individual fibers. This would be important for bioanodes involving direct electron transfer. Because the butanal modified chitosan distributes better than TBAB modified Nafion, the enzymes (and mediators) will have shorter distance to the conductive carbon fibers and lower transport resistances can be predicted. Due to the fact that butanal modified chitosan coats the individual fibres instead of forming a polymer layer on top of carbon paper as in the case of TBAB modified Nafion, less mass transport limitations can be also predicted.

3.2 Electrochemical Characterization of Immobilized ALDH Bioanode

3.2.1 Cyclic Voltammetry

Cyclic voltammetry was employed to evaluate the ALDH bioanodes containing both immobilization strategies. Results of the CV measurements of TBAB modified Nafion and butanal modified chitosan immobilized ALDH bioanodes and their controls are shown in Figure 2. The controls show similar curves, which represent the oxidation (~80 mV vs. SCE, negative current) and reduction (~25 mV vs. SCE, positive current) peak of the mediator.

Enzyme containing electrodes show higher oxidation peaks than the control electrodes (as shown in Table S1). The oxidation peak current of TBAB modified Nafion immobilized ALDH electrodes is 2.3 fold higher than the controls. The oxidation current (at 80 mV vs. SCE) of butanal modified chitosan immobilized ALDH electrodes is 5 fold higher than the controls. In the case of butanal modified chitosan immobilized ALDH electrodes, the oxidation peak doesn't show similar diffusion limitation as in the case of TBAB modified Nafion, and the oxidation peak increases all the way until i_{max} is reached. The reduction peak current of TBAB modified Nafion immobilized ALDH electrodes is similar to the controls, but there is no reduction peak observed with butanal modified chitosan immobilized ALDH electrodes. This means that the enzyme itself reduces the mediator very efficiently, not the actual electrode. This data suggests that the TBAB modified Nafion system is more mass transport limited than the butanal modified chitosan, which has also been noted in [17]. Transport values for caffeine (194.2 g/mol) both in TBAB modified Nafion and butanal modified chitosan membranes have been determined by Schrenk et al. [19] and Klotzbach et al. [20], respectively. According to the results, $KD^{1/2}$ value for caffeine is approximately four times higher in butanal modified chitosan membrane than in TBAB modified Nafion membrane. This indicates that the mass transfer of glucose (180.16 g/mol) is most likely slower in the modified Nafion layer. The mass transfer of the mediator, TMPD (164.25 g/mol), is probably also much slower in the modified Nafion layer than in the modified chitosan layer. The transfer of $Ru(bpy)_3^{2+}$ was shown to be similar in both polymers [19,20] which suggests that the ion transport of the radical cation form of the mediator, $TMPD^+$, is probably similar due to its charge.

Another common issue in immobilization technology is the enzyme inactivation. First, it can be due to the solvents in the polymer suspensions. In order to study this further, ALDH enzyme was exposed to different amounts

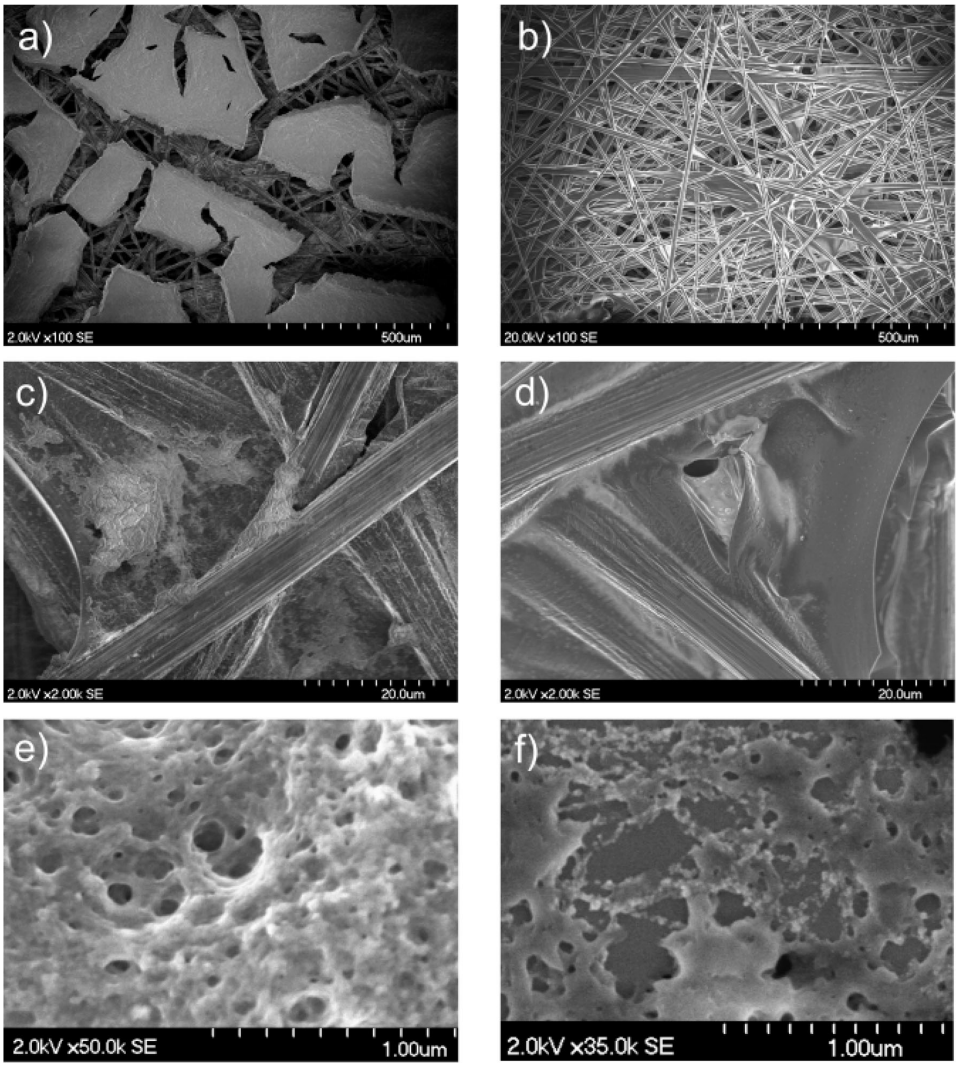

Fig. 1. SEM micrographs of TBAB modified Nafion/ALDH [a) 100× magnification, c) 2000× magnification] and butanal modified chitosan/ALDH [b) 100× magnification, d) 2000× magnification] on Toray paper. SEM micrographs of TBAB modified Nafion/ALDH (e) and butanal modified chitosan/ALDH (f) on Au grid.

of ethanol and acetic acid for 30 min and the enzyme activity was measured. The data in Table S2 shows that both the solvent for the Nafion suspension (ethanol) and the chitosan suspension (acetic acid) likely result in some enzyme inactivation, estimation for inactivation due to the solvents is 10% for TBAB modified Nafion and 3% for butanal modified chitosan (see supplementary information). However, this small degree of enzyme inactivation does not explain the significant observed differences in electrochemical performance

Second, both of the polymers provide different chemical microenvironments for the enzyme. Unmodified Nafion is very acidic with the pK_a value of −6 [21], in contrast to unmodified chitosan, which is more basic with the pK_a value of 6.5 [22]. Modification of Nafion dramatically decreases the acidity to near neutral pK_a values, so there is not a dramatic pH difference between modified chitosan and modified Nafion. However, literature has shown that hydrophobic modification of micellar polymers results in a change in chemical microenvironment that can stabilize the enzyme and does affect the enzyme activity [16–18]. In addition, it has been shown [23] that the enzyme activity can be increased using hydrophobically modified chitosan as the immobilizing polymer most

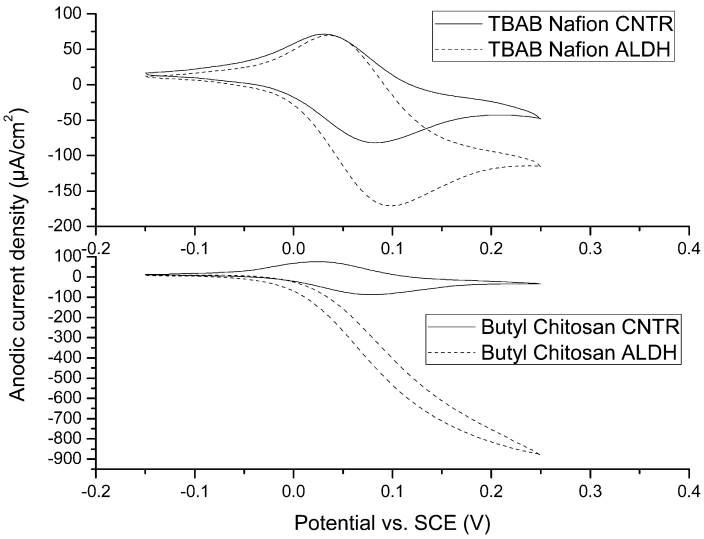

Fig. 2. CVs of TBAB modified Nafion (top) and butanal modified chitosan (bottom). CNTR: control electrode, ALDH: enzyme electrode. Half cell measurement with Pt counter electrode and SCE reference electrode. Scan rate of 5 mV/s. Electrolyte KPB with 0.5 mM of TMPD and 200 mM of glucose substrate.

probably due to a favourable protein aggregation, influenced by the chemical microenvironment provided by the polymer [24].

3.2.2 *Amperometric Evaluation of Glucose Bioelectrocatalysis*

Amperometry was performed with increasing injections of glucose concentrations. Limiting currents were measured and used to plot a calibration curve. The calibration curves of both TBAB modified Nafion and butanal modified chitosan ALDH bioanodes are shown in Figure 3. Also control electrodes were measured and they didn't show any current response to the addition of glucose. This confirms bioelectrocatalysis for both electrode systems.

TBAB modified Nafion immobilized ALDH bioanodes reach their maximum steady state current density of 121 ± 4 μA/cm^2 at 50 mM of glucose. After that, the addition of glucose doesn't affect the steade state current. Butanal modified chitosan immoblized ALDH bioanodes reach their maximum steady state current density of 493 ± 44 μA/cm^2 at 25 mM of glucose. After that, the addition of glucose decreases the steady state current. This may be due to leaching of the protein or inhibition effects.

The maximum current density of butanal modified chitosan is four times higher than that of TBAB modified Nafion, which is expected based on literature results. As discussed above, the mass transport of neutral glucose size molecule is four times higher in butanal modified chitosan membrane than in TBAB modified Nafion film.

Michaelis–Menten equation $I=(I_{max}\cdot c)/(K_m+c)$ was fitted into the results and the evaluated apparent K_m values were 2.9 ± 0.6 mM and 2.6 ± 0.6 mM for TBAB modified Nafion and butanal modified chitosan immobilized ALDH bioanodes, respectively. For soluble ALDH the K_m value was previously shown to be 0.7 mM [3]. This shows that both immobilization methods greatly alter the K_m values, but does not show significant differ-

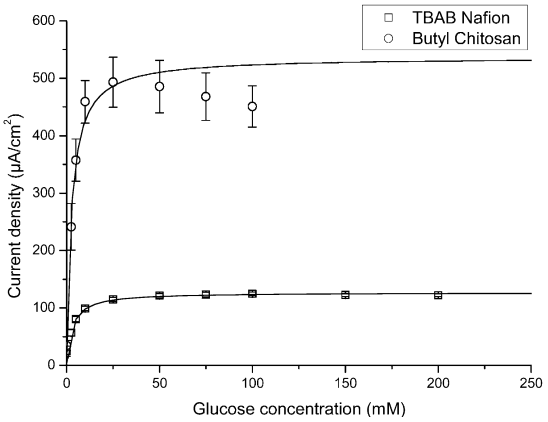

Fig. 3. Calibration curve of immobilized ALDH bioanode. Half cell measurement with Pt CE and SCE reference electrode. Potential of the anode 100 mV vs. SCE. Electrolyte KPB with 0.5 mM of TMPD. Addition of glucose every 10 min. Control electrodes didn't show any current response to the addition of glucose. The lines are fitting of Michaelis–Menten function.

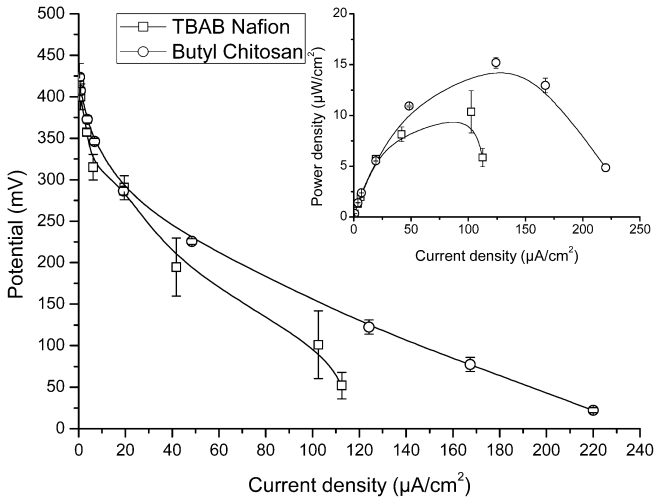

Fig. 4. Polarization curve (Main plot) and power density vs. current density curve (Inset) of a full cell with immobilized ALDH bioanode, Pt cathode and Nafion membrane. Electrolyte KPB with 0.5 mM of TMPD and 50 mM of glucose (anode), KPB (cathode). Change of the resistor was done every 20 min.

ence between each other. Hence the enzyme kinetics are similar in both systems.

When linear fitting is introduced to the data (from glucose concetration of 0–5 mM), the sensitivity of the bioanodes were 11.18 μA/mMcm^2 ($R^2=0.99$) and 64.62 μA/mMcm^2 ($R^2=0.97$) for TBAB modified Nafion and butanal modified chitosan immobilized ALDH bioanodes, respectively. In Li et al. [8] the sensitivity of screen printed PQQ-GDH carbon paste electrode was 31.0 μA/mMcm^2 in glucose range of 1–35 mM.

3.2.3 *Polarization Curve*

The calculated polarization (Main plot) and power density (Inset plot) curves of ALDH bioanode and platinum cathode full fuel cells are shown in Figure 4. Both cells having either TBAB modified Nafion or butanal modified chitosan immobilized ALDH bioanode show same beavior at the activation overpotential region of the polarization curve. The measured polarization curves show that both of the cell configurations have the same behaviour at very low current densities. This is the region of activation overpotential which describes the charge transfer kinetics. This result supports the previous finding that the K_m values are the same.

As the concentration overpotential region is reached, the potential of the cell with TBAB modified Nafion immobilized ALDH bioanode decreases faster than with butanal modified chitosan immobilized ALDH bioanode. As the current density increases, the concentration overpotential becomes significant which is mostly dependent on the ionic fluxes of the electrolyte and mass transport of the substrate. The cell with TBAB modified Nafion immobilized ALDH bioanode shows bigger concentration overpotential than the cell with butanal modified chitosan ALDH bioanodes, which further supports the previous results.

The maximum current densities were 112 ± 35 μA/cm^2 and 220 ± 31 μA/cm^2 for TBAB modified Nafion immobilized ALDH bioanode and butanal modified chitosan immobilized ALDH bioanode, respectively. The calculated maximum power densities were 10 ± 4 μW/cm^2 and 15 ± 1 μW/cm^2 for TBAB modified Nafion immobilized ALDH bioanode and butanal modified chitosan immobilized ALDH bioanode, respectively. This is further indication of the severe transport limitations in the modified Nafion membranes. The maximum current density was higher than that of the engineered PQQ-GDH/BOD biofuel cell reported by Yuhashi et al. [9] where the maximum current density was 61.4 μA/cm^2. The maximum power density of the engineered PQQ-GDH/BOD biofuel cell was 17.6 μW/cm^2 which is slightly higher than with ALDH bioanodes. It's important to note that the cathodes were different in these cell configurations, which affects on the cell potential and hence to the power.

3.3 Operational and Storage Stability of Immobilized ALDH Bioanode

3.3.1 *Potentiostatic Study*

The current density vs. time curves of half cell measurements are shown in Figure 5. The initial current density of TBAB modified Nafion ALDH bioanodes is significantly lower than that of butanal modified chitosan immobilized ALDH bioanodes, that is 59 ± 4 μA/cm^2 and 194 ± 19 μA/cm^2, respectively.

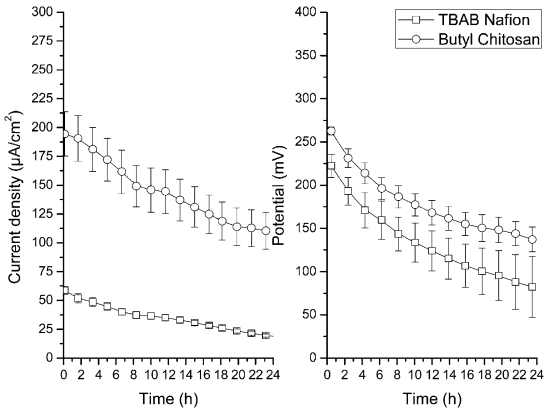

Fig. 5. Current density vs. time curve of immobilized ALDH bioanode (left). Half cell measurement with Pt CE and SCE reference electrode. Potential of the anode 100 mV vs. SCE. Electrolyte KPB with 0.5 mM of TMPD and 50 mM of glucose. Potential vs. time curve of immobilized ALDH bioanode (right). Full cell with immobilized ALDH bioanode, Pt cathode and Nafion membrane. Electrolyte KPB with 0.5 mM of TMPD and 50 mM of glucose (anode), KPB (cathode). Current held 25 $\mu A/cm^2$.

When the measured current densities are divided by the initial current densities the currents seem to decrease at the same rate after two hours of operation. The degradation could be due to enzyme inactivation, mediator degradation, crossover or all of the above. Either way there is no significant difference in the degradation of TBAB modified Nafion or butanal modified chitosan immobilized ALDH bioanodes. TBAB modified Nafion immobilized bioanodes reach 80% of the initial current density in four hours of operation and 60% in 12 hours. Butanal modified chitosan immobilized bioanodes reach 80% of the initial current density in eight hours of operation and 60% in 20 hours. In Smolander et al. [4] the performance of a carbon paste electrode with adsorbed mediator (phenazine methosulfate, PMS) and covalently immobilized enzyme in continuous operation was 22% of the initial response after 10 h of continuous operation. With soluble PMS the performance was 50% after 10 h. The most stable system was ALDH immobilized on glutaraldehyde activated controlled-pore glass with soluble PMS, the remaining response after 10 hours continuous operation was 87%. Comparing ALDH to GDH, in Yuhashi et al. [9] engineered PQQ-GDH/BOD cell showed 80% of the initial performance after 24 h of operation using external load of 200 kΩ.

3.3.2 Galvanostatic Study

The potential vs. time curves of full cell measurements are shown in Figure 5. The potential difference between TBAB modified Nafion and butanal modified chitosan immobilized ALDH bioanodes stays constant during the whole measurement, which is app. 40 mV, hence the potential of the fuel cells drops at the same rate. The potential drop for both cells is linear to the square root of time which indicates that the potential drop is due to diffusion, most probably due to the crossover of the mediator from the anode side to the cathode side. The calculated energy production after 24 h of operation was 75 ± 14 mWh and 102 ± 8 mWh for TBAB modified Nafion and butanal modified chitosan immobilized bioanode, respectively.

3.3.3 Storage Stability

The ratio of the oxidation current peak difference (between immobilized ALDH bioanodes and controls) and control electrodes on different days is shown in Figure S2. As ALDH enzyme is immobilized using TBAB modified Nafion, the performance of the bioanodes is very stable regardless if stored at 4 °C or at room temperature. During the first week, the performance decreases approximately 30–35% but after that it stays very stable.

The stability of butanal modified chitosan immobilized bioanodes is not as stable as TBAB modified Nafion bioanodes. After one week, the performance of electrodes stored at room temperature had decreased approximately 88% showing half of the current of TBAB modified Nafion immobilized electrodes. After three weeks of storing at room temperature, the electrodes had lost approximately 95% of their performance. In the case of electrodes that were stored in the fridge, the performance had decreased approximately 50% after one week showing twice the current of TBAB modified Nafion immobilized electrodes. After four weeks of storage, the butanal modified chitosan immobilized bioanodes had the same performance as TBAB modified Nafion immobilized bioanodes. After six weeks of storage in the fridge, the electrodes had lost app. 95% of their performance.

In Smolander et al. [3] the performance of the electrode based on ALDH was 50% of the original electrode response after five days of intermittent use. In Li et al. [8] a carbon paste electrode based on PQQ-GDH showed 93% performance after 2 weeks of storing at 5 °C and 87% after 4 weeks.

This shows that the storage stability of the TBAB modified Nafion is greater than the storage stability of butanal modified chitosan and the stability of butanal modified chitosan is more temperature dependent. The storage time stability tests show that TBAB modified Nafion immobilized ALDH bioanodes are very stable, not showing any significant loss in the electrode performance, regardless if stored at 4 °C or at room temperature. When butanal modified chitosan is used as the immobilizing polymer, the performance of the bioanodes decreases dramatically during the first week, and the drop is more significant when the bioanodes are stored at room temperature. This drop is probably due to enzyme leakage out of the polymer structure, because 25% of the enzyme leaches out during the first day.

It is important to note that these electrodes were stored in buffer, which enhances the enzyme leakage. In

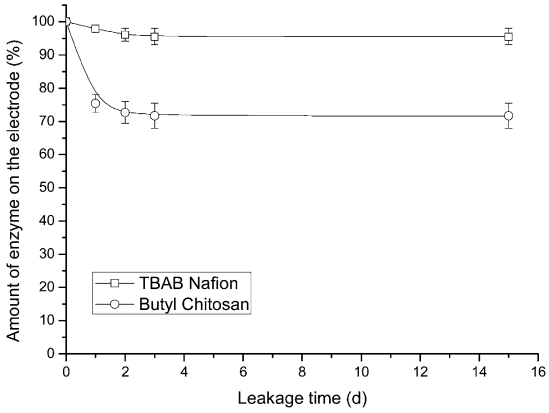

Fig. 6. Enzyme amount (as protein) on the Toray paper electrode vs. electrode storage time in 100 mM potassium phosphate pH 6 at 4 °C.

addition unmodified chitosan is soluble at pH 6 and although modified chitosan is less soluble it is still somewhat acid soluble, which also decreases the stability. If the electrodes were stored in fairly dry conditions the leakage would be minimal and hence the storage stability would be significantly better.

3.3.4 Enzyme Leaching from the Polymer

Enzyme leaching is a serious issue with bioelectrode stability and, although rarely studied, is quite important to understanding the effectiveness of enzyme immobilization and stabilization at bioelectrodes. The amount of immobilized enzyme retained on the carbon paper electrode is illustrated in Figure 6. Note: experiments were done in electrolyte solutions, but not in-situ in an electrochemical cell. When TBAB modified Nafion is used to immobilize ALDH, 2% of the enzyme leaches out during the first day. After that the leaching is very minimal and altogether 96% of the initial amount of the enzyme stays on the electrode. When butanal modified chitosan is used to immobilize ALDH, 25% of the enzyme leaches out during the first day. After that the leaching is minimal and altogether 72% of the initial amount of the enzyme stays on the electrode.

4 Conclusions

In this study two different polymers were used to immobilize PQQ-dependent aldose dehydrogenase enzyme for enzymatic bioanodes. The first polymer studied was non-biodegradable TBAB modified Nafion and the second biodegradable butanal modified chitosan.

All the studies indicate that the long term storage stability is better in the case of TBAB modified Nafion. The operational degradation was the same. The performance of the TBAB modified Nafion immobilized bioanodes stayed at 65–70% of the initial value after 60 days of storing, both at 4 °C and room temperature. The performance of butanal modified chitosan immobilized bioanodes stored at 4 °C decreased 50% of their initial value (still twice the current vs. TBAB modified Nafion immobilized electrodes) during the first week but stayed at that level until three weeks of storing. After six weeks, the performance of butanal modified chitosan immobilized bioanodes had decreased approximately 95%. In Smolander et al. [3] bioanodes using the same enzyme showed 50% of the initial performance after five days, which means the storage stability was greatly increased. It is important to note that the electrodes used for long term storage stability measurements were stored in buffer, which enhances enzyme leakage. If the electrodes were stored in fairly dry conditions, the leakage would be minimal and hence the storage stability could be significantly better for both polymer systems.

In contrast all electrochemical properties are worse with TBAB modified Nafion than with butanal modified chitosan. For an example, the steady state current and sensitivity of the butanal modified chitosan electrodes was four and six times higher than TBAB modified Nafion, respectively. It was shown though that the enzyme kinetics were the same (K_m values were app. four times higher compared to soluble ALDH) regardless which polymer was used to immobilize the enzyme, hence the operational difference between TBAB modified Nafion and butanal modified chitosan electrodes had to be explained in other ways. SEM pictures showed that TBAB modified Nafion forms a cracked layer of polymer on top of the carbon paper, but butanal modified chitosan coats individual carbon fibers with high enzymatic surface area. This means that both mass transfer of the substrate and ionic flux of the electrolyte of butanal modified chitosan immobilized ALDH bioanodes must be better than in the case of TBAB modified Nafion. In addition, there should be more active enzyme close to the carbon support in the case of butanal modified chitosan due to the higher coated surface area. All the electrochemical measurements indicate the same.

The question of which polymer is better depends on the potential application. If the application would be a disposable biosensor, higher sensitivity would be more important over long term storage stability in moist conditions, and butanal modified chitosan would be a good choice for enzyme immobilization. In the case of a biofuel cell with flowing fuel, long term stability is needed and TBAB modified Nafion would be more stable choice for enzyme immobilization.

Acknowledgements

Harry Boer and *Arja Kiema* (VTT) are thanked for supplying the ALDH enzyme preparation. In addition *Asta Pesonen* and *Anu Vaari* (VTT), *Rob Arechederra*, *Michael*

Moehlenbrock, and *Matthew Meredith* (SLU) are gratefully thanked for technical and academic assistance. The research was part of the Printed Enzymatic Power Source with embedded capacitor on next generation devices -project supported by *TEKES*, the *Finnish Funding Agency for Technology and Innovation*. Cofunding by companies is gratefully acknowledged. The authors would also like to acknowledge the *Air Force Office of Scientific Research* for providing the funding for the immobilization materials employed.

References

[1] M. Valkiainen, S. Tuurala, M. Smolander, O.-V. Kaukoniemi, *Innovations in Fuel Cell Technologies*, Printed Enzymatic Current Sources, RSC Publishing, London **2010**, ch. 1.
[2] M. Smolander, H. Boer, M. Valkiainen, R. Roozeman, M. Bergelin, J.-E. Eriksson, X.-C. Zhang, A. Koivula, L. Viikari, *Enzyme Microbial Technol.* **2008**, *43*, 93.
[3] M. Smolander, H. L. Livio, L. Räsänen, *Biosens. Bioelectron.* **1992**, *7*, 637.
[4] M. Smolander, J. Cooper, W. Schuhmann, M. Hämmerle, H.-L. Schmidt, *Anal. Chim. Acta* **1993**, *280*, 119.
[5] M. Smolander, J. Buchert, L. Viikari, *J. Biotechnol.* **1993**, *29*, 287.
[6] V. Laurinavicius, B. Kurtinaitiene, V. Liauksminas, A. Ramanavicius, R. Meskys, R. Rudomanskis, T. Skotheim, L. Boguslavsky, *Anal. Lett.* **1999**, *32*, 299.
[7] V. Laurinavicius, J. Razumiene, B. Kurtinaitiene, I. Lapenaite, I. Bachmatova, L. Marcinkeviciene, R. Meskys, A. Ramanavicius, *Bioelectrochemistry* **2001**, *55*, 29.
[8] G. Li, H. Xu, W. Huang, Y. Wang, Y. Wu, R. Parajuli, *Measurement Sci. Technol.* **2008**, *19*, 065203.
[9] N. Yuhashi, M. Tomiyama, J. Okuda, S. Igarashi, K. Ikebukuro, K. Sode, *Biosens. Bioelectron.* **2005**, *20*, 2145.
[10] J. Buchert, *J. Biotechnol.* **1991**, *18*, 103.
[11] M. Smolander, L. Gorton, H. S. Lee, T. Skotheim, H.-L. Lan, *Electroanalysis* **1995**, *7*, 941.
[12] M. J. Cooney, V. Svoboda, C. Lau, G. P. Martin, S. D. Minteer, *Energy Environ. Sci.* **2008**, *1*, 320.
[13] M. J. Moehlenbrock, S. D. Minteer, *Chem. Soc. Rev.* **2008**, *37*, 1188.
[14] J. Lim, P. Malati, F. Bonet, B. Dunn, *J. Electrochem. Soc.* **2007**, *154*, A140.
[15] R. Sahney, S. Anand, B. K. Puri, A. K. Srivastava, *Anal. Chim. Acta* **2006**, *578*, 156.
[16] C. M. Moore, N. L. Akers, A. D. Hill, Z. C. Johnson, S. D. Minteer, *Biomacromolecules* **2004**, *5*, 1241.
[17] T. L. Klotzbach, M. M. Watt, Y. Ansari, S. D. Minteer, *J. Membr. Sci.* **2008**, *311*, 81.
[18] G. B. Jiang, D. Quan, K. Liao, H. Wang, *Carbohydrate Polymer* **2006**, *66*, 514.
[19] M. J. Schrenk, R. E. Villigram, N. J. Torrence, S. J. Brancato, S. D. Minteer, *J. Membr. Sci.* **2002**, *205*, 3.
[20] T. Klotzbach, M. Watt, Y. Ansari, S. D. Minteer, *J. Membr. Sci.* **2006**, *282*, 276.
[21] J. M. Serpico, S. G. Ehrenberg, J. J. Fontanella, X. Jiao, D. Perahia, K. A. McGrady, E. H. Sanders, G. E. Kellogg, G. E. Wnek, *Macromolecules* **2002**, *35*, 5916.
[22] P. M. Claesson, B. W. Ninham, *Langmuir* **1992**, *8*, 1406.
[23] G. L. Martin, S. D. Minteer, M. J. Cooney, *Analyst* **2010**, *135*, 1131.
[24] G. L. Martin, S. D. Minteer, M. Cooney, *Chem. Commun.*, **2011**, *47*, 2083.

Supplementary Data

Novel Glucose Bioanode: Immobilization and Stabilization of PQQ-Dependent Aldose Dehydrogenase

Saara Tuurala[a,b,c], Carolin Lau[c], Plamen Atanassov[c], Maria Smolander[a*], and Shelley D. Minteer[b,d*]

[a] VTT Technical Research Centre of Finland, 02150 Espoo, Finland
[b] Saint Louis University, Department of Chemistry, St. Louis, MO USA
[c] The University of New Mexico, Department of Chemical and Nuclear Engineering, Albuquerque, NM USA
[d] University of Utah, Departments of Chemistry and Materials Science and Engineering, Salt Lake City, UT USA

*Joint corresponding authors Maria Smolander and Shelley D. Minteer:
maria.smolander@vtt.fi
Tel: +358 20 722 5836
Fax: +358 20 722 7071

minteer@chem.utah.edu
Tel: +1 801-587-8325
Fax: +1 801-581-8181

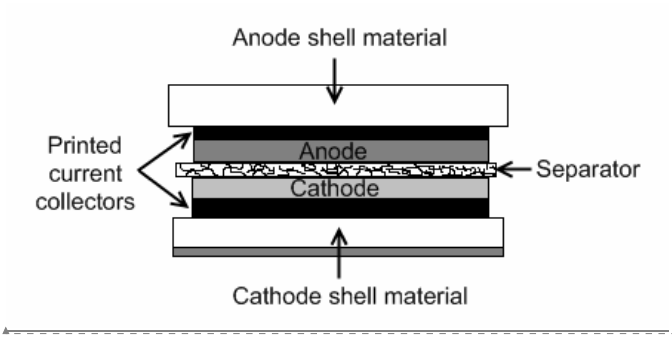

Figure S1. A schematic of a printed biofuel cell

Formatiert: Deutsch (Deutschland), Rechtschreibung und Grammatik nicht prüfen

Table S1. Values of oxidation (80 mV vs. SCE) and reduction (25 mV vs. SCE) currents of immobilized ALDH bioanodes and controls.

	TBAB modified Nafion		Butanal modified chitosan	
	Control electrode	Enzyme electrode	Control electrode	Enzyme electrode
i_{ox} (μA/cm^2)	-81.0 ± 0.5	-188 ± 13	-84 ± 3	-417 ± 24
i_{red} (μA/cm^2)	71 ± 1	80 ± 10	71 ± 4	-70 ± 1

Table S2. Activity of ALDH enzyme after exposure in different solvents for 30 min.

Ethanol (vol %)	Activity (%)
0	100
10	101
20	93
27	91
33	86
53	63
67	45
Acetic acid (vol %)	Activity (%)
0	100
2	95
3	83

The drying time for TBAB modified Nafion electrodes was app. 10 min from which one can estimate that 50 % ethanol (that was the used concentration for electrode preparation) led to app. 10 % decrease in enzyme activity. The drying time for butanal modified chitosan electrodes was app. 30 min.

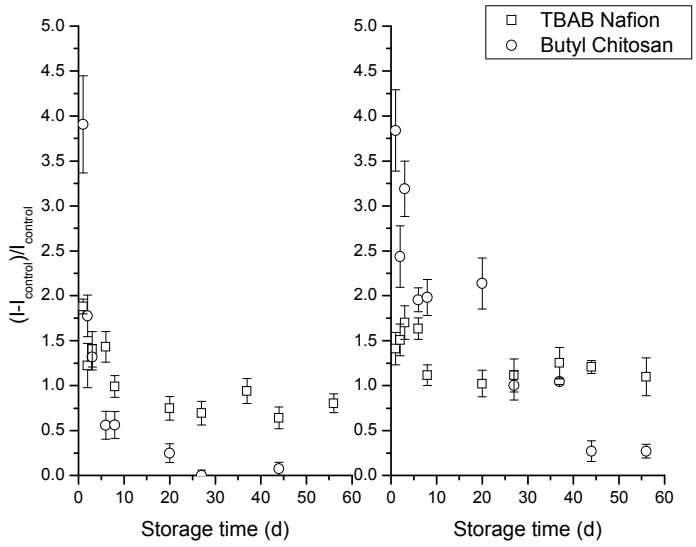

Figure S2. Peak current ratio between immobilized ALDH bioanodes and controls vs. storage time, stored at room temperature (left) and at 4 °C (right) in K-phosphate buffer (pH 6).

II

Jenkins, P., Tuurala, S., Vaari, A., Valkiainen, M., Smolander, M., and Leech, D. (2012) A compar-ison of glucose oxidase and aldose dehydrogenase as mediated anodes in printed glucose/oxygen enzymatic fuel cells using ABTS/laccase cathodes. *Bioelectrochemistry* ***87***, 172-177.

DOI: 10.1016/j.bioelechem.2011.11.011

Bioelectrochemistry 87 (2012) 172–177

Contents lists available at SciVerse ScienceDirect

Bioelectrochemistry

journal homepage: www.elsevier.com/locate/bioelechem

A comparison of glucose oxidase and aldose dehydrogenase as mediated anodes in printed glucose/oxygen enzymatic fuel cells using ABTS/laccase cathodes

Peter Jenkins [a], Saara Tuurala [b], Anu Vaari [b], Matti Valkiainen [b], Maria Smolander [b], Dónal Leech [a,*]

[a] National University of Ireland Galway, School of Chemistry, University Road, Galway, Ireland
[b] VTT Technical Research Centre of Finland, P.O. Box 1000, FI-02044 VTT, Finland

ARTICLE INFO

Article history:
Received 3 August 2011
Received in revised form 28 October 2011
Accepted 28 November 2011
Available online 7 December 2011

Keywords:
Biofuel cell
Printing
Laccase
Glucose oxidase
Aldose dehydrogenase

ABSTRACT

Current generation by mediated enzyme electron transfer at electrode surfaces can be harnessed to provide biosensors and redox reactions in enzymatic fuel cells. A glucose/oxygen enzymatic fuel cell can provide power for portable and implantable electronic devices. High volume production of enzymatic fuel cell prototypes will likely require printing of electrode and catalytic materials. Here we report on preparation and performance of, completely enzymatic, printed glucose/oxygen biofuel cells. The cells are based on filter paper coated with conducting carbon inks, enzyme and mediator. A comparison of cell performance using a range of mediators for either glucose oxidase (GOx) or aldose dehydrogenase (ALDH) oxidation of glucose at the anode and ABTS and a fungal laccase, for reduction of oxygen at the cathode, is reported. Highest power output, although of limited stability, is observed for ALDH anodes mediated by an osmium complex, providing a maximum power density of 3.5 μW cm^{-2} at 0.34 V, when coupled to a laccase/ABTS cathode. The stability of cell voltage in a biobattery format, above a threshold of 200 mV under a moderate 75 kΩ load, is used to benchmark printed fuel cell performance. Highest stability is obtained for printed fuel cells using ALDH, providing cell voltages over the threshold for up to 74 h, compared to only 2 h for cells with anodes using GOx. These results provide promising directions for further development of mass-producible, completely enzymatic, printed biofuel cells.

1. Introduction

Over the last 20 years research focused on biofuel cells has gained a significant amount of attention [1–3]. These electrochemical cells can convert chemical energy into electrical energy using biological catalysts. The biocatalysts can be highly specific enzymes, relatively cheap to produce, making them an attractive choice for incorporation in disposable, inexpensive, power sources for numerous applications.

One of the most studied enzymatic fuel cell (EFC) assemblies is based on utilization of glucose as the fuel, for application to powering portable or implantable electronic devices. Glucose is biocatalytically oxidized at the anode and the generated electrons are transferred through an external circuit to a suitable cathode, which often involves the biocatalytic reduction of dioxygen to water. Glucose oxidase (GOx) is a well characterized, stable, enzyme and has therefore been the anodic biocatalyst of choice for many prototype EFCs [1–3]. GOx oxidizes glucose to gluconolactone, with the transfer of electrons to the natural oxygen co-substrate, or to the anode or anodic mediator. One of the disadvantages of incorporating GOx into EFC, that depends upon oxygen reduction at a cathode, is therefore the sensitivity to oxygen at the anode. Oxygen as the natural acceptor of electrons from GOx, produces hydrogen peroxide, which has a high level of toxicity associated with it. Oxygen will also compete with the anode or anodic mediator for the electrons produced by GOx from oxidation of glucose. Aldose dehydrogenases (ALDH) provide interesting alternatives to GOx for use as anodic biocatalyst.

Here we report on a comparison of ALDH and GOx in assembled printed glucose/oxygen EFCs. The ALDH, isolated in this case from *Gluconobacter oxydans* as described previously, [4] is an 87.3 kDa pyrrolo-quinoline quinone (PQQ) dependent protein with optimum activity for glucose oxidation close to neutral pH. The PQQ redox potential is more positive than that of the $FADH_2$ in GOx, at approximately −110 mV *vs.* Ag/AgCl [4–6]. Nevertheless ALDH is relatively insensitive towards oxygen, preventing problems of peroxide formation and competition between anodic mediator and oxygen for electrons. Another advantage of ALDH is that, unlike GOx which specifically oxidizes glucose, ALDH can oxidize several other sugars, [4–7] resulting in a wider range of available fuels/substrates.

Immobilization of biocatalysts and mediators at electrodes is an active area of research with the constant development of novel methods aimed at producing both enhanced stability and improved signal/output. These biocatalytic electrodes can be subsequently exploited as biosensors or as bioanodes and biocathodes in fuel cells. The literature is full of examples of immobilization techniques including: physical adsorption, [8] entrapment in electro-polymerized matrices [9] and use of crosslinking agents to form redox hydrogels [10,11]. One immobilization technique which shows great promise for large-scale

* Corresponding author. Tel.: +353 91 493563.
E-mail address: donal.leech@nuigalway.ie (D. Leech).

1567-5394/$ – see front matter © 2011 Elsevier B.V. All rights reserved.
doi:10.1016/j.bioelechem.2011.11.011

manufacture is incorporation of biocatalysts into conducting inks. This technique has been realized for biosensors, where screen-printing techniques can be used to produce inexpensive, disposable biosensors for a wide range of different analytes [12–14]. Inks and printing provide a large scope for future research with new techniques like ink-jet printing [15,16] leading to more accurate and reproducible printing, as well improvements in response and stability resulting from the development of different ink compositions and ink additives [17–20].

By selecting suitable biocatalysts for anode and cathode, printed enzyme-based electrodes can be coupled together to produce a fully enzymatic printed biofuel cell. Printed hybrid EFCs have been constructed using printed zinc-based anodes coupled to a printed biocathode using *Trametes hirsuta* laccase (*Th*L) and 2,2′-azino-bis(3-ethylbenzthiazoline-6-sulfonic acid) (ABTS) as the cathodic mediator [21]. This fuel cell under humidity-controlled conditions could maintain a cell voltage between 0.6 and 0.8 V for several days under a 2.2 kΩ load. In a 'stand alone' biobattery configuration a cell was shown to be capable of maintaining a cell voltage of 0.7 V for 15 h under a load of 2.2 kΩ. More recently a fully enzymatic glucose/oxygen printed fuel cell has been developed [22] with the zinc anode replaced by printed ALDH anodes, and glucose oxidation mediated by either an osmium–polypyridyl complex or N,N,N′,N′-tetramethyl-phenylenediamine (TMPD). The highest power output in the biobattery configuration was achieved for a printed EFC containing ABTS as the cathode mediator, whilst the longest operational stability of the printed EFC under a 75 kΩ load was achieved using osmium-based mediators.

In this report, we extend evaluation of printed EFCs by investigating performance of EFCs prepared using two anode biocatalysts, ALDH and GOx, coupled to a printed *Th*L based oxygen-reducing cathode mediated by ABTS. The biocatalysts were incorporated into a conductive ink with a selection of different mediators and evaluated for application towards a fully enzymatic printed glucose/oxygen fuel cell.

2. Materials and methods

2.1. Materials

All chemicals and biochemicals were, unless otherwise stated, purchased from Sigma Aldrich and used as received. Carbon-based, water soluble ink was obtained from DuPont (Carbon 5067). Carbon nanotubes (multiwall, diameter 10–30 nm, purity > 80%) were purchased from Hydrocell. ALDH and *Th*L were produced and purified at VTT as described previously [5,6,23]. ALDH was identified as the 87.3 kDa quinoprotein glucose dehydrogenase P27175. The enzyme did not require added coenzyme for activity and could oxidize -glucose, -xylose, -galactose, -mannose and -arabinose. The enzyme had a molecular mass of 87 kDa and appeared as a single polypeptide.

Synthesis of the redox complexes was achieved using $(NH_4)_2OsCl_6$ as a starting material to prepare the *cis*-Os $(bpy)_2Cl_2$ (where, bpy = 2,2′-bipyridine), *cis*-Os $(dmobpy)_2Cl_2$ (where, dmbpy = 4,4′-dimethyl-2,2′-bipyridine), *cis*-Os $(dmobpy)_2Cl_2$ (where, dmobpy = 4,4′-dimethoxy-2,2′-bipyridine) complexes, and the subsequent ligand substitution of one of the chlorines with 4-aminomethylpyridine (4AMP) to yield the desired redox system, according to literature methods [24]. All buffers were prepared from solutions of the selected base then adjusted to the desired pH using solutions of the acid.

2.2. Enzymatic activity assays

The enzymatic activity of GOx and ALDH was calculated using spectrophotometric activity assays. For GOx the absorbance was monitored at 460 nm, where the increase in absorbance is a result of the oxidation of dianisidine through a peroxidase coupled system, using an extinction coefficient of 11,300 M^{-1} cm^{-1}, in phosphate buffer pH 6 [25]. For ALDH the absorbance was monitored at 600 nm, using phenazine methosulfate and dichlorophenol indophenol and an extinction coefficient of 21,000 M^{-1} cm^{-1}, in phosphate buffer pH 6 [4].

2.3. Preparation of inks and coatings

Biocatalytic inks were prepared by mixing carbon nanotubes (0.17 mg carbon nanotubes per mg dry carbon ink), enzyme (0.21 nkat per mg dry carbon ink, selected to achieve ~1 nkat cm^{-2} of electrode area) diluted in appropriate buffer (50 mM phosphate buffer pH 6 for ALDH and GOx and 50 mM succinate buffer pH 4.5 for *Th*L) and mediator (0.05 mmol for 400 nkat of enzyme, giving ~26 nmol mediator per mg dry carbon ink). Carbon nanotubes were added to enhance ink porosity and improve conductivity. The consistency of the ink was adjusted by addition of appropriate buffer. Coating was performed using a K Hand Coater (RK Print Coat Instruments Ltd) producing a wet layer of 40 μm, and filter paper (Whatman 1) was used as the substrate.

2.4. Electrochemical measurements

Solution phase experiments were performed using a CH Instruments 650 potentiostat containing an Ag/AgCl reference electrode (Bioanalytical System), a platinum counter electrode (Goodfellow) and a 3 mm Teflon-shrouded glassy carbon working electrode (IJ Cambria).

Printed fuel cell measurements were performed using two different configurations as described previously [20,21,26]. In power density plots with varying load a configuration with 6.25 cm^2 (2.5 × 2.5 cm) surface area was used. The cell was sandwiched between graphite plates and a dialysis membrane (cutoff 12–14 kDa, Medicell International Ltd) was used as a separator, as shown in Fig. 1. The anodic and cathodic potentials were measured with VMP® multichannel

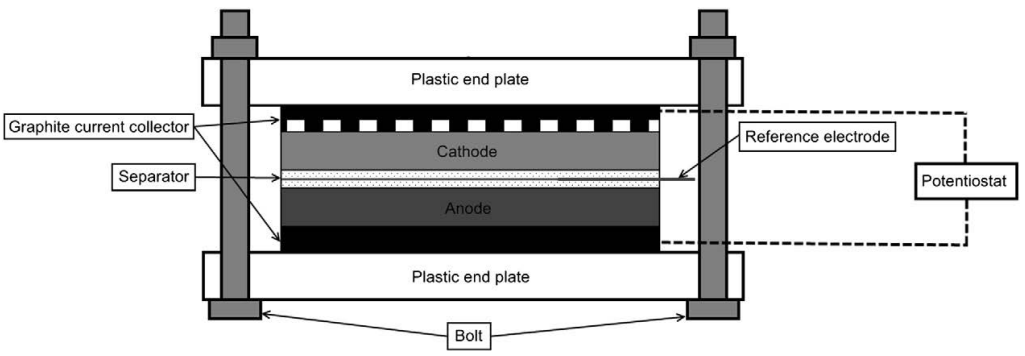

Fig. 1. Schematic of the three electrode system using the palladium-hydrogen reference, sandwiched between dialysis membrane.

potentiostat (Bio-Logic SAS) using three-electrode connection with a thin foil Pd–H_2 as a reference [26] and 200 μL of 50 mM succinate buffer pH 5, containing 25 mg of glucose powder as fuel was used to wet the biocatalytic prints. The open circuit voltage was monitored for 40 min, to ensure the system was stable, before 0.2 μA of current was drawn every minute until the cell voltage reached 0 V.

The cell was also operated in a 'stand alone' biobattery configuration, as described previously [20,21,26], where the anodic and cathodic prints (3.5 × 3.5 cm) were separated by dialysis membrane and sandwiched between two graphite plates all wetted by the electrolyte, Fig. 1. This configuration only differs from the previous cells in that there is no reference electrode and the size of the biocatalytic prints was increased. Due to the increase in print size the amount of electrolyte was increased to 400 μL of 50 mM succinate buffer pH 5, containing 50 mg of glucose powder as the fuel. After assembly the cells were connected to the measurement apparatus consisting a PC, voltage data logger (Agilent 34970A) and a resistor stack with variable resistors allowing 20 cells be measured simultaneously. After monitoring the open cell voltage (OCV) for 90 min a constant load of 75 kΩ was applied to the cells.

3. Results and discussion

3.1. Solution phase studies

One of the most important processes in a mediated enzymatic electrode is the interaction between the mediator and the enzyme. Evaluating a relative rate constant for enzyme-mediator electron transfer kinetics in solution, as a function of the driving force, chemical structure etc., may permit selection of target enzyme and mediator combinations for further study and eventual device development. Thus the electrochemical behavior of three different anodic mediators was evaluated by estimating pseudo-first order rate constants (k_f) for mediator-enzyme interactions using the method developed by Cass et al. [27] based on the Nicholson and Shain approach [28], for interactions with a solution of constant mediator concentration (0.2 mM) and enzymatic activity (5 U mL^{-1}). The peak current of the diffusional cyclic voltammogram (CV) of the mediator in the absence of enzyme is measured at the maximum intensity (i_d). Following addition of a sufficient amount of enzyme to yield a selected activity (5 U mL^{-1}) a change in shape of the CV is observed from the tailed diffusion-controlled peaks to a sigmoidal shaped curve typical of catalysis. The higher the enzymatic oxidation or reduction rate the larger the current increase will be. This catalytic oxidation or reduction current (i_k) is also measured and the k_f value calculated from ratio of the catalytic current to diffusional current over a range of scan rates. Homogeneous mediation with the enzyme and mediator free in solution has several disadvantages and therefore applications of such systems are very limited, however, they offer an insight into electron transfer mechanisms which can be applied to other electron transfer systems. Selected CVs in glucose-containing buffer, in the absence and presence of glucose-oxidizing enzyme are shown in Fig. 2, with the corresponding estimated pseudo-first order rate constants, and current ratios, for the interaction between GOx or ALDH presented in Table 1.

From the solution phase studies the increased current ratios, and the corresponding k_f values, observed for ALDH compared to GOx for both TMPD and Os $(bpy)_2Cl_2$ indicate the potential utility of this enzyme for application to bioanodes in a fuel cell. Interestingly for the [Os $(bpy)_2$(4AMP) Cl] PF_6 mediator and ALDH, although there is an increase in potential difference between the enzyme active site and mediator, yielding an increased thermodynamic driving force for electron transfer, the observed catalytic current and k_f value are smaller than that for the other mediators of lower redox potential (driving force). On the other hand GOx oxidation of glucose, mediated by [Os $(bpy)_2$(4AMP) Cl] PF_6, yields the largest current ratio and k_f value of all mediators tested here. However, use of mediators with such relatively high redox potentials is not compatible with an oxygen-reducing biofuel cell that can generate a useful cell voltage output.

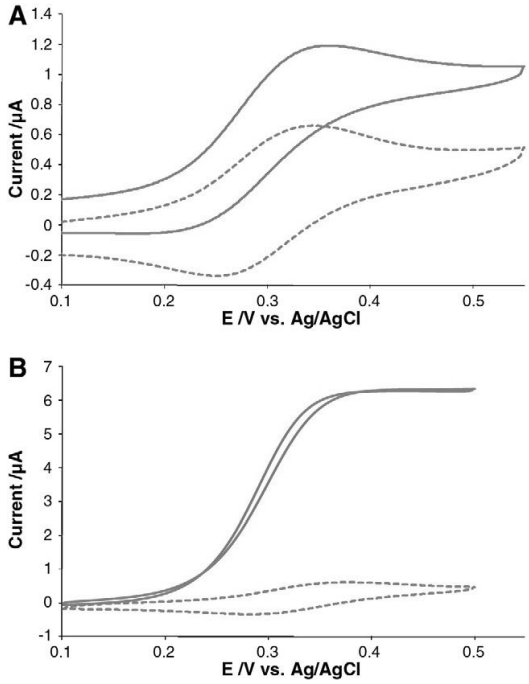

Fig. 2. CVs recorded in phosphate buffer, 5% DMSO, pH 7, 100 mM glucose at a scan rate of 5 mVs^{-1} for [Os $(bpy)_2$(AMP) Cl] PF_6 (0.2 mM) in the presence (solid) and absence (dotted) of 5 U mL^{-1} of ALDH (A) or GOx (B).

3.2. Performance of the printed ALDH anodes in the fuel cell construction

To test biofuel cell performance, ALDH was selected as the initial anodic biocatalyst and incorporated into inks with TMPD, Os $(dmbpy)_2Cl_2$, Os $(bpy)_2Cl_2$, [Os $(dmobpy)_2$(4AMP) Cl] PF_6 and [Os $(bpy)_2$(4AMP) Cl)]PF_6 as mediators. The printed anodes were coupled to printed cathodes containing *Th*L, mediated by ABTS, and the performance of the cells was evaluated, Table 2. Whilst the solution phase measurements were carried out at the optimal pH for ALDH and GOx, a compromise is required for the full EFC, as *Th*L has pH optimum of 4.5 [11,22]. Use of a succinate buffer, pH 5, was selected for this initial study, although the effect of identity and pH of the electrolyte should be investigated in order to fully optimize this system. Power density curves for each printed biofuel cell combination, except that of ALDH/ [Os $(dmobpy)_2$(4AMP) Cl] PF_6 due to the low power density it provided, are shown in Fig. 3.

A maximum OCV of approximately 0.6 V is observed with Os $(bpy)_2Cl_2$ as the anodic mediator. The decrease in OCV compared to a previously reported printed hybrid biofuel cell containing a Zn-based printed anode [21] corresponds to substituting the Zn-based

Table 1
Redox potential, estimated rate constant (k_f) and the ratio of catalytic to diffusional current (at a scan rate of 5 mVs^{-1}) for mediated glucose oxidation by 5 U mL^{-1} of either GOx or ALDH for different mediators (0.2 mM each). Conditions as in Fig. 1.

Mediator/0.2 mM	Redox potential/ mV *vs* Ag/AgCl	ALDH		GOx	
		k_f/s^{-1}	Current ratio	k_f/s^{-1}	Current ratio
Os $(bpy)_2Cl_2$	0	4.4	2.0	0.02	1.1
TMPD	70	8.9	3.3	0.04	1.3
[Os $(bpy)_2$(4AMP) Cl] PF_6	240	0.6	1.4	27	12.5

Table 2
Table of performance of biofuel cells using prints containing ALDH or GOx and anodic mediator, coupled to a printed *Th*L cathode mediated by ABTS. Conditions as in Figs. 2 and 3.

Anode enzyme	Anode mediator	Anode mediator redox potential/mV vs Ag/AgCl	Power density/μW/cm^2	Voltage at max power/V
ALDH	Os $(dmbpy)_2Cl_2$	−100	0.25	0.32
ALDH	Os $(bpy)_2Cl_2$	0	3.5	0.32
ALDH	TMPD	70	1.7	0.34
ALDH	[Os $(dmobpy)_2$(4AMP) Cl] PF_6	80	0.16	0.27
ALDH	[Os $(bpy)_2$(4AMP) Cl] PF_6	240	0.23	0.27
GOx	Os $(bpy)_2Cl_2$	0	0.17	0.24
GOx	TMPD	70	0.28	0.25
GOx	[Os $(bpy)_2$(4AMP) Cl] PF_6	240	0.11	0.24

printed anode, redox potential of ~−960 mV (*vs.* Ag/AgCl), with ALDH redox potential of ~−110 mV (*vs.* Ag/AgCl). A maximum power output of 3.5 μW cm^{-2} at a voltage of 0.32 V is achieved from a cell constructed from ALDH/Os $(bpy)_2Cl_2$ coupled to *Th*L/ABTS under the selected conditions. A cell constructed using ALDH/TMPD instead of ALDH/Os $(bpy)_2Cl_2$ generated only half the maximum power output, 1.7 μW cm^{-2} at a voltage of 0.35 V. For comparison, printed fuel cells assembled using conductive inks containing ABTS and TMPD mediators, but no biocatalysts, generated maximum power density of 0.045 μW cm^{-2} (not shown). Whilst a slight increase in maximum power density was observed using a TMPD mediated ALDH anode connected to an ABTS (no biocatalyst) cathode, the power generated is over 25 times smaller than that generated from inks containing biocatalyst and those mediators at both anode and cathode.

Printed biofuel cells assembled using other osmium-based mediators of ALDH all yielded maximum power densities lower than 0.26 μW cm^{-2}. The trend shows good agreement with the preliminary solution phase studies, where despite the increased thermodynamic driving force between [Os $(bpy)_2$(4AMP) Cl] PF_6 and ALDH the catalytic current for glucose oxidation diminishes compared to that observed for TMPD and Os $(bpy)_2Cl_2$.

3.3. Performance of the printed GOx anodes in the fuel cell construction

A printed biofuel cell using GOx was considered as an alternative, as GOx has a lower active site redox potential compared to ALDH, opening the possibility for use of mediators of lower redox potential, increasing the overall cell voltage output. GOx was incorporated into inks to form printed anodes, with TMPD, Os $(bpy)_2Cl_2$ and [Os $(bpy)_2$(4AMP) Cl] PF_6 as the mediators. Power density curves for printed biofuel cell combinations of GOx anodes coupled to printed cathodes containing *Th*L, mediated by ABTS are shown in Fig. 4 with the performance of the cells in Table 2. The power output of GOx printed biofuel cells for TMPD and Os $(bpy)_2Cl_2$ was lower than the corresponding cells containing ALDH. The sensitivity to O_2 and the subsequent production of H_2O_2 could have a significant effect on the performance of GOx based prints, as could the relative accessibility of the active site to the mediator. Moreover, our recent studies (unpublished) indicate incompatibility between GOx and the filter paper used as a printing substrate. Whilst the [Os $(bpy)_2$(4AMP) Cl] PF_6 mediator yielded high catalytic currents for glucose oxidation when used with GOx in solution phase, the printed biofuel cell using this enzyme/mediator combination resulted in the lowest observed power density of the combinations tested: 0.11 μW cm^{-2} at 0.24 V.

3.4. Performance of the printed anodes under constant load

The performance of the biofuel cells was also evaluated in a 'stand alone' configuration, with removal of the reference electrode and an increased anodic and cathodic print size area of 12.25 cm^2 using 400 μL succinate buffer, pH 5 containing 694 mM glucose as the electrolyte and operated under a constant load of 75 kΩ. The cell voltage was monitored, and the time taken for the cell voltage to decrease below a 200 mV threshold was recorded. The resistance and threshold voltage were chosen in relation to the power demands of potential applications, including active displays, sensors and radio frequency identity tags [29]. Plots of cell voltage against time for selected cells are shown in Fig. 5, and Table 3 lists the cell performance as a function of the anodic prints evaluated in the 'stand alone' configuration under a constant load, giving the time taken for the cell voltage to decrease below 200 mV and the corresponding energy content.

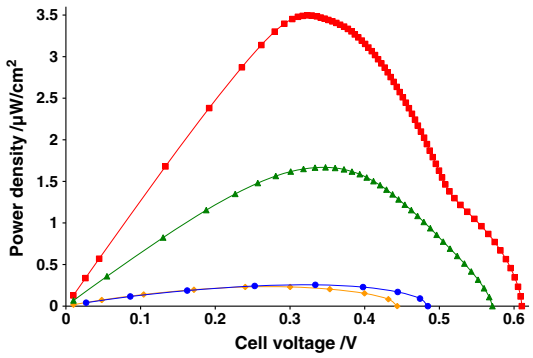

Fig. 3. Power curves derived from monitoring the cell voltage as 0.2 μA of current is drawn each minute for printed biofuel cells using *Th*L and ABTS as a cathode and, ALDH and either Os $(bpy)_2Cl_2$ (■), TMPD (▲), Os $(dmbpy)_2Cl_2$ (●) or [Os $(bpy)_2$(4-AMP) Cl] PF_6 (♦) as an anode, with 200 μL succinate buffer, pH 5, and 694 mM glucose as fuel.

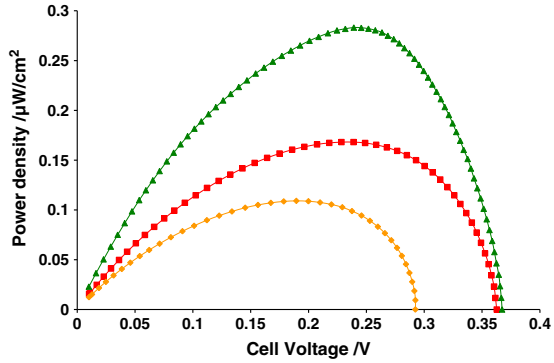

Fig. 4. Power curves derived from monitoring the cell voltage as 0.2 μA of current is drawn each minute for printed biofuel cells using *Th*L and ABTS as a cathode and, GOx mediated by either Os $(bpy)_2Cl_2$ (■), TMPD (▲) or [Os $(bpy)_2$(4AMP) Cl] PF_6 (♦) as an anode, with 200 μL succinate buffer, pH 5, and 694 mM glucose as fuel.

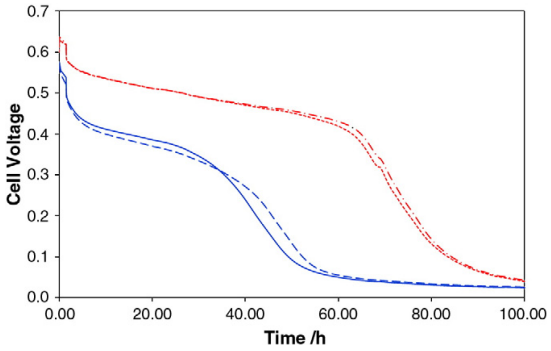

Fig. 5. Performance of 'stand alone' biofuel cells constructed from an ABTS mediated *Th*L cathode coupled to a ALDH anode mediated by either Os $(bpy)_2Cl_2$ (red) or TMPD (blue). OCV monitored for 90 min before cells were placed on a 75 kΩ load.

From these results there appears to be two different systems that show promise for further development. One system could consist of a printed biofuel cell that can maintain a cell voltage over 200 mV, under a relatively small load (75 kΩ), for a relatively long time period. When considering this possibility, the ALDH/TMPD: *Th*L/ABTS cell shows promise, taking approximately 74 h for the cell voltage to drop below 200 mV. The lifetime could be prolonged slightly by further wetting of the prints, indicating that voltage loss may be due to drying of the printed cell, in this configuration. The second system produces higher energy content but over a more limited lifetime. For example, ALDH/Os $(bpy)_2Cl_2$: *Th*L/ABTS cells show promise producing the highest energy content of approximately 14 μW h cm^{-2}, but over a lifetime of only 47 h. The second highest energy content was observed for ALDH/TMPD: *Th*L/ABTS cells producing an average of 8.5 μW h cm^{-2}, but with the advantage of being able to maintain a cell voltage, under a load, above the threshold voltage of 200 mV for 27 h longer than the ALDH/Os $(bpy)_2Cl_2$: *Th*L/ABTS cell. The reasons for the decrease in power of these cells cannot be determined from this experimental setup, but is likely to result from mediator instability and/or loss of activity of the enzyme biocatalysts. Whilst using small volumes of electrolyte helps to prevent the components from leaking from the cell, drying of the electrolyte can contribute to power loss. As the anodes are coupled to an enzymatic printed cathode the eventual loss in cell power can neither be attributed solely to anode instability with, for example issues with stability of ABTS as a laccase mediator previously highlighted [21,30]. None of the other mediators tested shows promise in the printed ALDH anode for this application/threshold setting. For example, although a cell constructed using an ALDH/[Os $(dmbpy)_2$(4-AMP) Cl] PF_6 anode took over 30 h for the cell voltage to decrease below the threshold voltage of 200 mV the resulting energy content was only 2.5 μW h cm^{-2}, approximately 5 times lower than the printed ALDH anodes mediated by TMPD and Os $(bpy)_2Cl_2$. Despite the power densities generated being smaller than several previously reported systems, they are sufficient to power simple electronic devices. Further cell optimization should focus on investigation into the mediator-enzyme-ink ratios, as well as improvement in both power generated and stability by using different ink additives and printing substrates.

Table 3
List of the different cells tested, time taken for the cell voltage to decrease below 200 mV and the energy content estimated over this time for the cell.

Anode coupled to ThL/ABTS printed cathode	V > 200 mV/h	Energy content/ μW h cm^{-2}
ALDH/TMPD	74.1 (±0.7)	8.5 (±4.9)
ALDH/[Os $(dmobpy)_2$(4AMP) Cl] PF_6	24.5 (±8.3)	1.9 (±0.6)
ALDH/[Os $(dmbpy)_2$(4AMP) Cl] PF_6	30.6	2.5
ALDH/[Os $(bpy)_2$(4AMP) Cl] PF_6	23.8 (±5.0)	2.1 (±0.4)
ALDH/Os $(bpy)_2Cl_2$	47.4 (±15.5)	14.5 (±5.5)
ALDH/Os $(dmobpy)_2Cl_2$	30.2	3.3
ALDH/Os $(dmbpy)_2Cl_2$	36.9	3.9
GOx/ferrocenemethanol	0.9	0.02
GOx/TMPD	2.0 (±0.3)	0.12 (±0.03)
GOx/[Os $(dmobpy)_2$(4AMP) Cl] PF_6	0.9	0.02
GOx/Os $(bpy)_2Cl_2$	0.8	0.02

GOx based inks were also tested in 'stand alone' cells, Table 3. As with the previous experiments the inks containing GOx performed poorly compared to the ALDH inks with many of the cell voltages decreasing below the 200 mV threshold voltage as soon as a load was applied. Even the best performing cell, based on a printed GOx/TMPD anode, was only able to maintain a cell voltage above 200 mV for 2 h producing an energy content of only 0.12 μW h cm^{-2}, significantly smaller than that observed with the ALDH anodes.

4. Conclusions

These results indicate that GOx is unsuitable for the application as an anodic enzyme for a fully enzymatic printed biofuel cell under the experimental criteria used in this study. In contrast inks containing ALDH mediated by TMPD and Os $(bpy)_2Cl_2$ show promise, generating energy content over a reasonable lifetime. Further studies are required to optimize the power output, and to understand the factors that limit the operational lifetime of these fully enzymatic printed biofuel cells, leading to improved printed EFC devices.

Acknowledgments

Support for this research was provided by an EU FP6 BIOMEDNANO EU STREP, contract NMP4-CT-2006-017350.

References

[1] S.C. Barton, J. Gallaway, P. Atanassov, Enzymatic biofuel cells for implantable and microscale devices, Chem. Rev. 104 (2004) 4867–4886.
[2] F. Davis, S.P.J. Higson, Biofuel cells — recent advances and applications, Biosens. Bioelectron. 22 (2007) 1224–1235.
[3] S.D. Minteer, B.Y. Liaw, M.J. Cooney, Enzyme-based biofuel cells, Curr. Opin. Biotechnol. 18 (2007) 228–234.
[4] J. Buchert, A xylose-oxidizing membrane-bound aldose dehydrogenase of Gluconobacter oxydans ATCC 621, J. Biotechnol. 18 (1991) 103–113.
[5] M. Smolander, J. Buchert, L. Viikari, Large-scale applicable purification and characterization of a membrane-bound PQQ-dependent aldose dehydrogenase, J. Biotechnol. 29 (1993) 287–297.
[6] K. Matsushita, E. Shinagawa, O. Adachi, M. Ameyama, Quinoprotein d-glucose dehydrogenase of the *Acinetobacter calcoaceticus* respiratory chain: membrane-bound and soluble forms are different molecular species, Biochemistry 28 (1989) 6276–6280.
[7] M. Smolander, G. Marko-Varga, L. Gorton, Aldose dehydrogenase-modified carbon paste electrodes as amperometric aldose sensors, Anal. Chim. Acta 302 (1995) 233–240.
[8] P. Peralta-Zamora, C.M. Pereira, E.R.L. Tiburtius, S.G. Moraes, M.A. Rosa, R.C. Minussi, N. Durán, Decolorization of reactive dyes by immobilized laccase, Appl. Catal., B 42 (2003) 131–144.
[9] S. Timur, N. Pazar-loglu, R. Pilloton, A. Telefoncu, Thick film sensors based on laccases from different sources immobilized in polyaniline matrix, Sens. Actuators, B 97 (2004) 132–136.
[10] B.A. Gregg, A. Heller, Redox polymer films containing enzymes. 2. Glucose oxidase containing enzyme electrodes, J. Phys. Chem. 95 (1991) 5976–5980.
[11] P.A. Jenkins, S. Boland, P. Kavanagh, D. Leech, Evaluation of performance and stability of biocatalytic redox films constructed with different copper oxygenases and osmium-based redox polymers, Bioelectrochemistry 76 (2009) 162–168.
[12] M. Albareda-Sirvent, A. Merkoçi, S. Alegret, Configurations used in the design of screen-printed enzymatic biosensors. Sensors and Actuators B: Chemical 69 (2000) 153–163.
[13] C. Zhang, Q. Gao, M. Aizawa, Flow injection analytical system for glucose with screen-printed enzyme biosensor incorporating Os-complex mediator, Anal. Chim. Acta 426 (2001) 33–41.
[14] C. Zhang, T. Haruyama, E. Kobatake, M. Aizawa, Disposable electrochemical capillary-fill device for glucose sensing incorporating a water-soluble enzyme/mediator layer, Anal. Chim. Acta 442 (2001) 257–265.
[15] L. Setti, A. Fraleoni-Morgera, B. Ballarin, A. Filippini, D. Frascaro, C. Piana, An amperometric glucose biosensor prototype fabricated by thermal inkjet printing, Biosens. Bioelectron. 20 (2005) 2019–2026.

[16] L. Setti, A. Fraleoni-Morgera, I. Mencarelli, A. Filippini, B. Ballarin, M. Di Biase, An HRP-based amperometric biosensor fabricated by thermal inkjet printing, Sens. Actuators, B 126 (2007) 252–257.
[17] A.L. Hart, W.A. Collier, Stability and function of screen printed electrodes, based on cholinesterase, stabilised by a co-polymer/sugar alcohol mixture, Sens. Actuators, B 53 (1998) 111–115.
[18] A.L. Hart, H. Cox, D. Janssen, Stabilization of lactate oxidase in screen-printed enzyme electrodes, Biosens. Bioelectron. 11 (1996) 833–837.
[19] G.A.M. Mersal, M. Khodari, U. Bilitewski, Optimisation of the composition of a screen-printed acrylate polymer enzyme layer with respect to an improved selectivity and stability of enzyme electrodes, Biosens. Bioelectron. 20 (2004) 305–314.
[20] J.T. Schumacher, I. Münch, T. Richter, I. Rohm, U. Bilitewski, Investigations with respect to stabilization of screen-printed enzyme electrodes, J. Mol. Catal. B: Enzym. 7 (1999) 67–76.
[21] M. Smolander, H. Boer, M. Valkiainen, R. Roozeman, M. Bergelin, J.E. Eriksson, X.C. Zhang, A. Koivula, L. Viikari, Development of a printable laccase-based biocathode for fuel cell applications, Enzyme Microb. Technol. 43 (2008) 93–102.
[22] P. Jenkins, S. Tuurala, A. Vaari, M. Valkiainen, M. Smolander, D. Leech, A mediated glucose/oxygen enzymatic fuel cell based on printed carbon inks containing aldose dehydrogenase and laccase as anode and cathode, Enzyme Microb. Technol. 50 (2012) 181–187.
[23] K. Rittstieg, A. Suurnakki, T. Suortti, K. Kruus, G. Guebitz, J. Buchert, Investigations on the laccase-catalyzed polymerization of lignin model compounds using size-exclusion HPLC, Enzyme Microb. Technol. 31 (2002) 403–410.
[24] E.M. Kober, J.V. Casper, B.P. Sullivan, T.J. Meyer, Synthetic routes to new polypyridyl complexes of osmium (II), Inorg. Chem. 27 (1988) 4587–4598.
[25] Worthington web-pages, http://www.worthington-biochem.com/GOP/assay.html2011.
[26] S. Tuurala, M. Smolander, J. Uotila, O.V. Kaukoniemi, H. Boer, M. Valkiainen, A. Vaari, A. Koivula, P. Jenkins, Performance of a printable enzymatic fuel cell: study on mediated ThL laccase cathode, ECS Trans. 25 (2010) 1–10.
[27] A.E.G. Cass, G. Davis, G.D. Francis, H.A.O. Hill, W.J. Aston, I.J. Higgins, E.V. Plotkin, L.D.L. Scott, A.P.F. Turner, Ferrocene-mediated enzyme electrode for amperometric determination of glucose, Anal. Chem. 56 (1984) 667–671.
[28] R.S. Nicholson, I. Shain, Theory of stationary electrode polarography. Single scan and cyclic methods applied to reversible, irreversible, and kinetic systems, Anal. Chem. 36 (1964) 706–723.
[29] A.K. Jones, R.R. Hoare, S.R. Dontharaju, S. Tung, R. Sprang, J. Fazekas, J.T. Cain, M.H. Mickle, An automated, reconfigurable, low-power RFID tag, Proceedings of the 43rd annual Design Automation Conference, ACM, San Francisco, CA, USA, 2006.
[30] J. Li, L.S. Chia, N.K. Goh, S.N. Tan, Silica sol-gel immobilized amperometric biosensor for the determination of phenolic compounds, Anal. Chim. Acta 362 (1998) 203–211.

III

Jenkins, P., Tuurala, S., Vaari, A., Valkiainen, M., Smolander, M., and Leech, D. (2012) A mediated glucose/oxygen enzymatic fuel cell based on printed carbon inks containing aldose dehydrogenase and laccase as anode and cathode. *Enzyme and microbial technology* ***50(3)***, 181-187.

DOI: 10.1016/j.enzmictec.2011.12.002

Enzyme and Microbial Technology 50 (2012) 181–187

Contents lists available at SciVerse ScienceDirect

Enzyme and Microbial Technology

journal homepage: www.elsevier.com/locate/emt

A mediated glucose/oxygen enzymatic fuel cell based on printed carbon inks containing aldose dehydrogenase and laccase as anode and cathode

Peter Jenkins [a], Saara Tuurala [b], Anu Vaari [b], Matti Valkiainen [b], Maria Smolander [b], Dónal Leech [a,*]

[a] School of Chemistry, National University of Ireland Galway, University Road, Galway, Ireland
[b] VTT Technical Research Centre of Finland, P.O. Box 1000, FI-02044 VTT, Finland

ARTICLE INFO

Article history:
Received 6 July 2011
Accepted 12 December 2011

Keywords:
Biofuel cell
Printing
Enzyme
Laccase
Aldose dehydrogenase
Mediator
Ink

ABSTRACT

Enzyme electrodes show great potential for many applications, as biosensors and more recently as anodes and cathodes in biocatalytic fuel cells for power generation. Enzymes have advantages over metal catalysts, as they provide high specificity and reaction rates, while operating under mild conditions. Here we report on studies related to development of mass-producible, completely enzymatic printed glucose/oxygen biofuel cells. The cells are based on filter paper coated with conducting carbon inks containing mediators and laccase, for reduction of oxygen, or aldose dehydrogenase, for oxidation of glucose. Mediator performance in these printed formats is compared to relative rate constants for the enzyme–mediator reaction in solution, for a range of anode and cathode mediators. The power output and stability of fuels cells using an acidophilic laccase isolated from *Trametes hirsuta* is greater, at pH 5, than that for cells based on *Melanocarpus albomyces* laccase, that shows optimal activity closer to neutral pH, at pH 6. Highest power output, although of limited stability, was observed for *Th*L/ABTS cathodes, providing a maximum power density of 3.5 $\mu W\,cm^{-2}$ at 0.34 V, when coupled to an ALDH glucose anode mediated by an osmium complex. The stability of cell voltage above a threshold of 200 mV under a moderate 75 kΩ load is used to benchmark printed fuel cell performance. Highest stability was obtained for a printed fuel cell using osmium complexes as mediators of glucose oxidation by aldose dehydrogenase, and oxygen reduction by *T. hirsuta* laccase, maintaining cell voltage above 200 mV for 137 h at pH 5. These results provide promising directions for further development of mass-producible, completely enzymatic, printed biofuel cells.

1. Introduction

Biological fuel cells are devices which are capable of transforming chemical energy to electrical energy involving biochemical pathways, using biomolecules such as enzymes or whole cells as the catalyst. Traditional fuel cells use expensive, transition metals with broad specificity as catalysts. Utilizing biological fuel cells for development of cheap disposable power sources for numerous applications has lead to increased attention in this area over recent years [1–3]. For example, diverse enzymes are available to catalyze oxidation of a wide range of fuels and enzymes can be highly specific, relatively cheap and generally operate under mild conditions, making them suitable biocatalysts for many applications.

One of the most widely studied biofuel cells is the glucose/O_2 system, typically using glucose oxidase (GOx) or glucose dehydrogenase combined with blue multi-copper oxygenases (BMCOs) such as laccases or bilirubin oxidases as the anode and cathode biocatalysts, respectively. For many applications the enzyme has to be immobilized, either alone or co-immobilized with a redox mediator. Mediators are artificial electron transferring agents (co-substrates) that can participate in redox reactions with the enzyme and help in the rapid transfer of electrons to and from the electrode. Research on immobilization of both enzyme and mediator has focused on physical adsorption, entrapment in electro-polymerized matrices and use of crosslinkers to form biocatalytic redox polymer hydrogels. An alternative method of immobilization involves incorporation of biomolecules into conductive inks. Biomolecules can be incorporated into conductive inks and sequentially deposited onto a substrate to produce low-cost, high-performance electrodes, using screen [4–6] or inkjet printing [7,8]. These methods have become of great interest in recent years due to the wide range of biomolecules and possible substrate materials available. More often than not the biomolecules are enzymes and disposable biosensors based on enzyme immobilized printed electrodes have been widely used for analysis of many enzyme substrates.

* Corresponding author. Tel.: +353 91493563; fax: +353 91525700.
E-mail addresses: pete175260@hotmail.co.uk (P. Jenkins), Saara.Tuurala@vtt.fi (S. Tuurala), Anu.Vaari@vtt.fi (A. Vaari), Matti.Valkiainen@vtt.fi (M. Valkiainen), Maria.Smolander@vtt.fi (M. Smolander), donal.leech@nuigalway.ie (D. Leech).

0141-0229/$ – see front matter © 2011 Elsevier Inc. All rights reserved.
doi:10.1016/j.enzmictec.2011.12.002

Printable biocatalytic inks offer advantages for mass-produced, cost-effective, reproducible enzymatic electrodes. For example, numerous biosensors have been developed for the analysis of glucose in clinical samples. The majority of these biosensors incorporate GOx as the biomolecule with a range of mediators, including tetrathiafulvalene [9], Prussian blue [10], hexaammineruthenium (III) chloride [11] and ferrocene and its derivatives [12]. Osmium complexes have also been widely used in the development of GOx-based screen printed electrodes [5,6,13].

An alternative to screen printing is inkjet printing and is fast emerging as an attractive manufacturing tool. Inkjet printing allows for the deposition of very small droplets onto virtually any surface, with a precision and reproducibility higher than that of screen printing [7]. Examples of biosensors fabricated in this way incorporating biocatalysts, including GOx and horseradish peroxidase have been presented in the literature [7,8], including different approaches to improve stability of the biocatalyst using ink additives [14–17]. To date nearly all the research on biocatalytic inks has focused on the production of biosensors, with a limited amount of work on the development of printable bioanodes and biocathodes for application to printed biofuel cells. Smolander et al. [18,19] reported on the performance of a printable oxygen-reducing biocathode based on the high redox potential fungal laccase from *Trametes hirsuta* (*Th*L). Laccases can be sourced from many different sources, including plants and fungi and oxidize a broad range of substrates coupled to four electron reduction of O_2 to water. Use of *Th*L was evaluated in different types of conducting inks using 2,2′-azino-bis(3-ethylbenzthiazoline-6-sulfonic acid) (ABTS) as the redox mediator [18]. Approximately 70% of the *Th*L activity was retained after heat treatment indicating a tolerance to different printing and drying processes. The properties of the printed biocathode were optimized by varying the ink composition and printing substrate. Improvements in performance could be achieved by selection of a printing substrate which maximizes the surface area of the ink and by optimizing the ink matrix structure. A prototype fuel cell was constructed using this printable laccase-based ink as the cathode and a printed Zn layer as the anode. Under humidity-controlled conditions a cell voltage between 0.8 and 0.6 V could be maintained for several days under a 2.2 kΩ load. Also a 'stand alone' configuration was shown to be able to maintain a cell voltage of 0.7 V for 15 h under a load of 2.2 kΩ [18].

A key characteristic of laccases is the standard reduction potential of the substrate-oxidizing T1 copper site [20–22]. In general plant laccases possess low T1 potential (~0.23 V *vs.* Ag/AgCl), while fungal laccases possess T1 sites of either mid range (~0.23–0.51 V *vs.* Ag/AgCl) or high range (~0.58 *vs.* Ag/AgCl) [1,20,21]. BMCOs with high T1 potentials show promise as biocatalysts for the oxygen reduction reaction in biofuel cell applications. A major drawback is that the optimum activity for high potential laccases is observed at low pH (<5.0) [20–22]. A number of laccases have been produced that display optimal activity closer to neutral pH, such as that isolated from *Melanocarpus albomyces* (r*Ma*L) [23,24]. However, increased activity at neutral pH comes at a cost, as the redox potential of T1 copper site of this laccase is in the low range (~0.27 V *vs.* Ag/AgCl).

The work presented here evaluates the performance of printed biocathodes using either *Th*L or r*Ma*L coupled to a printed bioanode using a glucose-oxidizing PQQ-dependent aldose dehydrogenase (ALDH) [25], mediated by a selection of inorganic and organic mediators, with the aim to produce the first reported fully enzymatic printable biofuel cell.

2. Materials and methods

2.1. Materials

All chemicals and biochemicals were, unless otherwise stated, purchased from Sigma–Aldrich and used as received. Carbon-based, water soluble ink was obtained from DuPont (Carbon 5067). Carbon nanotubes (multiwall, diameter 10–30 nm, purity > 80%) were purchased from hydrocell. ALDH, *Th*L and r*Ma*L were produced and purified in VTT as previously described [24–26].

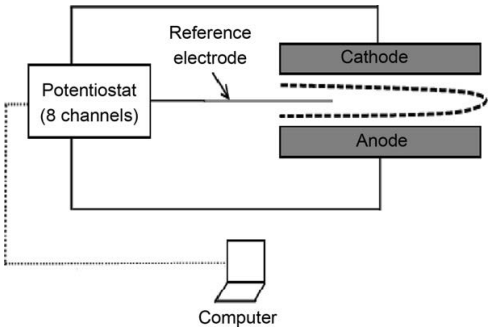

Fig. 1. Schematic of the three electrode system using the palladium–hydrogen reference, sandwiched between dialysis membrane.

Synthesis of the redox complexes was achieved using $(NH_4)_2OsCl_6$ as a starting material to prepare the *cis*-$Os(bpy)_2Cl_2$ (where, bpy = 2,2′-bipyridine), *cis*-$Os(dmbpy)_2Cl_2$ (where, dmbpy = 4,4′-dimethyl-2,2′-bipyridine), *cis*-$Os(dcbpy)_2Cl_2$ (where, dcbpy = 4,4′-dichloro-2,2′-bipyridine) complexes, and the subsequent ligand substitution of one of the chlorines with 4-aminomethylpyridine (4AMP) to yield the desired redox systems, according to literature methods [27]. All buffers were prepared from solutions of the selected base, then adjusted to the desired pH using solutions of the acid.

2.2. Preparation of inks and coatings

Biocatalytic inks were prepared by mixing carbon nanotubes (0.17 mg carbon nanotubes per mg dry carbon ink), enzyme (0.21 nkat per mg dry carbon ink, selected to achieve ~1 nkat cm^{-2} of electrode area) diluted in appropriate buffer (50 mM phosphate buffer pH 6 for ALDH, 50 mM succinate buffer pH 4.5 for *Th*L and 50 mM phosphate buffer pH 6.5 for r*Ma*L) and mediator (0.05 mmol for 400 nkat of enzyme, giving ~26 nmol mediator per mg dry carbon ink). Carbon nanotubes were used to enhance ink porosity and improve conductivity [18,19]. The consistency of the ink was adjusted by addition of the appropriate buffer. Coating was performed using a K Hand Coater (RK Print Coat Instruments Ltd) producing a wet ink layer of 40 μm, and filter paper (Whatman 1) was used as the printing substrate.

2.3. Electrochemical measurements

Solution phase experiments were performed using a CH Instruments 650 potentiostat connected to a cell containing an Ag/AgCl reference electrode (Bioanalytical System), a platinum counter electrode (Goodfellow) and a 3 mm Teflon-shrouded glassy carbon working electrode (IJ Cambria).

Printed fuel cell measurements were performed using two different configurations. In power density plots with varying load, printed anodes and cathodes with a surface area of 6.25 cm^2 were sandwiched between graphite plates and a dialysis membrane (cut-off 12–14 kDa, Medicell International Ltd) was used as a separator. The anodic and cathodic potentials were measured with a VMP® multichannel potentiostat (Bio-Logic SAS) connected to a PC using a three-electrode connection with a thin foil Pd–H_2 electrode as the reference, Fig. 1 [18,19].

200 μL of appropriate buffer containing 25 mg of glucose powder as fuel was used to wet the biocatalytic prints. The open circuit voltage was monitored for 40 min, to ensure the system was stable, before 0.2 μA of current was drawn every minute until the cell voltage reached 0 V. A similar experiment was also conducted where the open circuit voltage was monitored for 40 min, to ensure the system was stable, before 0.2 μA of current was drawn every hour until the cell voltage reached 0 V. The cell was also operated in a 'stand alone' configuration, Fig. 2, where the anodic and cathodic prints were separated by dialysis membrane (cut-off 12–14 kDa, Medicell International Ltd) and sandwiched between graphite plates.

After assembly the cells were connected to the measurement apparatus consisting of a PC, voltage data logger (Agilent 34970A) and a resistor stack with variable resistors allowing 20 cells to be measured simultaneously. After monitoring the open cell voltage (OCV) for 90 min a constant load of 75 kΩ was applied to the cells and the time taken for the cell voltage to decrease below 200 mV was recorded.

3. Results and discussion

The principal aim of the research was to develop a fully enzymatic printable biofuel cell. Initial studies focused on using *Th*L as

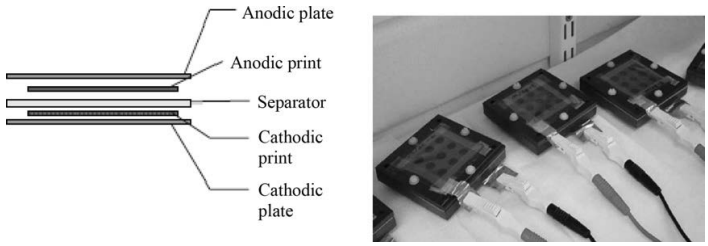

Fig. 2. Schematic structure of the printed biofuel test cell (left) and biofuel test cells enclosed between graphite plates (right).

the biocatalyst for oxygen reduction at the cathode, as this fungal laccase has a T1 copper site of high redox potential [28]. However there are some challenges associated with using *Th*L, as optimum activity is around pH 4.5, so if this biocathode is to be used in conjunction with a bioanode containing a fuel-oxidizing enzyme with an optimum activity closer to neutral pH then choice of supporting buffer would have to be a trade-off between the two pH values, which in turn could limit the performance of the biofuel cell. To try overcome this problem use of r*Ma*L as the oxygen-reducing biocatalyst was also tested, as it has the advantage of having an optimum activity at close to neutral pH, with however a T1 copper redox potential significantly lower than that of *Th*L.

3.1. Solution phase studies

Initially mediators and enzyme bioelectrochemistry was evaluated by estimating pseudo-first order rate constants (k_f) for mediator–enzyme kinetics using the method proposed by Cass et al. [29] based on the Nicholson and Shain approach [30]. Peak-shaped diffusional cyclic voltammograms (CV) are observed for mediators in presence of substrate but absence of enzyme, with a change in shape of CV to a sigmoidal shaped curve, typical of catalysis, upon addition of enzyme (not shown). The ratio of catalytic oxidation or reduction current to diffusional current provides an estimate of k_f.

Such solution-phase studies used a constant concentration of mediator (0.2 mM) and constant activity of enzyme (5 U mL^{-1} *Th*L activity at pH 4.5, 1.26 U mL^{-1} r*Ma*L activity at pH 7 using 2,2′-azino-bis(3-ethylbenzothiazoline-6-sulfonic acid), ABTS, as substrate and 5 U mL^{-1} ALDH activity at pH 6 using dichlorophenol indophenol DCIP as substrate) provided data compiled in Table 1. From the, although limited in number, estimated pseudo-first order rate constants it is clear that electron transfer is not dependent on thermodynamic driving force alone. For example, osmium complexes containing the 4AMP ligand or a chlorine functional group in the 4,4′ positions of the bipyridine produce k_f values considerably higher than other mediators of similar redox potential for *Th*L. The rate constant values obtained using *rMa*L indicate that there is efficient electron transfer occurring between enzyme and mediator, particularly given the lower enzyme activity used compared to *Th*L, although the different pH used makes direct comparison difficult. From these preliminary results r*Ma*L may have potential as a biocatalyst in biosensor and biofuel cell applications, where despite the lower redox potential of the T1 copper, substrate oxidizing, site of the enzyme, the rate constant is relatively rapid for the mediators studied here. From the solution phase studies for glucose oxidation, higher k_f values are observed for mediation of ALDH using N,N,N′,N′-tetramethyl-p-phenylenediamine (TMPD) and $Os(bpy)_2Cl_2$ as mediators, compared to that for $[Os(bpy)_2(4AMP)Cl]PF_6$. Not only does $[Os(bpy)_2(4AMP)Cl]PF_6$ display a relatively lower rate constant, but the relatively positive redox potential (>240 mV *vs.* Ag/AgCl) limits the use of this mediator in glucose-oxidizing anodes of a biofuel cell.

3.2. Performance of printed ThL cathodes in ALDH biofuel cells

To investigate power output from printed biofuel cells, a series of cathodic inks containing different mediators and enzymes were prepared and evaluated. These cathodes were coupled to two different printed ALDH glucose-oxidizing bioanodes, the first using TMPD as mediator, and the second $Os(bpy)_2Cl_2$ as mediator. Initially *Th*L was selected as the cathode biocatalyst and incorporated into conductive inks with ABTS, $K_4W(CN)_8$, $Os(dcbpy)_2Cl_2$, $[Os(dmbpy)_2(4AMP)Cl]PF_6$, $[Os(bpy)_2(4AMP)Cl]PF_6$ or $[Os(dcbpy)_2(4AMP)Cl]\cdot PF_6$ as the mediators. Table 2 summarizes the results from the different *Th*L-based inks coupled to the printed ALDH anodes, giving maximum power densities and cell voltages at which maximum power densities are obtained. Power density curves for the printed cathodes coupled to

Table 1
Pseudo-first order rate constant (k_f) for the enzyme–mediator interactions. Mediator 0.2 mM, 5% DMSO: using acetate buffer pH 4.5, 5 U mL^{-1} enzyme for *Th*L studies; phosphate buffer pH 7, 1.26 U/ml enzyme for r*Ma*L studies; and phosphate buffer pH 7, 100 mM glucose, 5 U mL^{-1} enzyme for ALDH studies.

Enzyme	Mediator	Redox potential (mV *vs.* Ag/AgCl)	k_f (s^{-1})
*Th*L	$[Os(dmbpy)_2(4AMP)Cl]PF_6$	190	2.2
*Th*L	$Os(dcbpy)_2Cl_2$	200	12
*Th*L	$[Os(bpy)_2(4AMP)Cl]PF_6$	240	1.7
*Th*L	$K_4W(CN)_8$	300	0.04
*Th*L	$[Os(dcbpy)_2(4AMP)Cl]PF_6$	445	14
*Th*L	ABTS	500	0.1
*rMa*L	$[Os(bpy)_2(4AMP)Cl]PF_6$	240	2.1
*rMa*L	$K_4W(CN)_8$	300	0.02
*rMa*L	ABTS	500	0.1
ALDH	$Os(bpy)_2Cl_2$	0	4.4
ALDH	TMPD	70	8.9
ALDH	$[Os(bpy)_2(4AMP)Cl]PF_6$	240	0.6

Table 2
Table listing the combinations of prints for evaluation of the *Th*L mediators, reporting maximum power densities and cell voltages at which maximum power densities are obtained, with conditions listed in Figs. 3 and 4.

Anode ALDH	Cathode *Th*L	Maximum power density (μW cm^{-2})	Voltage at maximum power density (V)
TMPD	ABTS	1.67	0.34
TMPD	$K_4W(CN)_8$	0.55	0.22
TMPD	$[Os(dmbpy)_2(4AMP)Cl]PF_6$	0.42	0.18
TMPD	$[Os(bpy)_2(4AMP)Cl]PF_6$	0.32	0.16
TMPD	$[Os(dcbpy)_2(4AMP)Cl]PF_6$	0.30	0.27
$Os(bpy)_2Cl_2$	ABTS	3.5	0.32
$Os(bpy)_2Cl_2$	$K_4W(CN)_8$	0.98	0.23
$Os(bpy)_2Cl_2$	$[Os(dmbpy)_2(4AMP)Cl]PF_6$	0.62	0.19
$Os(bpy)_2Cl_2$	$[Os(bpy)_2(4AMP)Cl]PF_6$	0.46	0.21
$Os(bpy)_2Cl_2$	$[Os(dcbpy)_2(4AMP)Cl]PF_6$	0.39	0.31
$Os(bpy)_2Cl_2$	$Os(dcbpy)_2Cl_2$	0.34	0.20

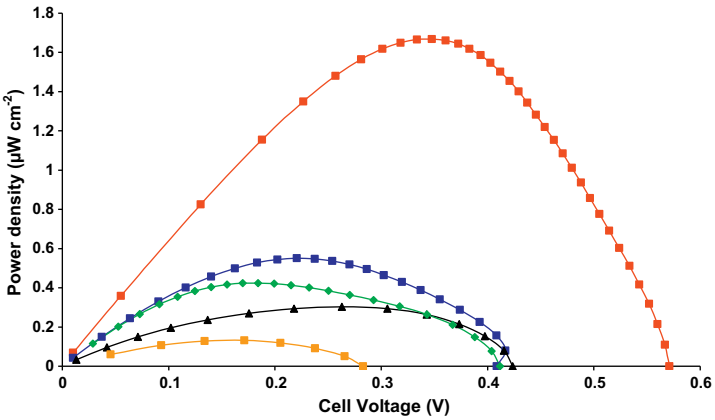

Fig. 3. Power curves derived from monitoring cell voltage as 0.2 μA of current is drawn every minute. Anodic ink contains ALDH mediated by TMPD, cathodic ink contains *Th*L mediated by either ABTS (■), $K_4W(CN)_8$ (■), $[Os(dmbpy)_2(4AMP)Cl]PF_6$ (◆), $[Os(bpy)_2(4AMP)Cl]PF_6$ (■) or $[Os(dcbpy)_2(4AMP)Cl]PF_6$ (▲), 200 μL succinate buffer pH 5, glucose 694 mM.

printed anodes containing ALDH, mediated by TMPD at a pH of 5 are given in Fig. 3. The highest power density of 1.67 μW cm^{-2} at 0.34 V is obtained using ABTS, correlating well with results from the solution phase studies. Nevertheless instability of ABTS had previously been reported [31–33] potentially limiting the long term stability of printed ABTS-based biofuel cells. Other mediators tested produced significantly lower (0.3–0.55 μW cm^{-2}) power densities compared to the printed ABTS/*Th*L cathode. The low power densities are somewhat surprising, as the osmium complexes of general formula $[Os(N{-}N)_2(4AMP)Cl]PF_6$ displayed more efficient electron transfer kinetics with *Th*L in solution.

The printed cathodes were also coupled to a printed anode containing ALDH mediated by $Os(bpy)_2Cl_2$, and resulting power density curves are represented in Fig. 4 with results summarized in Table 2. Replacing the printed TMPD/ALDH anode with an anode incorporating ALDH mediated by $Os(bpy)_2Cl_2$ increased the overall maximum power densities of all cells constructed using the different cathodes. The $Os(bpy)_2Cl_2$ mediator has a more negative redox potential compared to that of TMPD, so although some of the thermodynamic driving force for electron transfer from the active site of the anodic enzyme to the anodic mediator is lost, this loss is compensated for in the power output by the increase in cell voltage of the biofuel cell.

3.3. Performance of printed rMaL cathodes in ALDH biofuel cells

An issue with fuel cells containing ALDH and *Th*L is that both these enzymes have different optimal pHs and careful consideration must be taken when selecting an appropriate cell pH. If the pH of the supporting buffer is too high this could limit the activity of *Th*L decreasing the effectiveness of the cathode. One way to try and address this problem is to incorporate r*Ma*L into the cathodic ink as a replacement biocatalyst to *Th*L. The r*Ma*L has a pH optimum close to neutral but the T1 copper site of *Th*L has higher redox potential (~570 mV *vs.* Ag/AgCl), compared to that in r*Ma*L (~270 mV *vs.* Ag/AgCl). This lower redox potential could result in a lower overall cell voltage and ultimately limit the maximum power output of a printed r*Ma*L-based biocatalytic fuel cell.

The *rMa*L was incorporated into inks with ABTS, $Os(dcbpy)_2Cl_2$, $[Os(bpy)_2(4AMP)Cl]PF_6$ and $[Os(dcbpy)_2(4AMP)Cl]{\cdot}PF_6$ as mediators. Power density results for the printed cathodes coupled to a printed anode containing ALDH, mediated by TMPD or $Os(bpy)_2Cl_2$ at pH of 6.5 are summarized in Table 3. Biofuel cells using ALDH/$Os(bpy)_2Cl_2$ anodes result in higher power densities compared to ALDH/TMPD anodes, with the same trends in cathodic mediators as observed for *Th*L-based cathodes. Again differences in power densities can be attributed to the higher overall cell voltages produced using anodes incorporating $Os(bpy)_2Cl_2$ compared to TMPD. Although r*Ma*L could be considered as an alternative to *Th*L as a potential cathodic biocatalyst, biofuel cells incorporating r*Ma*L produce significantly lower power outputs compared to cells containing *Th*L as the biocatalyst, under these experimental conditions, most likely due to the lower redox potential of the T1 copper of the r*Ma*L.

3.4. Performance of the printed cathodes under constant load

The performance of the cathodic prints was also evaluated in a 'stand alone' configuration, Fig. 2, with a load of 75 kΩ applied after 90 min, using 400 μL succinate buffer, pH 5 containing 694 mM glucose, as the supporting electrolyte. The cell voltage was recorded until it decreased below a threshold voltage selected to be 200 mV. Table 4 lists the cathodic prints coupled to an ALDH anode mediated by either TMPD or $Os(bpy)_2Cl_2$, in a 'stand alone' configuration under a constant load, the time taken for the cell voltage to decrease below 200 mV and the corresponding estimated energy content. With the exception of when coupled to the *Th*L/ABTS cathode, the ALDH/$Os(bpy)_2Cl_2$ anodes give higher energy content and maintained cell voltages above the threshold voltage for longer, compared to the equivalent ALDH/TMPD anodes. On average the cells containing ALDH/$Os(bpy)_2Cl_2$ anodes maintained cell voltages above 200 mV for approximately twice as long and

Table 3
Table listing the combinations of prints for evaluation of the r*Ma*L mediators, reporting maximum power densities and cell voltages at which maximum power densities are obtained, with all conditions as listed in Figs. 3 and 4, except using a pH of 6.5.

Anode ALDH	Cathode r*Ma*L	Maximum power density (μW cm^{-2})	Voltage at maximum power density (V)
TMPD	ABTS	0.39	0.35
TMPD	$Os(dcbpy)_2Cl_2$	0.13	0.14
TMPD	$[Os(bpy)_2(4AMP)Cl]PF_6$	0.29	0.27
$Os(bpy)_2Cl_2$	ABTS	0.50	0.40
$Os(bpy)_2Cl_2$	$Os(dcbpy)_2Cl_2$	0.17	0.16
$Os(bpy)_2Cl_2$	$[Os(bpy)_2(4AMP)Cl]PF_6$	0.39	0.25

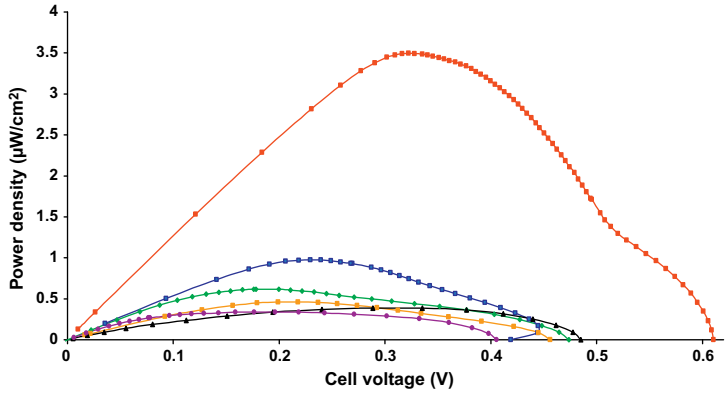

Fig. 4. Power curves derived from monitoring cell voltage as 0.2 μA of current is drawn every minute. Anodic ink contains ALDH mediated by $Os(bpy)_2Cl_2$, cathodic ink contains *Th*L mediated by either ABTS (■), $K_4W(CN)_8$ (■), $[Os(dmbpy)_2(4\text{-}AMP)Cl]PF_6$ (◆), $[Os(bpy)_2(4\text{-}AMP)Cl]PF_6$ (■), $[Os(dcbpy)_2(4AMP)Cl]PF_6$ (▲) or $Os(dcbpy)_2Cl_2$ (●), 200 μL succinate buffer, pH 5, glucose 694 mM.

generated an energy content three times larger than cells containing ALDH/TMPD anodes. This is not surprising due to the larger cell voltages previously observed for ALDH/$Os(bpy)_2Cl_2$ anodes compared to ALDH/TMPD anodes.

A plot of cell voltage against time, for the loaded cells consisting of a printed ALDH/$Os(bpy)_2Cl_2$ anode coupled to a printed *Th*L cathode mediated by $K_4W(CN)_8$, $[Os(dmbpy)_2(4AMP)Cl]PF_6$, $[Os(bpy)_2(4AMP)Cl]PF_6$ or $Os(dcbpy)_2Cl_2$ is given in Fig. 5. The previous experiments to evaluate performance of cathodic inks focused on drawing large amounts of current over a short period of time, with the ALDH/$Os(bpy)_2Cl_2$: *Th*L/ABTS cell generating the maximum power output of 3.5 μW cm^{-2}. If the application only requires a limited load (75 kΩ) but requires a longer lifetime then other cells may prove to be more effective. For example the printed biofuel cell constructed from ALDH/$Os(bpy)_2Cl_2$: *Th*L/$Os(dcbpy)_2Cl_2$ produced a maximum power density 10 times smaller compared to the ALDH/$Os(bpy)_2Cl_2$: *Th*L/ABTS cell. Despite this, under a limited load the ALDH/$Os(bpy)_2Cl_2$: *Th*L/$Os(dcbpy)_2Cl_2$ cell was able to operate for almost three times longer maintaining a cell voltage above the threshold 200 mV, under a 75 kΩ load for approximately 137 h. In comparison, the ALDH/$Os(bpy)_2Cl_2$: *Th*L/ABTS cell maintained a cell voltage over 200 mV for only 47 h. In fact all of the biofuel cells containing osmium complexes as anodic and cathodic mediators maintained cell voltages over 200 mV, under a constant load of 75 kΩ, for considerably longer time periods and in general give rise to higher energy contents compared to cells mediated by ABTS, TMPD or $K_4W(CN)_8$. When drawing high current, the complexes with the general formula $[Os(N\text{–}N)_2(4AMP)Cl]PF_6$ have not performed well as enzymatic mediators compared to other mediators, such as ABTS and $K_4W(CN)_8$. Despite this in a 'stand alone' configuration, under a limited load, these complexes generate energy content over longer lifetimes compared to *Th*L cathodes mediated by ABTS and $K_4W(CN)_8$. This highlights the need for careful consideration on how to evaluate performance metrics of these printed biofuel cells with respect to the eventual application.

The performance of r*Ma*L prints were also evaluated in a 'stand alone' configuration, with the same load of 75 kΩ applied after 90 min, using 400 μL succinate buffer, pH 6.5 containing 694 mM glucose, as supporting electrolyte, Table 5. As before the cell voltage was recorded until it decreased below the threshold voltage of 200 mV. Using r*Ma*L as the cathodic biocatalyst resulted in lower cell voltages compared to similar cells containing *Th*L. One of the most notable differences is the poor performance of the $Os(dcbpy)_2Cl_2$ mediated r*Ma*L cathodes. The cathode incorporating $Os(dcbpy)_2Cl_2$ and r*Ma*L coupled to an ALDH/$Os(bpy)_2Cl_2$ anode maintained a cell voltage over the threshold 200 mV for only 0.83 h and produced an energy content of 0.05 μW h cm^{-2}, which was considerably lower than equivalent cells mediated by either ABTS or $[Os(bpy)_2(4AMP)Cl]PF_6$. In contrast the equivalent cell

Table 4
List of the different cells tested in 400 μL succinate buffer, pH 5 containing 694 mM glucose, as supporting electrolyte; the time taken for the cell voltage to decrease below 200 mV; and the energy content of the cell. Cells were run in duplicate, with median of two readings ± the maximum/minimum given in brackets.

Cell	*V* >200 mV (h)	Energy content (μW h cm^{-2})
ALDH/TMPD: *Th*L/ABTS	74.1 (±0.7)	10.7 (±2.8)
ALDH/TMPD: *Th*L/$K_4W(CN)_8$	15 (±4)	1.1 (±0.2)
ALDH/TMPD: *Th*L/$[Os(dmbpy)_2(4AMP)Cl]PF_6$	39 (±7)	2.8 (±0.6)
ALDH/TMPD: *Th*L/$[Os(bpy)_2(4AMP)Cl]PF_6$	60 (±5)	4.1 (±0.1)
ALDH/TMPD: *Th*L/$[Os(dcbpy)_2(4AMP)Cl]PF_6$	58 (±4)	4.4 (±0.1)
ALDH/TMPD: *Th*L/$Os(dcbpy)_2Cl_2$	88 (±26)	5.6 (±1.9)
ALDH/$Os(bpy)_2Cl_2$: *Th*L/ABTS	47 (±16)	11.1 (±5.5)
ALDH/$Os(bpy)_2Cl_2$: *Th*L/$K_4W(CN)_8$	107 (±3)	14.0 (±0.7)
ALDH/$Os(bpy)_2Cl_2$: *Th*L/$[Os(dmbpy)_2(4AMP)Cl]PF_6$	120 (±18)	12.4 (±2.3)
ALDH/$Os(bpy)_2Cl_2$: *Th*L/$[Os(bpy)_2(4AMP)Cl]PF_6$	127 (±16)	16.1 (±5.7)
ALDH/$Os(bpy)_2Cl_2$: *Th*L/$[Os(dcbpy)_2(4AMP)Cl]PF_6$	123 (±14)	16.3 (±2.2)
ALDH/$Os(bpy)_2Cl_2$: *Th*L/$Os(dcbpy)_2Cl_2$	137 (±24)	11.8 (±2.6)

Table 5
List of the different cells tested in succinate buffer, pH 6.5 containing 694 mM glucose, as supporting electrolyte; the time taken for the cells voltage to decrease below 200 mV; and the energy content of the cell.

Cell	*V* >200 mV (h)	Energy content (μW h cm^{-2})
ALDH/TMPD: r*Ma*L/$W(CN)_8$	0.02	<0.1
ALDH/TMPD: r*Ma*L/ABTS	78	9
ALDH/TMPD: r*Ma*L/$Os(dcbpy)_2Cl_2$	2.0	0.1
ALDH/TMPD: r*Ma*L/$[Os(bpy)_2(4AMP)Cl]PF_6$	57	4
ALDH/$Os(bpy)_2Cl_2$: r*Ma*L/$W(CN)_8$	0.13	0.01
ALDH/$Os(bpy)_2Cl_2$: r*Ma*L/ABTS	98	15
ALDH/$Os(bpy)_2Cl_2$: r*Ma*L/$Os(dcbpy)_2Cl_2$	0.83	0.05
ALDH/$Os(bpy)_2Cl_2$: r*Ma*L/$[Os(bpy)_2(4AMP)Cl]PF_6$	87	7

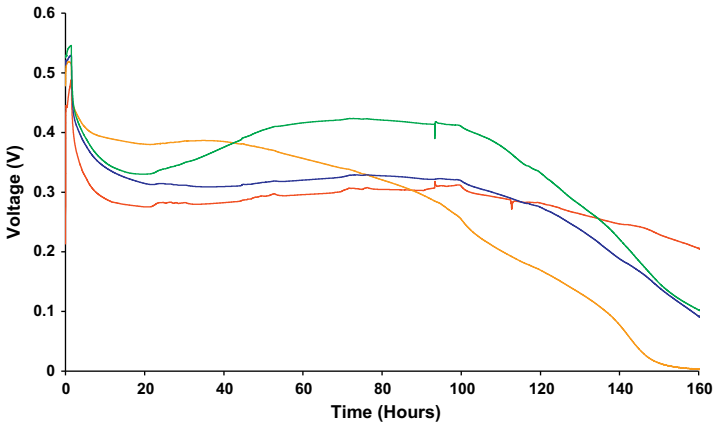

Fig. 5. Performance of 'stand alone' biofuel cells constructed from an $Os(bpy)_2Cl_2$ mediated ALDH anode coupled to a *Th*L cathode mediated by either $K_4W(CN)_8$ (gold), $[Os(dmbpy)_2(4AMP)Cl]PF_6$ (blue), $[Os(bpy)_2(4AMP)Cl]PF_6$ (green), or $Os(dcbpy)_2Cl_2$ (red). OCV monitored for 90 min before cells were loaded with 75 kΩ load. (For interpretation of the references to color in this figure legend, the reader is referred to the web version of the article.)

containing *Th*L instead of r*Ma*L, proved to be one of the best evaluated, maintaining a cell voltage over 200 mV for 137 h. As with the cells containing *Th*L, the r*Ma*L based cathodes which were coupled to ALDH anodes mediated by $Os(bpy)_2Cl_2$ give higher cell voltages over TMPD mediated anodes, resulting in longer lifetimes.

The printed ABTS mediated r*Ma*L cathodes give the largest energy content, 15 $\mu W\,h\,cm^{-2}$, when coupled to a ALDH/$Os(bpy)_2Cl_2$ anode, compared to 7 $\mu W\,h\,cm^{-2}$ for the cells using $[Os(bpy)_2(4AMP)Cl]PF_6$ as a mediator for r*Ma*L. This, despite $[Os(bpy)_2(4AMP)Cl]PF_6$ yielding the highest observed rate constant for mediation of oxygen reduction by this enzyme in solution, compared to ABTS or $K_4W(CN)_8$. Thus despite rapid electron transfer, the decrease in mediator redox potential when selecting this mediator results in a lower overall power output for printed fuel cells.

4. Conclusions

Production of printed cathodes of *Th*L and ABTS, when coupled to printed glucose-oxidizing ALDH mediated anodes are capable of producing relatively high initial power outputs, but however, have a limited operational lifetime. In contrast, under a limited load use of osmium-based mediators in printed enzymatic fuel cells result in systems that display power output over longer lifetimes. Attempts to use a fungal laccase with a pH optimum closer to that of the glucose-oxidizing ALDH, did not result in appreciable improvement to power output, nor to power output stability. The eventual decrease in power output of the cells is likely to be due to several factors including leaching or decomposition of the mediators, denaturing/inhibition of the enzymatic biocatalysts and/or the depletion of fuel and oxidant required to keep the fuel cell running. Further studies would be required to not only optimize the power output, but also the operational lifetime of these fully enzymatic printed biofuel cells.

Acknowledgment

Funding for this research was provided by an EU FP6 award NMP4-CT-2006-17350 'Biomednano',

References

[1] Barton SC, Gallaway J, Atanassov P. Enzymatic biofuel cells for implantable and microscale devices. Chem Rev 2004;104:4867–86.
[2] Davis F, Higson SPJ. Biofuel cells: recent advances and applications. Biosens Bioelectron 2007;22:1224–35.
[3] Minteer SD, Liaw BY, Cooney MJ. Enzyme-based biofuel cells. Curr Opin Biotechnol 2007;18:p228–34.
[4] Albareda-Sirvent M, Merkoçi A, Alegret S. Configurations used in the design of screen-printed enzymatic biosensors. A review. Sens Actuators B: Chem 2000;69:53–163.
[5] Zhang C, Gao Q, Aizawa M. Flow injection analytical system for glucose with screen-printed enzyme biosensor incorporating Os-complex mediator. Anal Chim Acta 2001;426:33–41.
[6] Zhang C, Haruyama T, Kobatake E, Aizawa M. Disposable electrochemical capillary-fill device for glucose sensing incorporating a water-soluble enzyme/mediator layer. Anal Chim Acta 2001;442:257–65.
[7] Setti L, Fraleoni-Morgera A, Ballarin B, Filippini A, Frascaro D, Piana C. An amperometric glucose biosensor prototype fabricated by thermal inkjet printing. Biosens Bioelectron 2005;20(10):2019–26.
[8] Setti L, Fraleoni-Morgera A, Mencarelli I, Filippini A, Ballarin B, Di Biase M. An, HRP-based amperometric biosensor fabricated by thermal inkjet printing. Sens Actuators B: Chem 2007;126:252–7.
[9] Newman JD, Turner APF, Marrazza G. Ink-jet printing for the fabrication of amperometric glucose biosensors. Anal Chim Acta 1992;262:13–7.
[10] Lupu A, Compagnone D, Palleschi G. Screen-printed enzyme electrodes for the detection of marker analytes during winemaking. Anal Chim Acta 2004;513:67–72.
[11] Cui G, Yoo JH, Woo BW, Kim SS, Cha GS, Nam H. Disposable amperometric glucose sensor electrode with enzyme-immobilized nitrocellulose strip. Talanta 2001;54:1105–11.
[12] Nagata R, Yokoyama K, Durliat H, Comtat M, Clark SA, Karube I. An enzyme-containing ink for screen-printed glucose sensors. Electroanalysis 1995;7:1027–31.
[13] Gao Q, Yang X. Layer-by-layer electrodeposition of redox polymers and enzymes on screen-printed carbon electrodes for the preparation of reagentless biosensors. Chem Commun 2004;1:30–1.
[14] Hart AL, Collier WA. Stability and function of screen printed electrodes, based on cholinesterase, stabilised by a co-polymer/sugar alcohol mixture. Sens Actuators B: Chem 1998;53:111–5.
[15] Hart AL, Cox H, Janssen D. Stabilization of lactate oxidase in screen-printed enzyme electrodes. Biosens Bioelectron 1996;11:833–7.
[16] Mersal GAM, Khodari M, Bilitewski U. Optimisation of the composition of a screen-printed acrylate polymer enzyme layer with respect to an improved selectivity and stability of enzyme electrodes. Biosens Bioelectron 2004;20:305–14.
[17] Schumacher JT, Munch I, Richter T, Rohm I, Bilitewski U. Investigations with respect to stabilization of screen-printed enzyme electrodes. J Mol Catal B: Enzym 1999;7:67–76.
[18] Smolander M, Boer H, Valkiainen M, Roozeman R, Bergelin M, Eriksson JE, et al. Development of a printable laccase-based biocathode for fuel cell applications. Enzyme Microb Technol 2008;43:93–102.
[19] Tuurala S, Smolander M, Uotila J, Kaukoniemi OV, Boer H, Valkiainen M, et al. Performance of a printable enzymatic fuel cell: study on mediated ThL laccase cathode. ECS Trans 2010;25:1–10.
[20] Solomon EI, Sundaram UM, Machonkin TE. Multicopper oxidases and oxygenases. Chem Rev 1996;96:2563–606.
[21] Yaropolov AI, Skorobogatko OV, Vartanov SS, Varfolomeyev SD. Laccase—properties, catalytic mechanism, and applicability. Appl Biochem Biotechnol 1994;49:257–80.

[22] Xu F, Shin WS, Brown SH, Wahleithner JA, Sundaram UM, Solomon EI. A study of a series of recombinant fungal laccases and bilirubin oxidase that exhibit significant differences in redox potential, substrate specificity, and stability. Biochim Biophys Acta: Protein Struct Mol Enzymol 1996;1292:303–11.
[23] Kavanagh P, Jenkins P, Leech D. Electroreduction of O_2 at a mediated *Melanocarpus albomyces* laccase cathode in a physiological buffer. Electrochem Commun 2008;10:970–2.
[24] Kiiskinen LL, Viikari L, Kruus K. Purification and characterisation of a novel laccase from the ascomycete *Melanocarpus albomyces*. Appl Microb Biotechnol 2002;59:198–204.
[25] Smolander M, Buchert J, Viikari L. Large-scale applicable purification and characterization of a membrane-bound PQQ-dependent aldose dehydrogenase. J Biotechnol 1993;29:287–97.
[26] Rittstieg K, Suurnakki A, Suortti T, Kruus K, Guebitz G, Buchert J. Investigations on the laccase-catalyzed polymerization of lignin model compounds using size-exclusion HPLC. Enzyme Microb Technol 2002;31:403–10.
[27] Kober EM, Caspar JV, Sullivan BP, Meyer TJ. Synthetic routes to new polypyridyl complexes of osmium(II). Inorg Chem 1988;27:4587–98.
[28] Shleev S, Pita M, Yaropolov AI, Ruzgas T, Gorton L. Direct heterogeneous electron transfer reactions of *Trametes hirsuta* laccase at bare and thiol-modified gold electrodes. Electroanalysis 2006;18:1901–8.
[29] Cass AEG, Davis G, Francis GD, Hill HAO, Aston WJ, Higgins IJ, et al. Ferrocene-mediated enzyme electrode for amperometric determination of glucose. Anal Chem 1984;56:667–71.
[30] Nicholson RS, Shain I. Theory of stationary electrode polarography. Single scan and cyclic methods applied to reversible, irreversible, and kinetic systems. Anal Chem 1964;36:706–23.
[31] Li KC, Xu F, Eriksson KEL. Comparison of fungal laccases and redox mediators in oxidation of a nonphenolic lignin model compound. Appl Environ Microbiol 1999;65:2654–60.
[32] Kurniawati S, Nicell JA. Efficacy of mediators for enhancing the laccase-catalyzed oxidation of aqueous phenol. Enzyme Microb Technol 2007;41:353–61.
[33] Farneth WE, Diner BA, Gierke TD, D'Amore MB. Current densities from electrocatalytic oxygen reduction in laccase/ABTS solutions. J Electroanal Chem 2005;581:190–6.

IV

Tuurala, S., Kaukoniemi, O.V., von Hertzen, L., Uotila, J., Vaari, A., Bergelin, M., Sjöberg, P., Eriksson, J.E., and Smolander, M. (2014) Scale-up of manufacturing of printed enzyme electrodes for enzymatic power source applications. *Journal of Applied Electrochemistry* ***44(7)***, 881-892.

DOI: 10.1007/s10800-014-0702-2

V

Tuurala, S., Kallio, T., Smolander, M., and Bergelin, M. (2015) Increasing performance and stability of mass-manufacturable biobatteries by ink modification. *Sensing and Bio-Sensing Research* ***4***, 61-69.

DOI: 10.1016/j.sbsr.2015.03.003

Sensing and Bio-Sensing Research 4 (2015) 61–69

Contents lists available at ScienceDirect

Sensing and Bio-Sensing Research

journal homepage: www.elsevier.com/locate/sbsr

Increasing performance and stability of mass-manufacturable biobatteries by ink modification

Saara Tuurala [a,*], Tanja Kallio [b], Maria Smolander [a], Mikael Bergelin [c]

[a] VTT Technical Research Centre of Finland, Tietotie 3, Espoo, FI-02044 VTT, Finland
[b] Department of Chemistry, Aalto University, P.O. Box 16100, FI-00076 AALTO, Finland
[c] Åbo Akademi, Process Chemistry Centre, Biskopsgatan 8, FI-20500 Åbo, Finland

ARTICLE INFO

Keywords:
Enzymatic electrode
Self-powered biosensor
Biobattery
Stability
Mass-manufacturing
Printing

ABSTRACT

In this work, biobatteries assembled using roll-to-roll screen printed enzymatic electrodes were characterised in terms of their electrical performance and storage stability. The enzymes and mediators used on the anode and cathode were glucose oxidase with ferrocenemethanol and laccase with ABTS, respectively. This study shows that besides rheological properties of enzyme inks used for the printing of the biobattery electrodes also adhesion of these electrodes to the printing substrate can be adjusted by varying the amount and composition of the binder in the ink. Another important observation is that the mediator has a strong impact on both the performance and the stability of the anode electrode. Consequently, electrochemical performance of biobatteries can be enhanced by adding fresh mediator into the battery during activation or by some other method preserving the activity of the mediator. Hence, this study discusses and sheds light on important practical aspects for up-scaling production process of biobatteries and also other printed bioelectronics.

1. Introduction

Printing of enzymes on paper or cardboard can add valuable functionalities to the substrate. These functionalized paper-based products could be used in low-cost diagnostics [24,53], indicators [7,9,41] or bioelectronics. In bioelectronics the functionality of the device is typically based on catalytic reactions of enzymes or affinity sensing due to formation of specific antigen–antibody complexes [48]. Typical examples of bioelectronic devices are potentiometric and amperometric biosensors [6,10,21], and enzymatic power sources [5].

Traditional amperometric biosensors require an external power supply for the signal-reading because the current generated in the detection reaction of the sensor is measured at controlled potential versus reference electrode. However, power supplies (e.g. batteries) are difficult to miniaturise. In addition, sensor designs allowing easy replacement or recharging of the battery are bulky. Another challenge in designing amperometric biosensors is interference current resulting from nonspecific redox reactions of other redox-active species upon application of potential on the working electrode.

In order to solve the challenges described above, biobattery configuration consisting of two electrodes has been introduced as a self-powered biosensor (SPB) device [1,18,57]. The operational principle of SPB is very simple; there is no voltage or current in the absence of the fuel, but the presence of the fuel in the anode induces voltage and current, and thus generates power. The induced current density and thus the power density are functions of the concentration of the fuel. Hence, the sensor itself provides the power for the sensing device when achieving the analytical signal. Still, in order to make SPBs as commercial products their electrical performance and stability need to be ensured. In addition, their mass-manufacturability has to be tested, and especially paper-based biosensors have drawn attention due to their inexpensive and renewable substrate material and disposability.

Although biocatalysts have been successfully applied on paper-based substrates possessing many desirable characteristics (including selectivity, non-toxicity, reproducibility and low-cost), their marginal stability has prevented or delayed their implementation for mass-manufacturing. As enzymes are removed from their natural environment and applied onto a paper-based surface, their hydration-level, pH and temperature are typically not optimal. For this reason their stability is poor. For an example, Khan et al. [20] reported half-lives of alkaline phosphatase (ALP) and horseradish peroxidase (HRP) adsorbed on paper of 22 days and 10 days at 23 °C, respectively, whereas ALP incubated at 37 °C in 50% glycerol solution is stable at least for 4 weeks and lyophilized HRP is stable at room temperature for 3 weeks (stability values are given by the enzyme manufacturers).

* Corresponding author. Tel.: +358 401843818.
E-mail address: saara.tuurala@vtt.fi (S. Tuurala).

http://dx.doi.org/10.1016/j.sbsr.2015.03.003
2214-1804/

The enzyme immobilization procedure is critical for the fabrication of enzymatic bioelectronics. The enzyme activity should be retained while favouring its electrical connection with the underlying conductive electrode material, directly or via a redox mediator. It has been seen that the bioelectrochemical interface in bioelectronic devices plays an important role in the performance of the device [56]. Immobilisation of enzymes into solid structures is one of the most used methods for stabilising enzymes [13,29]. This can be done by incorporating enzymes into printable inks and it is considered as one of the promising approaches for large-scale manufacturing processes for enzyme-containing electrodes. Hence, modification of the enzyme-containing inks in order to increase the enzymatic stability of the printed layers is an important challenge. One natural approach is to carefully select the solvents (usually water) and binders according to the enzymes used. For an example, Khan et al. [19] reported that water soluble polymers increased the adsorption of ALP on paper by around 50% and prevented enzyme desorption/leaching upon rewetting of the paper compared to non-treated paper. However, they also found out that the type of polymers affects the thermal stability and the ageing of ALP on paper, and in their case the thermal stability of ALP on paper decreased when polymers were used. For this reason, components of enzymatic inks must be chosen carefully.

We have previously demonstrated that biocatalyst-based electrodes can be produced on paper-based substrates by printing and in large scale [16,17,39,42,44]. In this work, biobattery assemblies using roll-to-roll (R2R) printed enzymatic electrodes were characterised by electrochemical methods. Storage stability was studied over one month period and optimisation of the printed anode was done by improving ink formulation. Rheological properties of enzyme containing inks and adhesion of these electrodes to the current collector can be adjusted by varying the amount and composition of the binder in the ink. Moreover, the mediator has a strong impact on both the performance and the stability of the anode electrode. Hence, this study reveals important practical aspects for up-scaling the printing production process of bioelectronics.

2. Material and methods

2.1. Materials

Materials for base inks were graphite powder (<20 μm, Aldrich 282863), polyethylene oxide (PEO, Aldrich 189456), and chitosan (Sigma 448877). The mediators and enzymes used in the inks were ferrocenemethanol (FeMeOH, Aldrich 335061), 2,2′-Azino-bis(3-ethylbenzothiazoline-6-sulfonic acid) diammonium salt (ABTS, Sigma A1888), glucose oxidase from *Aspergillus niger* (GOx, Sigma G7141) and laccase (EcoL, AB Enzymes Ecostone LCL 45, EC 1.10.3.2), respectively.

Materials for printing process and assembling the cells were polyethylene (PE) coated cardboard (Stora Enso Classic Bar PE 175 + 15 g/m^2), insulator paper (Delfortgroup, Terkab Ilam), current collector ink (Peters HAL SD-2843), dialysis membrane (Medicell International Ltd, visking code DTV12000.11.000), D-glucose (VWR 101176K) and succinic acid (Sigma–Aldrich 398055). The chemicals were used as received without further purification and distilled water was used in all the experiments.

2.2. Electrode preparation

2.2.1. Inks

A base ink was prepared by mixing graphite and binders (PEO and chitosan) together in different ratios as described in Table 1. The enzyme containing inks were prepared by mixing enzyme and mediator into the base ink. GOx and FeMeOH (dissolved in ethanol) were used for anode inks and EcoL and ABTS for the cathode inks. 50 mM Na-succinate buffer (pH 4.5) was used to adjust the viscosity of the ink (Table 1).

2.2.2. Printing and curing

Pilot printing trials were carried out using VTT's modular ROKO R2R pilot line (Fig. 1). The printing speed was 2 m min^{-1} and Gallus BY/RS Mesh 64 (thickness 200 μm) printing screens were used with all inks. PE-coated cardboard was used as the printing substrate and the ink was deposited on the PE-coated side. First, current collectors were printed using commercial carbon-based ink and cured on the printing line at 145 °C. The enzyme containing inks were printed as a separate layer (the geometrical electrode area was 9 cm^2) on top of the current collector layers and cured on the printing line at approximately 70 °C. The layers were cured using three 0.9 m long box ovens; hence the accumulative curing time was 81 s. The printed cardboard rolls (Fig. 2) were stored at room temperature. The first electrochemical measurements were performed after 1 week of manufacturing due to transportation from the pilot printing line to laboratory.

Experimental laboratory printing trials were carried out using a semi-automatic Kent SP-400 screen printer. The printing substrate was insulator paper (A4-size) and the screen mesh was NMC EX 31-100. The printed electrodes (the geometrical electrode area was 12.25 cm^2) were dried and stored at room temperature and characterised on the next day after manufacturing.

2.3. Cell assembly

Printed electrodes were stored at room temperature and cut from the printing substrate for assembly. As pilot-printed

Table 1
Compositions of enzymatic inks tested. The pilot anode ink 1 and cathode ink were prepared as previously published by Tuurala et al. [42] and the compositions are reprinted here with permission.

Component	Anode ink 1 for the 1st pilot run	Cathode ink for the pilot run	Experimental anode ink 1	Experimental anode ink 2	Experimental anode ink 3	Anode ink 2 for the 2nd pilot run
Graphite (g)	25	25	25	23	25	25
PEO (g) (5 wt% in H_2O)	18	18	18	16	35	35
Chitosan solution (g) (in 1% acetic acid)	–	–	4.3 different concentrations*	4 (1.5 wt%)	6.7 different concentrations*	7 (0.5 wt%)
Enzyme (nkat)	40,500	36,700	36,400	52,550	25,000	40,550
Mediator (mg) [μmol nkat^{-1}]	86 [0.01]	217 [0.01]	86 [0.01]	Different concentrations**	54 [0.01]	188 [0.02]
Solvent (ml) (ethanol)	0.4	0	0.4	0.4	0.4	0.6
Buffer (ml)	10–12	10–12	–	–	–	–

* Four different chitosan solutions were prepared: 0.5, 1.0, 1.5 and 2 wt% in 1% acetic acid and added into the experimental inks 1 and 3.
** Four different FeMeOH amounts were tested: 0.01, 0.03, 0.05 and 0.08 μmol nkat^{-1} (of GOx enzyme).

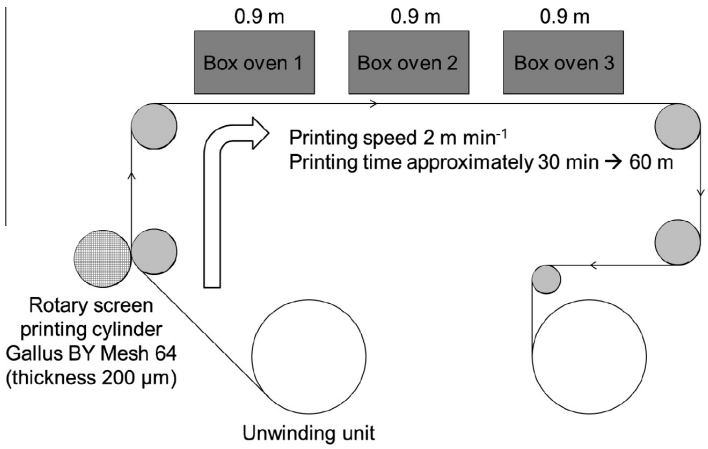

Fig. 1. Schematic of VTT's ROKO R2R pilot line. Printing of biobatteries can be seen in a YouTube video clip (https://www.youtube.com/watch?v=DS44BpavARk).

electrodes were characterised, anode (9 cm^2) was moisturised with 200 µl of 50 mM Na-succinate buffer (pH 4.5) and 50 mg of glucose. A piece of a dialysis membrane separator (16 cm^2) was set on top of the anode. Cathode (9 cm^2) was moisturised with 100 µl of buffer and assembled on top of the anode-separator layer so that the printed sides of the electrodes were facing each other. The cell assembly was fixed between planar graphite plates and the cell was connected to a potentiostat with alligator clips from the printed current collectors.

As the laboratory manufactured electrodes were assembled, anode (12.25 cm^2) and cathode (12.25 cm^2) were sandwiched between graphite current collector plates so that the printed sides of the electrodes were facing the graphite. Hence no additional separator was needed. There was a gasket (thickness 250 µm) between the anode and the cathode. The graphite plate on the cathode side had holes, and the cell was activated via the holes with 50 mg of glucose in 400 µl of buffer. The cell was connected to a potentiostat with alligator clips from the graphite current collectors.

2.4. Electrochemical measurements and data analysis

The electrochemical performance of the cells was measured using multichannel potentiostat (BioLogic VMP) in two electrode connection. At least three individual repetitions were measured and the error bars were calculated as standard error of the mean (SM). Student's *t*-test was used to evaluate the statistical significance between measurement sets. All the measurements are listed in Table 2.

In chronopotentiometry (CP) cells were measured at open circuit potential (OCP) for 1.5 h after which a constant current was drawn from the cells until the cell potential decreased to 0 V. The cell potential was recorded in 60 s intervals. The energy output of the cells was calculated by integrating the area until the cell potential decreased to (a) 200 mV and (b) 150 mV. In chronoamperometry (CA) cells were measured at OCP for 1.5 h after which the cell potential was decreased from 300 mV to 0 mV in 25 mV steps every 10 min. The steady state current was measured.

2.5. Characterisation of the morphology of the electrode

Thickness of the pilot printed electrodes was determined using a Dektak stylus profilometer. Roughness was measured using a Wyko white light interferometer and the area measured was 0.91 mm × 1.20 mm. Three Au layers were sputtered on top of the samples prior to measurement. The number of samples was at least three and three measurement points were analysed from each sample.

3. Results and discussion

3.1. Performance of the pilot anode ink 1

In our previous work we optimised the composition of the pilot inks in the perspective of the drying process on the ROKO R2R printing line [42]. However, the pilot anode ink 1 has a poor mechanical stability rendering assembling of the cells difficult. The ink has also high water-solubility which reduces the functionality and operational lifetime of the cell because the enzyme is not immobilized into the ink and the electrical conductivity is lost as the electrode wets. For this reason, the amount of binder was increased in the laboratory experimental inks (see Section 3.2).

As stability is one of the major issues in biobatteries, performance of the pilot cells was investigated. The OCP and the maximum power density of 1 week old pilot cells is (343 ± 4) mV and (0.40 ± 0.03) µW cm^{-2} (at 225 mV), respectively. The energy outputs of the 1 week old pilot cells are (0.59 ± 0.09) µW h cm^{-2} ($E_{cut\text{-}off}$ = 200 mV) and (0.67 ± 0.09) µW h cm^{-2} ($E_{cut\text{-}off}$ = 150 mV). Our fresh laboratory manufactured cells have an OCP of (380 ± 8) mV [42]. This data suggests that already 1 week of storing decreases the OCP and hence the power and energy outputs. After 10 weeks the performance of the cells has decreased close to zero, which can be seen in Fig. 3. The inset of Fig. 3 shows that in 10 weeks the OCP has decreased to 200 mV indicating that either the anodic and/or cathodic mediator is degrading.

In order to find out whether it is the anode or the cathode side of the cell that had degraded, 13 weeks old electrodes were tested against newly manufactured electrodes. The fresh electrodes were printed in laboratory on insulator paper using a semi-automatic screen printer. The results of the CP measurements are seen in Fig. 4a.

It can be seen that the cell performance is poor as both the anode and cathode are stored for 13 weeks. The same is observed with an aged anode and fresh cathode. In contrast, when a fresh anode was tested with an aged cathode the performance of the

Fig. 2. A roll of printed bioelectrodes on cardboard.

cells was significantly better. This indicates that the anode ageing is limiting the performance of the cells. This interpretation agrees with the results by Smolander et al. [39] and [50,51] where the enzymatic stability of printed laccase on a paper substrate is several months.

The next step was to investigate the degradation of the anode mediator. This was done by adding small amount of the fresh FeMeOH mediator into the activation electrolyte which was injected into the aged anodes. Addition of aged FeMeOH was also tested with electrolyte solutions prepared 1 and 2 weeks (stored at 4 °C) before the injection and measurement. Results of CP measurements with addition of fresh and aged FeMeOH via the activation electrolyte can be seen in Fig. 4b.

These measurements showed that by adding the fresh mediator solution on the anode side both OCP and energy output of the aged cells increases. Addition of 1 mM fresh FeMeOH (0.2 μmol) is enough to achieve the same performance level as with 1 week old cells (the amount of printed mediator is approximately 1.3 μmol per electrode) which shows that the enzyme is still active; 0.2 μmol of FeMeOH alone is not enough to produce the electrical energy (25 μA h) discharged during the CP measurement.

However, 1 and 2 weeks old 1 mM FeMeOH solutions did not increase the cell performance as much. This indicates that FeMeOH rapidly either loses its ability to work as an electron shuttle between the enzyme and the carbon particles or there is a chemical reaction that changes the FeMeOH to another compound which has a higher redox potential (300–350 mV vs. Ag/AgCl) than that of FeMeOH (200–250 mV vs. Ag/AgCl [42]).

Stability of ferrocene-based mediator has been studied earlier. Wang et al. [45] and Patel et al. [26] developed ferrocene-based systems showing 70% and 75% of the initial activity after one month as samples were stored at 4 °C and 25 °C, respectively. A study by Li et al. [22] reported a $Fe(CN)_3^{3-/4-}$-based sensor retaining 78% of its initial performance after one month (stored at 4 °C).

Table 2
Cells measured during this work.

	Anode	Age	Cathode	Age	Number of cells	Printing substrate (electrode size)	Measurement
Cell 1	Pilot ink 1	1 wk	Pilot ink	1 wk	3	Cardboard (9 cm^2)	CA
Cell 2	Pilot ink 1	1 wk	Pilot ink	1 wk	6	Cardboard (9 cm^2)	CP, 10 μA
Cell 3	Pilot ink 1	3 wk	Pilot ink	3 wk	3	Cardboard (9 cm^2)	CP, 10 μA
Cell 4	Pilot ink 1	5 wk	Pilot ink	5 wk	3	Cardboard (9 cm^2)	CP, 10 μA
Cell 5	Pilot ink 1	11 wk	Pilot ink	11 wk	3	Cardboard (9 cm^2)	CP, 10 μA
Cell 6	Pilot ink 1	13 wk	Pilot ink	13 wk	3	Cardboard (9 cm^2)	CP, 10 μA
Cell 7	Pilot ink 1	13 wk	Pilot ink	1 d	3	Cardboard/insulator paper (9 cm^2)	CP, 10 μA
Cell 8	Pilot ink 1	1 d	Pilot ink	13 wk	3	Insulator paper/cardboard (9 cm^2)	CP, 10 μA
Cell 9	Exp ink 10 wt% chit	1 d	Pilot ink	1 d	3	Insulator paper (12.25 cm^2)	CP, 15 μA
Cell 10	Exp ink 10.09 wt% chit	1 d	Pilot ink	1 d	3	Insulator paper (12.25 cm^2)	CP, 15 μA
Cell 11	Exp ink 10.17 wt% chit	1 d	Pilot ink	1 d	3	Insulator paper (12.25 cm^2)	CP, 15 μA
Cell 12	Exp ink 10.26 wt% chit	1 d	Pilot ink	1 d	3	Insulator paper (12.25 cm^2)	CP, 15 μA
Cell 13	Exp ink 10.34 wt% chit	1 d	Pilot ink	1 d	3	Insulator paper (12.25 cm^2)	CP, 15 μA
Cell 14	Exp ink 20.01 μmol nkatFeMeOH	1 d	Pilot ink	1 d	3	Insulator paper (12.25 cm^2)	CA
Cell 15	Exp ink 20.03 μmol nkatFeMeOH	1 d	Pilot ink	1 d	3	Insulator paper (12.25 cm^2)	CA
Cell 16	Exp ink 20.05 μmol nkatFeMeOH	1 d	Pilot ink	1 d	3	Insulator paper (12.25 cm^2)	CA
Cell 17	Exp ink 20.08 μmol nkatFeMeOH	1 d	Pilot ink	1 d	3	Insulator paper (12.25 cm^2)	CA
Cell 18	Exp ink 30 wt% chit	1 d	Pilot ink	1 d	3	Insulator paper (12.25 cm^2)	CP, 15 μA
Cell 19	Exp ink 30.13 wt% chit	1 d	Pilot ink	1 d	3	Insulator paper (12.25 cm^2)	CP, 15 μA
Cell 20	Exp ink 30.27 wt% chit	1 d	Pilot ink	1 d	3	Insulator paper (12.25 cm^2)	CP, 15 μA
Cell 21	Exp ink 30.40 wt% chit	1 d	Pilot ink	1 d	3	Insulator paper (12.25 cm^2)	CP, 15 μA
Cell 22	Exp ink 30.53 wt% chit	1 d	Pilot ink	1 d	3	Insulator paper (12.25 cm^2)	CP, 15 μA
Cell 23	Pilot ink 2	1 wk	Pilot ink	19 wk	3	Cardboard (9 cm^2)	CA
Cell 24	Pilot ink 2	1 wk	Pilot ink	19 wk	3	Cardboard (9 cm^2)	CP, 10 μA
Cell 25	Pilot ink 2	3 wk	Pilot ink	21 wk	3	Cardboard (9 cm^2)	CP, 10 μA
Cell 26	Pilot ink 2	5 wk	Pilot ink	23 wk	3	Cardboard (9 cm^2)	CP, 10 μA

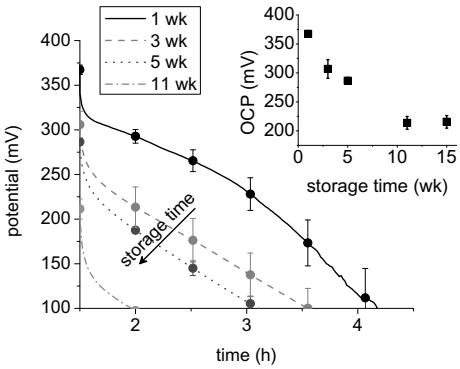

Fig. 3. Curves of chronopotentiometric measurement (constant current of 10 μA) and OCP (inset) of aged GOx/EcoL cells. Pilot anode ink 1 was used in these cells. The geometrical area of the cells was 9 cm^2. The data points represent mean ± SM (n = 3–6).

Chen et al. [4] demonstrated a FeMeOH-based creatinine biosensor which showed 94% of the initial current after more than 6 month storage period as dry at room temperature. These studies indicate that the ferrocene-based redox-systems are fairly stable.

On the other hand, lyophilized GOx is very stable; at 0 °C it is stable for 2 years and at −15 °C for 8 years [2]. In solution the stability of GOx is dependent on the pH; it is most stable at around pH 5 [49]. In a study by Liu et al. [23] there was nearly no decrease in the GOx-based biosensor after storing the biosensor for 15 days at 4 °C. Lawrence et al. [21] reported 98% of the initial performance of a GOx-based biosensor after four months (stored at 4 °C as dry). In a study presented by Onda et al. [25], GOx was assembled with polycations in the preparation of molecular films. The films that were stored in water at 25 °C showed drastic decrease in activity, and approximately only 30% of the activity was retained after 4 weeks. The films which were kept in a buffer at 4 °C did not show a significant decrease in enzymatic activity over 14 weeks. The films stored in air at 4 °C showed 10% decrease in the first week

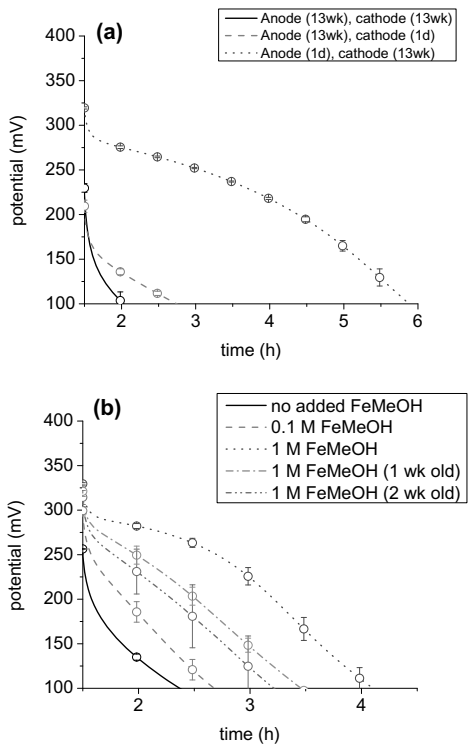

Fig. 4. Curves of chronopotentiometric measurement (constant current of 10 μA) of GOx/EcoL cells (a) as aged (13 weeks old) and fresh electrodes (1 day old) were tested together and (b) as aged (15 weeks old) electrodes were tested with fresh and aged FeMeOH in the activation electrolyte. Geometrical area of the cells was 9 cm^2. The data points represent mean ± SM (n = 3).

but the activity was maintained during the following 13 weeks. The conclusion is that the stability of GOx-based bioelectronics is highly dependent on the storing conditions, and low storing temperature seems to be the key factor.

R2R screen-printed GOx-electrodes without FeMeOH (dried at around 70 °C during the printing process) retained approximately 60% of their initial activity as stored dry for one month (both at room temperature and 4 °C) [42]. However, the presence of FeMeOH in the GOx-electrodes reduced the performance to approximately 30% after one month. This leads to a conclusion that the FeMeOH is the limiting factor in the case of storing stability of GOx-electrodes. The reason for this is still unknown and this phenomenon will be studied in the future. We speculate that FeMeOH gets protonated during the ink preparation process by the succinic acid (dicarboxylic acid) used for the stabilisation of GOx. This reaction leads to elimination the hydroxyl group from FeMeOH forming α-ferrocenyl carbocation (S_N1 reaction on FeMeOH has been studied by Peljo et al. [28]). The formed α-ferrocenyl carbocation reacts with the dicarboxylic acid forming an insoluble ferrocenecarboxylic acid compound, and thus leads to increase in the redox potential of the mediator. Ferrocenecarboxylic acid has a redox potential close to 350 mV vs. Ag/AgCl and has a voltammetric response with GOx starting at 300 mV vs. Ag/AgCl [42]. This potential correlates well with the OCP of the aged cells.

Moreover, a reaction between α-ferrocenyl carbocation and the cofactor of GOx (FAD) is also possible leading to denaturation of GOx. If the enzyme and/or the mediator could be stabilised the anode electrodes were more stable. For this reason, addition of chitosan into experimental anode inks was tested in order to increase stability. This topic is discussed more in the next chapter.

3.2. Optimisation of the anode ink

Experimental inks for the anode were made in order to improve the printability and mechanical stability of the printed anode layer, as well as enzyme and mediator stability. Adhesive behaviour of graphite-based inks can be tailored by controlling the binder to graphite ratio [30]. In addition, ink composition affects also stability as delamination of thin films increases in moist environment [46]. Adding hydrophobic chitosan into the experimental anode inks was tested to improve adhesive behaviour of the electrode. This is kind of a passive corrosion protection which is typically done by fabricating a hydrophobic film that prevents wetting and direct contact with water and/or corrosive liquids thus decreasing corrosion (Samyn [37]). For an example, Höhne et al. [12] synthesized superhydrophobic aluminium surfaces by depositing a chitosan layer and poly(octadecene-alt-maleic anhydride) on microroughened substrates. Ivanova and Philipchenko [15] developed a method to make hydrophobic fabrics by using chitosan-based hydrophobic nanoparticles. Song et al. [40] used chitosan-based polymer to prepare durable superhydrophobic films using a simple and low-cost phase separation method. Hence, chitosan has been used in many applications in order to add hydrophobicity to surfaces.

Chitosan has also been successfully used as an immobilisation and stabilisation polymer-matrix for enzymes [11,22,23,34,35,38,43,47] as well as for iron-based redox couples [11,22,45] in numerous studies. In the perspective of enzymes, PEO is essentially an inert hydrophilic polymer [14], whereas chitosan is hydrophobic, pseudo-natural cationic polymer [8,33]. In hydrophobic solvents a higher amount of water remains associated with the enzyme structure, and thus they exhibit higher activity in hydrophobic solvents than in hydrophilic ones [32]. Additionally, cationic chitosan is a suitable polymer for anionic GOx (pKa 4.2 [27]) because of attractive forces induced by their opposite charges. Hence, hydrophobic characteristic of a chitosan-containing ink can protect the enzyme from dehydration and prevent denaturation.

Moreover, chitosan may act as a stabiliser for FeMeOH. Chitosan has nucleophilic amino groups that can be modified by mild chemical reactions [31]. A chemical synthesis of a ferrocene-chitosan based derivative is also possible [52] as well as a mild synthesis process of a lactic acid-grafted chitosan copolymer [3]. Bhattarai et al. [3] dehydrated chitosan lactate salts for copolymerisation using heat (70–90 °C) to form an amide linkage. This synthesis process is very close to our electrode preparation process where chitosan is mixed with succinic acid (at pH 4.5) and FeMeOH. During the ink drying process one carboxylic acid functional group of succinic acid molecule can react with one amine group of chitosan and the other with α-ferrocenyl carbocation

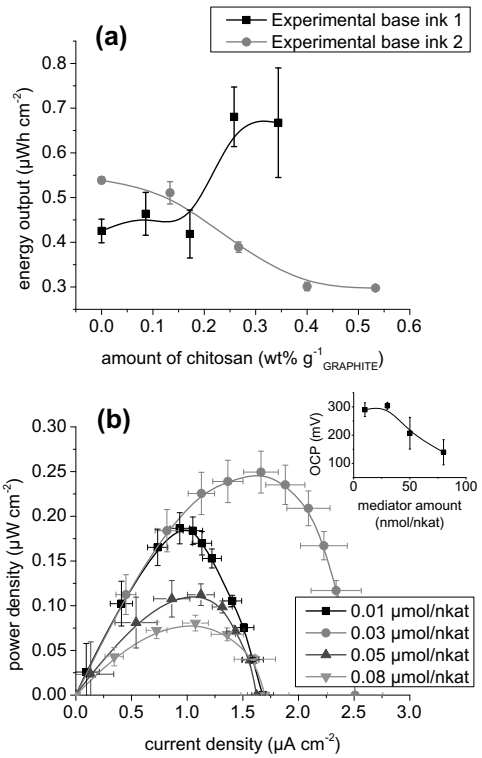

Fig. 5. (a) Energy outputs calculated from chronopotentiometric measurement (constant current of 15 μA, $E_{cut\text{-}off}$ = 150 mV) of experimental base inks containing different amounts of PEO and chitosan. (b) Curves of chronoamperometric measurement and OCP (inset) of experimental inks containing different amounts of FeMeOH. Geometrical area of the cells was 12.25 cm^2. The data points represent mean ± SM (n = 3).

Table 3
Average thickness and roughness of pilot printed anode ink 2 layers. The errors are calculated standard deviations. The values of the pilot anode ink 1 are reprinted from Tuurala et al. [42] with permission.

	Anode ink 1	Anode ink 2
Thickness (μm)	103 ± 22	98 ± 21
Ra[a]	9 ± 1	5.8 ± 0.7
Rq[b]	11 ± 3	7 ± 1

[a] Aritmetic mean.
[b] Quatratic mean.

forming a stabilised ferrocene-chitosan derivative. It must be emphasised though that this reaction has not been verified and will be studied in more detail in the future.

Addition of different amounts of chitosan and FeMeOH into the anode ink was tested in order to increase printability, adhesion and stability of the anode layers. CP and CA curves of three different experimental anode inks are presented in Fig. 5. It can be seen that addition of chitosan into the PEO-containing inks has effect on the energy output (Fig. 5a). If there is low amount of PEO (3.6 wt% $g^{-1}_{GRAPHITE}$) in the ink, increasing amount of chitosan increases the energy output. On the other hand, if there is a high amount of PEO (7 wt% $g^{-1}_{GRAPHITE}$) in the ink, increasing the amount of chitosan decreases the energy output. However, in all the cases higher amount of chitosan in the ink makes the printing process better and increases the ink adhesion to the printing substrate. For this reason, addition of small amount of chitosan is needed for good printing process and print quality.

Addition of different amounts of FeMeOH into the ink was also tested and it can be seen that there is a clear optimum (Fig. 5b). For this particular ink composition, 0.03 μmol $nkat^{-1}$ (of GOx enzyme activity) is the optimum. If the mediator amount is increased further there is significant drop in the power density most probably due to denaturation of the enzyme by the excess amount of the mediator. For this reason, 0.02 μmol $nkat^{-1}$ (of GOx enzyme activity) was seen as a safe amount of FeMeOH for the pilot anode ink 2.

3.3. Performance of the pilot anode ink 2

On the bases of the anode ink optimisation experiments, the amount of binder was doubled and in addition to PEO small amount of chitosan was used in the pilot anode ink 2. Furthermore, the amount of anodic mediator per dry ink was approximately 2-fold compared to the pilot anode ink 1 to increase the cell performance and stability. From the point of view of the printing process, PEO seems to function well as a flow-adding component whereas chitosan adds viscosity to the ink. Thus combination of PEO and chitosan resulted in better ink-flow and printing quality compared to the pilot anode ink 1.

The thickness of the new anode layer was the same as in the previous batch (see Table 3). However, the roughness of the new anodes was 36% lower than that of the anodes using pilot anode ink 1. In addition, the surface topography (see Fig. 6) shows that the difference between the highest and the lowest point of the surface is around 50 μm whereas it was roughly 80 μm in the anodes printed using the pilot ink 1 [42]. This means that the pilot anode

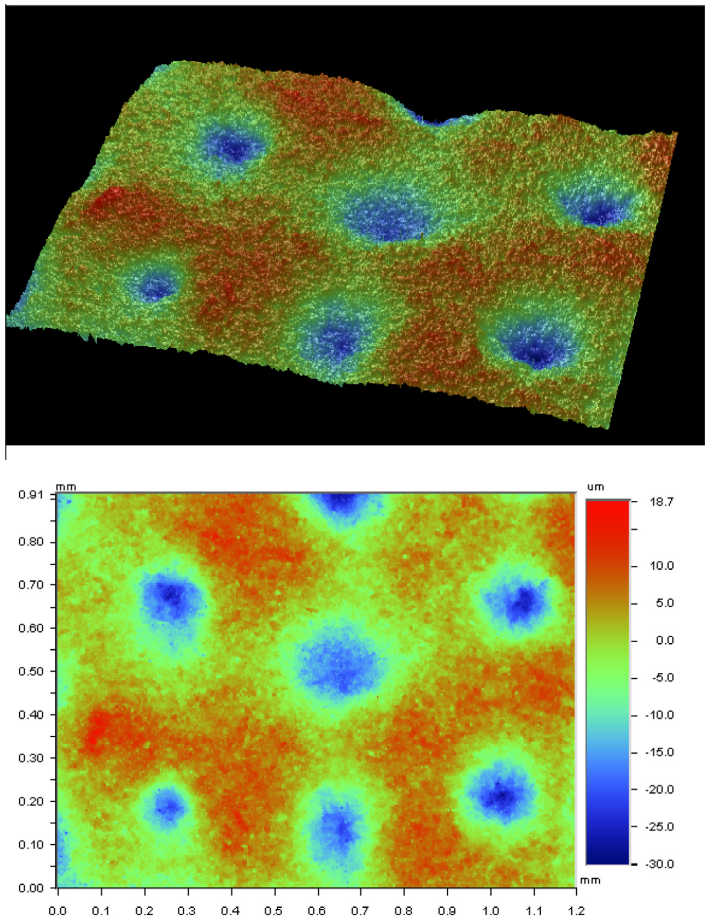

Fig. 6. An optical image (magnification 5.2) of the surface (0.91 mm × 1.20 mm) of the anode layer printed using the pilot anode ink 2 on cardboard. The equivalent image of the anode layer printed using the pilot anode ink 1 can be seen in the Supplementary material 5 (Fig. 3) of our previous publication [42].

ink 2 settles better than the pilot anode ink 1 during printing process leading to more even print quality.

The electrochemical performance of the new anode batch was also studied. The OCP of the 1 week old pilot cells is (341 ± 1) mV and the maximum power density is (0.59 ± 0.02) μW cm^{-2} (at 200 mV). The OCP is the same whereas the maximum power density is 1.5-fold compared to the cells fabricated using the pilot anode ink 1 (see Fig. 7a). The energy outputs calculated from CP measurements (Fig. 7b) are (0.88 ± 0.01) μW h cm^{-2} ($E_{cut\text{-}off}$ = 200 mV) and (1.07 ± 0.02) μW h cm^{-2} ($E_{cut\text{-}off}$ = 150 mV), which are 1.5-fold and 1.6-fold compared to those obtained with the pilot anode ink 1, respectively. The increase in the electrochemical performance is most probably due to 1.75-fold amount of mediator per electrode compared to the mediator amount per electrode in the case of the pilot anode ink 1. In addition, these values are in good correlation with the laboratory manufactured cells (see Section 3.2). Both the maximum power density and the energy output ($E_{cut\text{-}off}$ = 150 mV) are approximately two times higher than that of laboratory manufactured cells which is explained by the different printing screens. The ink layer is two times thicker in the case of pilot printing; hence there is two times more enzyme and mediator in the pilot printed electrodes.

Although we were able to increase the performance of the printed bioanodes, the values achieved seem modest compared to power densities of glucose/O_2 biofuel cells studied by other research groups. For an example, Zhou et al. [55] has demonstrated

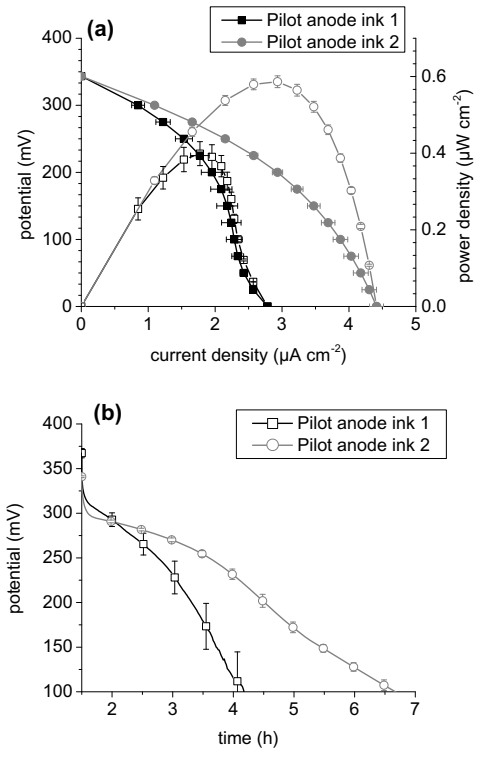

Fig. 7. (a) Potential curve (*full symbols*) and power curve (*hallow symbols*) of chronoamperometric measurement, and (b) chronopotentiometric (constant current of 10 μA) measurement of pilot printed GOx/EcoL cells. Two different pilot anode inks were used. Part of the results of the pilot anode ink 1 were previously published by Tuurala et al. [42] and they are presented here with permission. Geometrical area of the cells was 9 cm^2. The data points represent mean ± SM (n = 3–6).

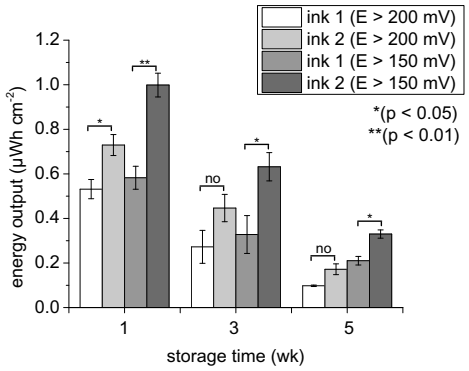

Fig. 8. Energy output calculated from chronopotentiometric measurement (constant current of 10 μA) of pilot printed GOx/EcoL cells versus storage time. Two different pilot anode inks were used. The data points represent mean ± SM (n = 3–6). The p represents the p-value of Student's t-test.

a glucose dehydrogenase (GDH) laccase cell based on highly ordered mesoporous carbon with power density of 38.7 μW cm^{-2}. Sakai et al. [36] build a high-power GDH/laccase cell based on carbon-fibre sheets which resulted in power density of 1.45 mW cm^{-2}. In addition, Zebda et al. [54] fabricated a high-power mediatorless GOx/laccase cell based on compressed multi-walled carbon nanotubes and demonstrated a power density of 1.3 mW cm^{-2}. We want to emphasise though that they used much higher amount of enzyme on the anodes than us; as the power output is calculated by anode enzyme activity the numbers are different 2.3 μW U^{-1}, 12.9 μW U^{-1} and 0.3 μW U^{-1}, respectively. Our bioelectrodes contain approximately 0.7 U cm^{-2} of enzyme activity and thus the power output is 0.8 μW U^{-1}. In addition, the anode is 20–30 times thicker than in our case, which means smaller amount of electrolyte in the anode compartment and thus higher mass-transfer limitations.

We have previously reported an OCP, maximum power density and energy output of (380 ± 8) mV, (1.4 ± 0.1) μW cm^{-2} and (5.5 ± 0.2) μW h cm^{-2}, respectively, for laboratory manufactured cells [42]. The amount of GOx and FeMeOH in the electrodes produced in laboratory was approximately 0.6- and 4-fold, respectively, compared to the pilot anode ink 2. In addition, the laboratory-manufactured cells were printed on a different substrate and dried at room temperature. Because there are many variables that have been changed (the amount of enzyme and mediator, printing substrate and drying temperature), interpretation of the differences in the electrochemical performance is not straightforward. However, these previous results together with the above described experiments with the different FeMeOH concentrations (Figs. 4 and 5b) show that the amount of the mediator plays an important role in the performance and stability of the GOx-electrodes.

In addition to improved electrochemical behaviour, higher binder amount results in a more rigid anode ink layer, decreasing the delamination of the enzymatic layer from the conductive current collector layer. This is observed as more reproducible samples (i.e. decreased error bars in Fig. 7) and significantly higher energy outputs for stored samples as shown in Fig. 8. However, due to the degradation process of the anode mediator the cells degrade at the same pace regardless of the anode ink used.

3.4. Conclusions

R2R printed enzymatic electrodes were manufactured on a cardboard material. During assembling the cells it was observed

that the anode ink layer cracked very easily as dry rendering the assembling of the cells difficult. The anode ink was also very water soluble which decreases the functionality and operational lifetime of the cells, because the enzyme was not immobilized properly into the ink and the conductive layer was lost. The cathode ink layer was more rigid than the anode ink and did not show any problems during the cell assembly. In addition, the electrochemical performance of the cells decreased dramatically during the storage due to the self-degradation of the anodic mediator.

Due to the challenges with the first pilot anode ink a new pilot anode ink was fabricated containing two times more binder than the initial one. In addition to PEO a small amount of chitosan was added to the ink to increase the viscosity (i.e. better printability) and adhesion of the ink as well as the enzyme and mediator stability. Furthermore, two times higher amount of the mediator was used compared to the initial anode ink, which lead to 1.75 times higher amount of the mediator per each electrode. The new anode ink was tested in the R2R printing process and it functioned better than the initial anode ink; the printed layers became more rigid and did not crack during the assembly. In addition to more facile printing process, approximately 1.5 times higher electrochemical performance was obtained with the cells fabricated from the latter ink compared to ones using the initial anode ink. Moreover, the stability and reproducibility of the cells was increased. However, the stability of the anode mediator was not increased.

In the future, degradation of the anode side mediator will be studied in more detail in order to increase the stability of the cells. On the other hand, adding fresh mediator into the biobatteries during their activation was shown to improve the performance, but from the user point of view it is not practical. Another possibility could be adding the mediator as a separate dry layer, as it is storable as dry.

Conflict of interest

None declared.

Acknowledgements

Tiina Maaninen, Pekka Ontero, Mikko Hietala and Arto Rantala-Panula (VTT) are thanked for their assistance in the R2R manufacturing and characterisation of enzymatic electrodes. In addition, Asta Pesonen (VTT), Anu Vaari (VTT) and Prof. Kyösti Kontturi (Aalto University) are gratefully thanked for technical and academic assistance. The research was funded by the Printed Enzymatic Power Source with embedded capacitor on next generation devices – Project (PEPSecond) supported by Tekes, the Finnish Funding Agency for Technology and Innovation.

References

[1] R.L. Arechederra, S.D. Minteer, Anal. Bioanal. Chem. 400 (2011) 1605–1611.
[2] R. Bentley, Glucose oxidase, in: P. Boyer, H. Lardy, K. Myrback (Eds.), The Enzymes, Academic Press, New York, 1963, p. 567.
[3] N. Bhattarai, H.R. Ramay, S.-H. Chou, M. Zhang, Int. J. Nanomed. 1 (2006) 181–187.
[4] P. Chen, Y. Peng, M. He, X. Yan, Y. Zhang, Y. Liu, Int. J. Electrochem. Sci. 8 (2013) 8931–8939.
[5] M.J. Cooney, V. Svoboda, C. Lau, G. Martin, S.D. Minteer, Energy Environ. Sci. 1 (2008) 320.
[6] W. Dungchai, O. Chailapakul, C.S. Henry, Anal. Chem. 81 (2009) 5821–5826.
[7] W. Dungchai, O. Chailapakul, C.S. Henry, Anal. Chim. Acta 674 (2010) 227–233.
[8] P. Dutta, J. Dutta, V. Tripathi, J. Sci. Ind. Res. (India) 63 (2004) 20–31.
[9] L. Feng, X. Li, H. Li, W. Yang, L. Chen, Y. Guan, Anal. Chim. Acta 780 (2013) 74–80.
[10] D. Grieshaber, R. MacKenzie, J. Voeroes, E. Reimhult, Sensors 8 (2008) 1400–1458.
[11] M. Hedström, F. Plieva, I.Y. Galaev, B. Mattiasson, Anal. Bioanal. Chem. 390 (2008) 907–912.
[12] S. Höhne, C. Blank, A. Mensch, M. Thieme, R. Frenzel, H. Worch, M. Müller, F. Simon, Macromol. Chem. Phys. 210 (2009) 1263–1271.
[13] A. Illanes, Electron. J. Biotechnol. 2 (1999) 7–15.
[14] J. Israelachvili, Proc. Natl. Acad. Sci. 94 (1997) 8378–8379.
[15] N.A. Ivanova, A.B. Philipchenko, Appl. Surf. Sci. 263 (2012) 783–787.
[16] P. Jenkins, S. Tuurala, A. Vaari, M. Valkiainen, M. Smolander, D. Leech, Enzyme Microb. Technol. 50 (2012) 181–187.
[17] P. Jenkins, S. Tuurala, A. Vaari, M. Valkiainen, M. Smolander, D. Leech, Bioelectrochemistry 87 (2012) 172–177.
[18] E. Katz, A. Bückmann, I. Willner, J. Am. Chem. Soc. 123 (2001) 10752–10753.
[19] M.S. Khan, S.B.M. Haniffa, A. Slater, G. Garnier, Colloids Surf. B 79 (2010) 88–96.
[20] M.S. Khan, X. Li, W. Shen, G. Garnier, Colloids Surf. B 75 (2010) 239–246.
[21] C.S.K. Lawrence, S.N. Tan, C.Z. Floresca, Sens. Actuators B 193 (2014) 536–541.
[22] W. Li, R. Yuan, Y. Chai, L. Zhou, S. Chen, N. Li, J. Biochem. Biophys. Methods 70 (2008) 830–837.
[23] Y. Liu, M. Wang, F. Zhao, Z. Xu, S. Dong, Biosens. Bioelectron. 21 (2005) 984–988.
[24] A.W. Martinez, S.T. Phillips, G.M. Whitesides, E. Carrilho, Anal. Chem. 82 (2010) 3–10.
[25] M. Onda, K. Ariga, T. Kunitake, J. Biosci. Bioeng. 87 (1999) 69–75.
[26] H. Patel, X. Li, H.I. Karan, Biosens. Bioelectron. 18 (2003) 1073–1076.
[27] J.H. Pazur, K. Kleppe, Biochemistry 3 (1964) 578–583.
[28] P. Peljo, L. Qiao, L. Murtomäki, C. Johans, H.H. Girault, K. Kontturi, Chemphyschem 14 (2013) 311–314.
[29] K.M. Polizzi, A.S. Bommarius, J.M. Broering, J.F. Chaparro-Riggers, Curr. Opin. Chem. Biol. 11 (2007) 220–225.
[30] J. Rangel, A. Del-Real, V. Castano, Chem. Chem. Technol. 2 (2008) 305–308.
[31] M. Rekha, C. Sharma, Trends Biomater. Artif. Organs 21 (2008) 107–115.
[32] K. Rezaei, E. Jenab, F. Temelli, Crit. Rev. Biotechnol. 27 (2007) 183–195.
[33] M. Rinaudo, Prog. Polym. Sci. 31 (2006) 603–632.
[34] R.A. Rincón, C. Lau, H.R. Luckarift, K.E. Garcia, E. Adkins, G.R. Johnson, P. Atanassov, Biosens. Bioelectron. 27 (2011) 132–136.
[35] R.A. Rincón, C. Lau, K.E. Garcia, P. Atanassov, Electrochim. Acta 56 (2011) 2503–2509.
[36] H. Sakai, T. Nakagawa, Y. Tokita, T. Hatazawa, T. Ikeda, S. Tsujimura, K. Kano, Energy Environ. Sci. 2 (2009) 133–138.
[37] P. Samyn, J. Braz. Chem. Soc. 25 (5) (2014) 947–960.
[38] K. Sjoholm, M. Cooney, S. Minteer, ECS Trans. 19 (2009) 1–7.
[39] M. Smolander, H. Boer, M. Valkiainen, R. Roozeman, M. Bergelin, J.-E. Eriksson, X.-C. Zhang, A. Koivula, L. Viikari, Enzyme Microb. Technol. 43 (2008) 93–102.
[40] W. Song, V.S. Gaware, Ö.V. Rúnarsson, M. Másson, J.F. Mano, Carbohyd. Polym. 81 (2010) 140–144.
[41] A. Swerin, I. Mira, Sens. Actuators B 195 (2014) 389–395.
[42] S. Tuurala, O.-V. Kaukoniemi, L. von Hertzen, J. Uotila, A. Vaari, M. Bergelin, P. Sjöberg, J.-E. Eriksson, M. Smolander, J. Appl. Electrochem. 44 (2014) 881–892.
[43] S. Tuurala, C. Lau, P. Atanassov, M. Smolander, S.D. Minteer, Electroanalysis 24 (2012) 229–238.
[44] S. Tuurala, M. Smolander, J. Uotila, O.-V. Kaukoniemi, H. Boer, M. Valkiainen, A. Vaari, A. Koivula, P. Jenkins, ECS Trans. 25 (2010) 1–10.
[45] H. Wang, Q. Pan, G. Wang, Sensors 5 (2005) 266–276.
[46] P. Waters, The Effects of Moisture on Thin Film Delamination and Adhesion, University of South Florida, 2005.
[47] R. Vazquez-Duhalt, R. Tinoco, P. D'Antonio, L.D. Topoleski, G.F. Payne, Bioconjugate Chem. 12 (2001) 301–306.
[48] I. Willner, E. Katz (Eds.), Bioelectronics: From Theory to Applications, WILEY-VCH, Weinheim, 2005.
[49] R. Wilson, A. Turner, Biosens. Bioelectron. 7 (1992) 165–185.
[50] H. Virtanen, H. Orelma, T. Erho, M. Smolander, Process Biochem. 47 (2012) 1496–1502.
[51] H. Virtanen, K. Vehmas, T. Erho, M. Smolander, Packag. Technol. Sci. 27 (2014) 819–830.
[52] W. Yang, H. Zhou, C. Sun, Macromol. Rapid Commun. 28 (2007) 265–270.
[53] A.K. Yetisen, M.S. Akram, C.R. Lowe, Lab Chip 13 (2013) 2210–2251.
[54] A. Zebda, C. Gondran, A. Le Goff, M. Holzinger, P. Cinquin, S. Cosnier, Nat. Commun. 2 (2011) 370.
[55] M. Zhou, L. Deng, D. Wen, L. Shang, L. Jin, S. Dong, Biosens. Bioelectron. 24 (2009) 2904–2908.
[56] M. Zhou, S. Dong, Acc. Chem. Res. 44 (2011) 1232–1243.
[57] M. Zhou, J. Wang, Electroanalysis 24 (2012) 197–209.

VI

Tuurala, S., Kallio, T., Smolander, M., and Bergelin, M. (2015) Increasing operational lifetime of printed enzymatic power sources using superabsorbent polymers as anode support. *Energy Technology* ***3***, 1080-1083.

DOI: 10.1002/ente.201500163

Increasing the Operational Lifetime of a Printed Enzymatic Power Source using Superabsorbent Polymers as the Anode Support

Saara Tuurala,*[a] Tanja Kallio,[b] Maria Smolander,[a] and Mikael Bergelin[c]

Superabsorbent polymers (SAPs) were added as a dry powder to the anode side of a printed enzymatic power source. SAPs partially eliminated delamination of the cathode electrode from the current collector and decreased the ohmic losses in the cells. SAPs also retained moisture inside the cells and increased water diffusion through the membrane from the anode side to the cathode side. Moreover, the degradation process of the operational cells was slower due to using the SAPs. Consequently, the operational lifetime of the cells was increased; the electric charge and energy output of the cells doubled in the presence of the SAPs at the anode.

Environmentally friendly, disposable batteries are needed because portable electronics are getting more and more common in our everyday activities. The demand for thin and flexible batteries is growing as wearable technology and the "internet of things" are brought to the market. For this reason, we have developed a fully printable biobattery for low-power applications. Its chemistry is based on enzyme catalysis where glucose is oxidized at the anode by glucose oxidase and air is reduced by laccase at the cathode. The electrons produced at the anode are circulated using an external circuit to the cathode and thus the chemical energy is converted to electrical energy.

There are still many challenges in battery technology. For instance, contact between the electrode and the current collector plays an important role in the overall battery capacity and lifetime.[1] Thus, as printed electrodes are manufactured, good adhesion between the printing substrate and catalyst-containing ink has to be guaranteed. In addition to the adhesion, cracking of the catalyst layer causes problems. Thinner layers can prevent cracking[2] but this also means smaller amount of active materials and 3D surface area, which may not be sufficient for battery applications. Moreover, lack of moisture and uneven contacts between the anode/membrane/cathode interfaces hinders the ion transfer through the membrane from one electrode to the other. In the case of enzymatic electrodes, the lack of electrolyte buffer also hinders diffusion of the substrate and reaction products to and from the active sites of the enzymes. Enzymes require a certain minimum amount of water in their structure to maintain their natural conformation; hence their catalytic activity and stability are strongly influenced by hydration levels.[3]

Our previous unpublished studies have revealed contact problems and electrolyte leakage in our printed biobatteries. During disassembling the cells, it was observed that the cathode layer had completely delaminated from the current collector (Figure 1a). The anode layer stayed attached to the current collector most likely due to using double the amount of binder in the ink at the anode (7.14 wt% of graphite) than in the cathode ink (3.6 wt% of graphite). Additionally, the electrolyte used to moisturize the cells leaked out from the anode side as illustrated in Figure 2a. Therefore, we wanted to find a biocompatible glue-like substance to ensure proper adhesion between each layer and to increase the operational lifetime of our printed biobattery.

Choosing an appropriate enzyme support (in our case the enzyme-containing ink) and adding certain salt hydrates have been important strategies to adjust the moisture content in an enzymatic reaction medium.[3] Our approach was to use superabsorbent polymers[4] (SAPs), which are capable of absorbing and holding large amounts of water compared to their weight, even under some compression pressure. The swelling capacity is typically 40–50 wt% but, for example, poly(acrylic acid) (PAA) hydrogels can exhibit swelling of more than 99 wt%.[4b] Due to these water-retaining properties as well as biocompatibility, SAPs have been used in wide variety of applications ranging from the forest and plant industry[5] to diapers,[6] and from drug release systems[7] to batteries[8] and fuel cell technology.[9] For instance, Iwakura et al.[8a] reported that the use of a PAA-based electrolyte in nickel–metal-hydride batteries increased the charge–discharge and capacity retention characteristics compared with a similar type of cell assembled using an aqueous solution of potassium hydroxide. In addition, Magasinski et al.[8e] demonstrated that carbon-coated silicon anodes with PAA binders have stable performance for more than 100 cycles and the coulombic efficiency was 99%. Hence, we viewed SAPs as good candidates for anode supports in our printed biobatteries. We chose two commercial products from which the first (SAP1) is typically used for chemical spills and the other (SAP2) for baby diapers.

We observed that the SAPs increase the adhesion between the cathode layer and the current collector (Figure 1b). The

[a] S. Tuurala, Dr. M. Smolander
Printed Sensors and Electronic Devices
VTT Technical Research Centre of Finland Ltd
P.O. Box 1000, FI-02044 VTT (Finland)
E-mail: saara.tuurala@vtt.fi

[b] Dr. T. Kallio
Department of Chemistry
Aalto University
P.O. Box 16100, FI-00076 AALTO (Finland)

[c] Dr. M. Bergelin
Process Chemistry Centre
Åbo Akademi
Biskopsgatan 8, FI-20500 ÅBO (Finland)

Supporting information for this article is available on the WWW under http://dx.doi.org/10.1002/ente.201500163.

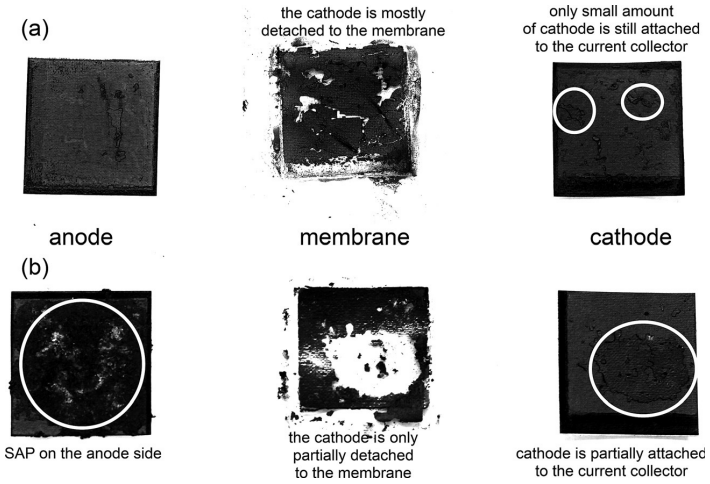

Figure 1. Photos of electrodes and membrane after electrochemical measurements (a) without and (b) with superabsorbent polymer on the anode side.

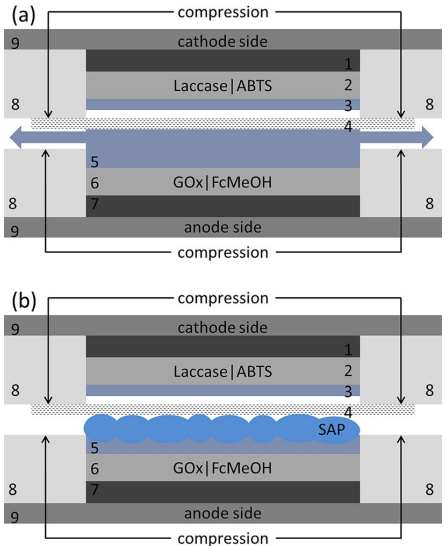

Figure 2. Cross-sectional schematic of the cell assembly (a) without and (b) with SAP on the anode side. The numbers indicate different layers of the cell: 1) printed current collector, 2) printed cathode, 3) cathode electrolyte, 4) membrane, 5) anode electrolyte, 6) printed anode, 7) printed current collector, 8) rubber seal, and 9) printing substrate (cardboard). The properties (e.g., thickness) of the layers are presented in Table S1 (Supporting Information).

presence of SAPs also increases diffusion of water from the anode to the cathode (Supporting Information, Figure S2 and S3). Based on gravimetric analysis (Figure S4, Supporting Information), the moisture retention of the cells is slightly increased by using SAPs. These positive effects were observed in the long-term electrochemical measurements. However, only small differences between the cells were observed in chronoamperometric (CA) measurements (Figure 3a). The maximum current densities of the cells were $I_{max}^{noSAP} = 4.4 \pm 0.1$, $I_{max}^{SAP1} = 4.2 \pm 0.1$, and $I_{max}^{SAP2} = 4.0 \pm 0.1\ \mu A\,cm^{-2}$. Hence, the addition of SAPs on the anode slightly increases the diffusion overpotentials of the cells. The maximum power densities of the cells were $P_{max}^{noSAP} = 0.59 \pm 0.01$, $P_{max}^{SAP1} = 0.58 \pm 0.01$, and $P_{max}^{SAP2} = 0.63 \pm 0.01\ \mu W\,cm^{-2}$. The small increase in the power density in the case of SAP2 indicates decreased ohmic losses. At 30 min after the CA measurement, the open-circuit potentials (OCP) of the cells recovered to 85% (no SAP), 88% (SAP1), and 91% (SAP2) of the initial OCP

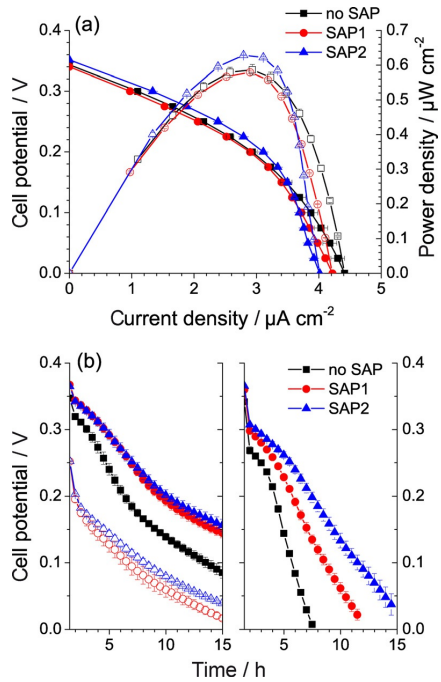

Figure 3. (a) Polarization curve (full symbols) and power curve (hollow symbols) of printed GOx||EcoL cells without and with the addition of superabsorbent polymer on the anode side. (b) Curves of chronopotentiometric measurement (left: 5 μA constant current, right: 15 μA constant current) of printed GOx||EcoL cells without (hollow symbols) and with (full symbols) glucose. The geometrical cell area was 9 cm^2. The data represents the mean ±SM ($n=3$).

value. This indicates that the degradation of the batteries is slower in the case of SAPs on the anode. The average energy output (EO) and electrical charge (EC) values calculated from the CA measurements are $0.91 \pm 0.03\ \mu Wh\,cm^{-2}$ and $7.3 \pm 0.2\ \mu Ah\,cm^{-2}$, respectively, which are the minimum values to be expected from the chronopotentiometric (CP) measurements.

CP measurements (Figure 3b) show that the operational lifetime of the cells is significantly increased by applying SAPs at the anode. First, the *IR*-drop decreases by 14% by using SAPs. Secondly, both the EC and EO values increase significantly [1.6–1.7 fold (SAP1) and 2.1–2.2 fold (SAP2)] compared to cells without SAPs (Table 1). This effect is attributed to the swelling of the SAPs, which leads to tighter cell assembly and thus increased adhesion of the cathode ink to the current collector as well as to better contact at the anode/membrane/cathode interfaces, thereby increasing the diffusion of protons from the anode to the cathode. Moreover, laccase inhibition due to H_2O_2 formation on the anode[10] is reduced as the SAP-layer blocks the diffusion of H_2O_2 from the anode to the cathode. The blocking reaction is assumed to be a degradation process of the SAPs following Fenton's chemistry.[11]

Cells without glucose (i.e., fuel) were also tested, which showed that addition of the SAPs does not have significant discharge property for a cut-off voltage of 200 mV (Table 1); the EC and EO values are 5% of those from the glucose-containing cells. However, as the cut-off voltage is less than 150 mV, the EC is 25–40% and the EO is 13-20% compared to glucose-containing cells. The reason is most likely the combination of PAA and ferrocene methanol (FcMeOH, anode mediator). PAA is an anionic polymer and tends to lose protons, and, at the same time, FcMeOH becomes oxidized to release electrons. Each anode contains 2–3 μmol of FcMeOH, which corresponds to an EC value of 6–9 $\mu Ah\,cm^{-2}$, which agrees well to the results (Table 1). The oxidation potential of FcMeOH is 0.244 V (vs. Ag/AgCl)[12] and the half-wave potential of 2,2′-azino-bis(3-ethylbenzothiazoline-6-sulfonic acid) (ABTS, cathode mediator) is 0.498 V (vs. Ag/AgCl),[13] which generates a cell potential of 0.254 V. This corresponds well to the OCP of the cells without glucose (Table 1).

In summary, the contact between the anode and cathode prints as well as moisture management in the cells was improved by using glue-like biocompatible polymers as anode support. The addition of the SAPs decreased the delamination of the cathode layer from the current collector and improved the contact at the anode/membrane/cathode interface, thereby increasing the proton diffusion from the anode to the cathode. The *IR*-drop was decreased by 14% and degradation of the operational cells was hindered. Thus, the operational lifetime of the cells was increased and both the EC and EO values were doubled. Cells without glucose also generated power, presumably due to the combination of SAP and FcMeOH on the anode, but it is not a problem in the case of a battery application as long as the functionality of FcMeOH as an enzyme mediator is not significantly interfered with by the SAP used. Although the performance of our biobattery is still rather modest compared to glucose/air biofuel cells studied by other research groups, we want to emphasize that they used much higher amounts of enzymes on the electrodes than we did, as well as thicker structures and higher amounts of electrolyte as discussed in our previous publications.[12,14] In this study, our experiments showed that SAPs can be used in our printed biobatteries as a biocompatible adhesive and stabilizing component. Our future studies will include optimizing the enzyme as well as SAP amount in the cells to achieve higher performance.

Experimental Section

Materials: The materials for the enzyme-containing inks were ferrocene methanol (FcMeOH, Aldrich 335061), glucose oxidase from *Aspergillus niger* (GOx, Sigma G7141), ABTS (Sigma A1888), laccase (EcoL, AB Enzymes Ecostone LCL 45, EC 1.10.3.2), graphite powder (<20 μm, Aldrich 282863), polyethylene oxide (PEO, Aldrich 189456), chitosan (Aldrich 448877), succinic acid (Sigma–Aldrich 398055), and acetic acid (Sigma–Aldrich 33209). The materials for printing and cell assembly were polyethylene-coated cardboard (Stora Enso Classic Bar PE $175+15\ g\,m^{-2}$), current-collector ink (Peters SD 2843 HAL), dialysis membrane (Medicell International Ltd, visking code DTV12000.11.000), and D-glucose (VWR 101176K). Superabsorbent polymers were Engulf (SAP1, Oy NCH Suomi Ab/Certified Laboratories) and poly(acrylic acid) (SAP2, LG Chem. Korea). Distilled (DI) water was used in all experiments and 50 mM Na-succinate (pH 4.5) was used as buffer-electrolyte.

Printed electrodes: Cathode ink was prepared by mixing together graphite (25 g), PEO (5 wt% in H_2O, 18 g), and 50 mM sodium succinate (pH 4.5, 10 g). This ink (50 g) was mixed with

Table 1. Electrical characteristics of printed enzymatic cells without and with addition of SAPs on the anode.

	OCP [V]	Electrical charge [$\mu Ah\,cm^{-2}$]			Energy output [$\mu Wh\,cm^{-2}$]		
		$E>200$ mV	$E>150$ mV	$E>25$ mV	$E>200$ mV	$E>150$ mV	$E>25$ mV
without SAP (5 μA)	0.347 ± 0.004	2.7 ± 0.1	4.2 ± 0.2	11.9 ± 0.7	0.73 ± 0.02	0.99 ± 0.03	1.59 ± 0.08
without SAP (15 μA)	0.342 ± 0.002	4.52 ± 0.05	5.64 ± 0.04	9.3 ± 0.1	1.14 ± 0.02	1.33 ± 0.03	1.64 ± 0.04
with SAP1 (5 μA, no glucose)	0.252 ± 0.001	0.22 ± 0.03	1.2 ± 0.3	6.9 ± 0.5	0.05 ± 0.01	0.22 ± 0.01	0.66 ± 0.07
with SAP1 (5 μA)	0.367 ± 0.004	4.4 ± 0.3	7.1 ± 0.5	17.7 ± 0.9	1.24 ± 0.03	1.69 ± 0.04	2.6 ± 0.2
with SAP1 (15 μA)	0.360 ± 0.002	7.1 ± 0.2	9.3 ± 0.2	16.4 ± 0.6	1.87 ± 0.01	2.24 ± 0.03	2.9 ± 0.1
with SAP2 (5 μA, no glucose)	0.252 ± 0.001	0.30 ± 0.01	1.7 ± 0.2	8.8 ± 0.3	0.07 ± 0.01	0.30 ± 0.01	0.84 ± 0.02
with SAP2 (5 μA)	0.364 ± 0.001	4.8 ± 0.4	8.0 ± 0.7	23 ± 1	1.32 ± 0.03	1.87 ± 0.06	3.1 ± 0.2
with SAP2 (15 μA)	0.366 ± 0.003	9.9 ± 0.4	13.0 ± 0.6	22.2 ± 0.8	2.63 ± 0.05	3.18 ± 0.08	4.0 ± 0.2

2200 U of EcoL and 0.4 mmol of ABTS. The anode ink was prepared by mixing together graphite (25 g), PEO (5 wt% in H_2O, 35 g), and chitosan (0.5 wt% in 1 wt% acetic acid, 7 g). This ink (50 g) was mixed with 2430 U of GOx and 0.8 mmol of FcMeOH. PE-coated cardboard was used as the printing substrate. Current collectors were printed first and cured at 145 °C. The enzyme-containing inks were printed on the current collector layer and dried at approximately 70 °C. The printing process and ink optimization are explained in detail in our previous publications.[12,14] The electrodes were stored at room temperature.

Cell assembly: Square samples were cut from the cardboard for measurements. First, an anode (9 cm^2) was moisturized by pipetting 200 μL of electrolyte and 50 mg of glucose, which corresponds to 1.39 M glucose concentration. A separator (16 cm^2) was set on top of the anode. A cathode (9 cm^2) was moisturized by pipetting 100 μL of electrolyte and assembled on top of the anode–separator layer (Figure 2a). The electrodes were sandwiched between flat graphite plates (Figure S1, Supporting Information) to ensure even pressure such that the rubber seals, and hence anode/separator/cathode layers, were compressed together. The properties of the layers of the assembled cell are shown in Table S1 (Supporting Information). If SAPs were used, 15 mg of the SAP-powder was spread on the anode before moisturizing it (Figure 2b). The SAP-powder absorbed most of the anode electrolyte and swelled before the cells were assembled, whereas some of the anode electrolyte floated on the anode layer in the cases that the SAP-powder was not used. As the electrolyte was absorbed into the SAP-powder it added ionic conductivity to the polymer[8c].

Electrochemical measurements: The electrochemical performance of the cells was measured using a multichannel potentiostat (BioLogic VMP), in two electrode connection. The reference cells were assembled as illustrated in Figure 2a (no SAP). In chronoamperometry (CA), cells were measured at open-circuit potential (OCP) for 1.5 h, after which the cell potential was decreased from 300 to 0 mV in 25 mV steps every 10 min, and the steady-state current was measured. In chronopotentiometry (CP), the cells were measured at OCP for 1.5 h, after which a constant current (5 or 15 μA) was drawn from the cells until the cell potential decreased to 25 mV. The cell potential was measured in 1 min intervals. The electrical charge (EC) and energy output (EO) of the cells was calculated from the CP data using multiple cut-off voltages ($E_{cut-off}$) a) 200 mV, b) 150 mV, and c) 25 mV. The *IR*-drop was calculated using $R = U/I$, in which U is the instant potential drop from OCP as the constant current I (either 5 or 15 μA) is applied. Three individual repetitions were measured and the error bars are the standard error of the mean (SM).

Acknowledgements

Tiina Maaninen, Pekka Ontero, Mikko Hietala, Arto Ranta-Panula, Asta Pesonen, Anu Vaari (VTT), and Prof. Emer. Kyösti Kontturi (Aalto University) are gratefully thanked for their technical and academic assistance. The research was funded by the Printed Enzymatic Power Source with embedded capacitor on next generation devices -project (PEPSecond) supported by TEKES, the Finnish Funding Agency for Technology and Innovation.

Keywords: batteries · enzyme catalysis · fuel cells · print processing · superabsorbent polymers

[1] a) C. K. Chan, H. Peng, G. Liu, K. McIlwrath, X. F. Zhang, R. a. Huggins, Y. Cui, *Nat. Nanotechnol.* **2008**, *3*, 31–35; b) S. Yoshihara, H. Katsuta, H. Isozumi, M. Kasai, K. Oyaizu, H. Nishide, *J. Power Sources* **2011**, *196*, 7806–7811.

[2] J. Li, A. K. Dozier, Y. Li, F. Yang, Y.-T. Cheng, *J. Electrochem. Soc.* **2011**, *158*, A689–A694.

[3] K. Rezaei, E. Jenab, F. Temelli, *Crit. Rev. Biotechnol.* **2007**, *27*, 183–195.

[4] a) K. Horie, R. B. Fox, J. He, M. Hess, J. Kahovec, T. Kitayama, P. Kubisa, W. Mormann, R. F. T. Stepto, D. Tabak, E. S. Wilks, W. J. Work, *Pure Appl. Chem.* **2009**, *76*, 889–906; b) A. B. Kinney, A. B. Scranton in *Superabsorbent Polymers* (Eds.: F. Buchholz, N. Peppas), American Chemical Society, Washington DC, **1994**, pp. 2–26.

[5] a) M. Casquilho, A. Rodrigues, F. Rosa, *Agric. Sci.* **2013**, *4*, 57–60; b) K. M. Raju, M. P. Raju, *Adv. Polym. Technol.* **2001**, *20*, 146–154; c) K. M. Raju, M. P. Raju, Y. M. Mohan, *J. Appl. Polym. Sci.* **2002**, *85*, 1795–1801; d) G. Cannazza, A. Cataldo, E. De Benedetto, C. Demitri, M. Madaghiele, A. Sannino, *Water* **2014**, *6*, 2056–2069.

[6] a) M. C. Hermansen, M. Buches, *Pediatrics* **1988**, *81*, 428–431; b) A.-M. Beguin, E. Malaquin-Pavan, C. Guihaire, A.-M. Hallet-Lezy, S. Souchon, V. Homann, P. Zöllner, M. Swerev, R. Kesselmeier, F. Hornung, H. Smola, *BMC Geriatr.* **2010**, *10*, 86.

[7] a) M. Sadeghi, F. Soleimani, *Int. J. Chem. Eng. Appl.* **2011**, *2*, 314–316; b) M. Pandey, M. C. I. Mohd Amin, N. Ahmad, M. M. Abeer, *Int. J. Polym. Sci.* **2013**, *2013*, 1–10; c) A. Kikuchi, T. Okano, *Adv. Drug Delivery Rev.* **2002**, *54*, 53–77.

[8] a) C. Iwakura, S. Nohara, N. Furukawa, H. Inoue, *Solid State Ionics* **2002**, *148*, 487–492; b) S. Thayumanasundaram, V. S. Rangasamy, N. De Greef, J. W. Seo, J.-P. Locquet, *Eur. J. Inorg. Chem.* **2015**, 1290–1299; c) Y. Ismail, H. Haliman, A. Mohamad, *Int. J. Electrochem. Sci.* **2012**, *7*, 3555–3566; d) A. A. Mohamad, *J. Power Sources* **2006**, *159*, 752–757; e)
A. Magasinski, B. Zdyrko, I. Kovalenko, B. Hertzberg, R. Burtovyy, C. F. Huebner, T. F. Fuller, I. Luzinov, G. Yushin, *ACS Appl. Mater. Interfaces* **2010**, *2*, 3004–3010.

[9] a) S.-H. Ge, X.-G. Li, I.-M. Hsing, *J. Electrochem. Soc.* **2004**, *151*, B523–B528; b) Q. Qin, Q. Tang, Q. Li, B. He, H. Chen, X. Wang, P. Yang, *Int. J. Hydrogen Energy* **2014**, *39*, 4447–4458; c) Q. Tang, J. Wu, Z. Tang, Y. Li, J. Lin, *J. Mater. Chem.* **2012**, *22*, 15836.

[10] a) R. D. Milton, F. Giroud, A. E. Thumser, S. D. Minteer, R. C. T. Slade, *Phys. Chem. Chem. Phys.* **2013**, *15*, 19371–19379; b) R. D. Milton, S. D. Minteer, *J. Electrochem. Soc.* **2014**, *161*, H3011–H3014.

[11] A. Neira, M. Tarraga, R. Catalan, *J. Chil. Chem. Soc.* **2007**, *52*, 1314–1317.

[12] S. Tuurala, O.-V. Kaukoniemi, L. von Hertzen, J. Uotila, A. Vaari, M. Bergelin, P. Sjöberg, J.-E. Eriksson, M. Smolander, *J. Appl. Electrochem.* **2014**, *44*, 881–892.

[13] M. Smolander, H. Boer, M. Valkiainen, R. Roozeman, M. Bergelin, J.-E. Eriksson, X.-C. Zhang, A. Koivula, L. Viikari, *Enzyme Microb. Technol.* **2008**, *43*, 93–102.

[14] S. Tuurala, T. Kallio, M. Smolander, M. Bergelin, *Sens. Bio-Sensing Res.* **2015**, *4*, 61–69.

Received: May 29, 2015
Revised: July 29, 2015
Published online on September 11, 2015

Energy Technology

Supporting Information

Increasing the Operational Lifetime of a Printed Enzymatic Power Source using Superabsorbent Polymers as the Anode Support

Saara Tuurala,*[a] Tanja Kallio,[b] Maria Smolander,[a] and Mikael Bergelin[c]

ente_201500163_sm_miscellaneous_information.pdf

Properties of the layers of an assembled cell

Properties of the layers of an assembled cell are shown in Table S1. The total amount of electrolyte that was estimated to be absorbed into the layer structures was approximately 300 µl which was calculated according to the area, thickness and porosity of each layer. The anode was moisturized with 200 µl and the cathode with 100 µl of anode and cathode electrolyte solutions, respectively. The reason why the amount of electrolyte on the anode side was higher than on the cathode side was because 100 µl of electrolyte was instantly absorbed into the cathode structure, however higher amount of electrolyte ran over the electrode as it was assembled on top of the anode-separator layer.

Table S1. Area, thickness and porosity of the layers.

Layer	Area [cm^2]	Thickness [µm]	Porosity [%]	Estimation of buffer absorption capacity [µl]
Printed current collector	9	80	25	18
Printed cathode	9	100	52	47
Printed anode	9	100	60	54
Membrane	16	35	N/A	30
Rubber seal		250	-	-
Area between printed electrode and membrane	9	70	100	63

Water diffusion tests with dummy cells and water retention of the cells

Cleanroom paper (Spec-Wipe 3, VWR) was used as the dummy electrode material. The thickness of the paper was close to that of the printed electrodes (200 µm). The dummy cells were assembled as the actual cells, except the moisturizing electrolyte was red-colored DI-water (200 µl) on the dummy-anode side and DI-water (100 µl) on the dummy-cathode side. In addition to plain graphite plates open-cathode was tested (Figure S2). The cells were kept assembled for 24 h. Figures S3 and S4 show that in both cases (closed and open-cathode configurations) the colored DI-water has diffused better from the anode side to the cathode side as SAP was used.

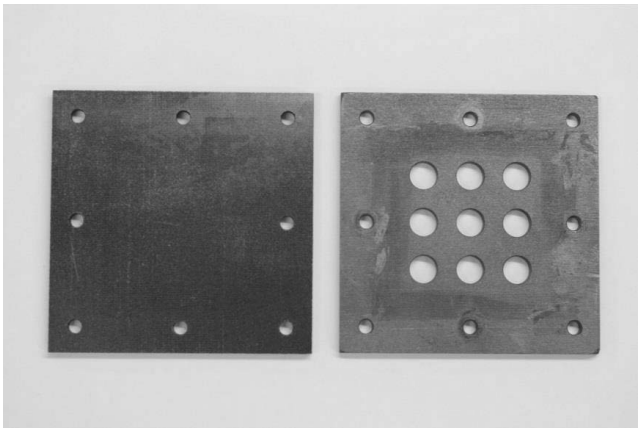

Figure S1. Graphite plates used in the electrochemical measurements. Two flat graphite plates (left) were used in closed test cell configuration. One flat and one holed graphite plate (right) were used in open-cathode configuration.

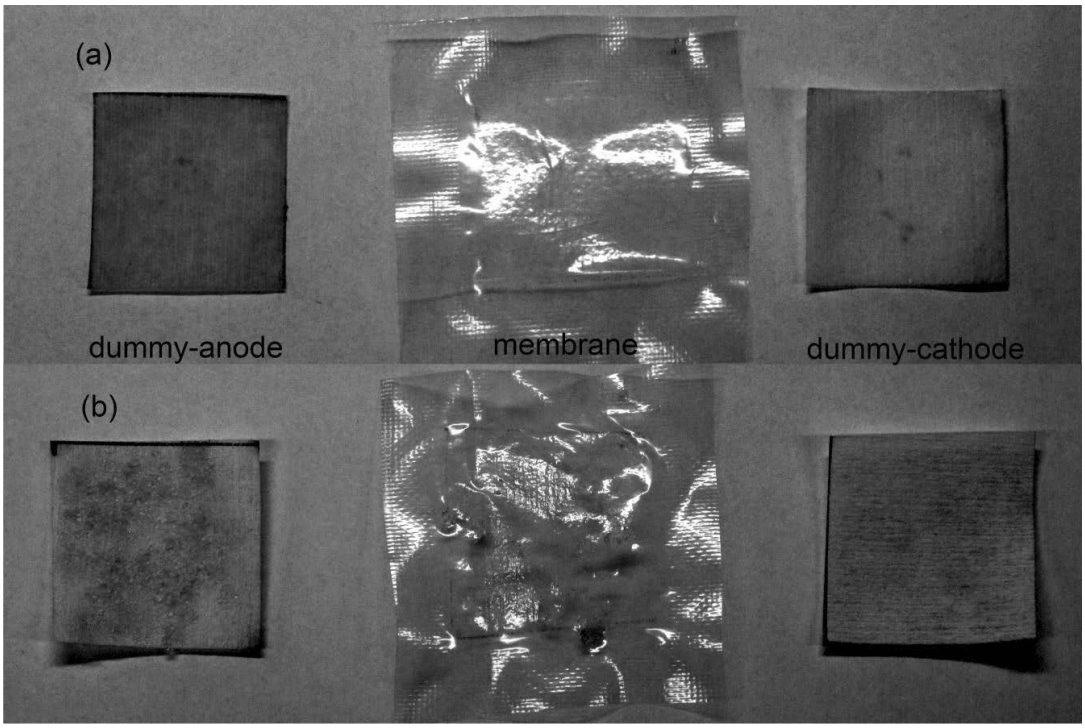

Figure S2. Colored DI-water on clean room paper placed in closed test cell (a) without and (b) with superabsorbent polymer. The cells were kept assembled for 24 h.

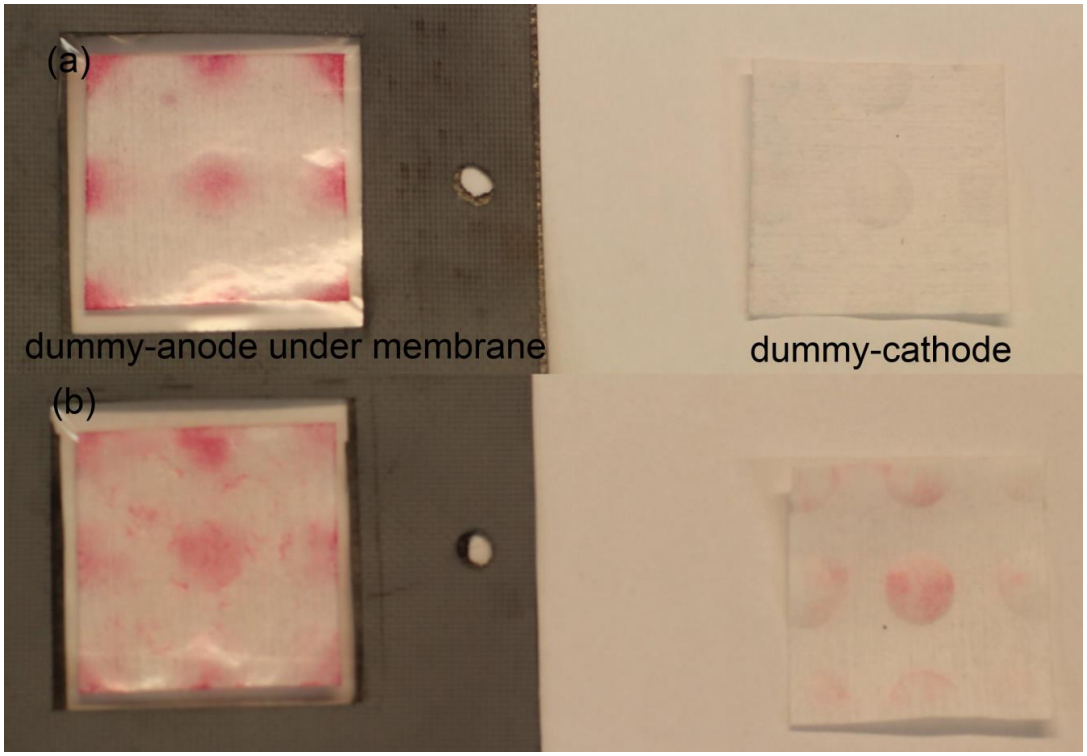

Figure S3. Colored water on clean room paper placed in open-cathode test cell (a) without and (b) with superabsorbent polymer. The cells were kept assembled for 24 h.

Water retention of the cells was measured by weighing the assembled cells. The cells were assembled using printed electrodes. Both closed and open-cathode cell configurations were tested. The anode was moisturized with 200 µl and the cathode with 100 µl of DI-water.

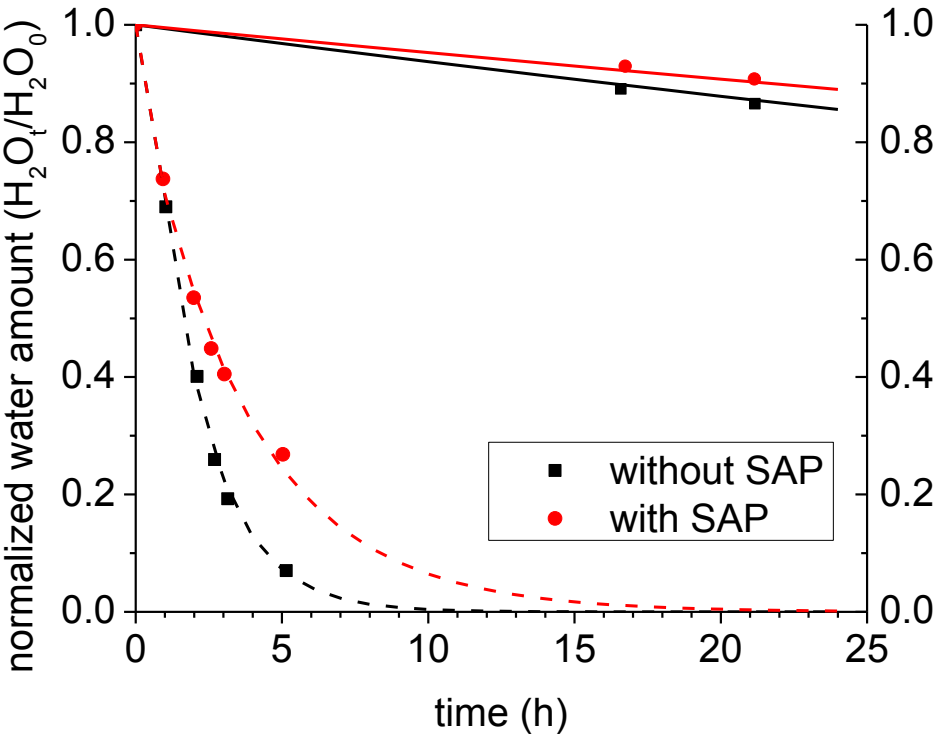

Figure S4. Amount of water in a test cell without and with superabsorbent polymer on the anode side. Closed cell configuration (solid line) and open-cathode configuration (dashed line) were tested.

Aalto-DD 83/2017
VTT SCIENCE 152

Printed enzymatic glucose/air batteries

The enzymatic biofuel cell (EBFC) converts the chemical energy of biofuel into electricity via bioelectrochemical reactions. In this thesis, laminar EBFCs were assembled using printed enzymatic electrodes and characterised by means of electrochemistry. **The performance** of the printed EBFCs was in the range of microwatts. The power output could be increased by adding biocatalysts and active electrode area. **The stability** of printed and hot-dried enzymatic electrodes was 60-80% after 28 days of storage at room temperature. Incorporating mediators into the inks degraded the electrodes faster and only 20-30% of the enzymatic activity was maintained during the same storage time. **The mass-manufacturing** of printed EBFCs was demonstrated on VTT's modular roll-to-roll screen printer. The performance of the EBFCs manufactured at the pilot facility was 10-50% of the laboratory manufactured EBFCs, due to decreased amount of active components in the inks and elevated drying temperatures of the inks.

ISBN 978-952-60-7412-2 (printed)
ISBN 978-952-60-7411-5 (pdf)
ISSN-L 1799-4934
ISSN 1799-4934 (printed)
ISSN 1799-4942 (pdf)

978-951-38-8537-3 (printed)
978-951-38-8536-6 (pdf)
2242-119X
2242-119X (printed)
2242-1203 (pdf)

Aalto University
School of Chemical Engineering
Department of Chemistry and Materials Science
www.aalto.fi

BUSINESS + ECONOMY

ART + DESIGN + ARCHITECTURE

SCIENCE + TECHNOLOGY

CROSSOVER

DOCTORAL DISSERTATIONS